



저작자표시-비영리-변경금지 2.0 대한민국

이용자는 아래의 조건을 따르는 경우에 한하여 자유롭게

- 이 저작물을 복제, 배포, 전송, 전시, 공연 및 방송할 수 있습니다.

다음과 같은 조건을 따라야 합니다:



저작자표시. 귀하는 원저작자를 표시하여야 합니다.



비영리. 귀하는 이 저작물을 영리 목적으로 이용할 수 없습니다.



변경금지. 귀하는 이 저작물을 개작, 변형 또는 가공할 수 없습니다.

- 귀하는, 이 저작물의 재이용이나 배포의 경우, 이 저작물에 적용된 이용허락조건을 명확하게 나타내어야 합니다.
- 저작권자로부터 별도의 허가를 받으면 이러한 조건들은 적용되지 않습니다.

저작권법에 따른 이용자의 권리는 위의 내용에 의하여 영향을 받지 않습니다.

이것은 [이용허락규약\(Legal Code\)](#)을 이해하기 쉽게 요약한 것입니다.

[Disclaimer](#)

Ultra Low Latency 71 ~ 76 / 81 ~ 86 GHz

E-band Radiolink Design

Young Su Kim

Electrical Engineering

Graduate School of UNIST

2014


Ultra Low Latency 71 ~ 76 / 81 ~ 86 GHz E-band Radiolink Design

A dissertation submitted to the Graduate School of UNIST
in partial fulfillment of the requirements
for the degree of Doctor of Philosophy

Young Su Kim

Jun. 17, 2014

Approved by




Major Advisor
Franklin Bien

Ultra Low Latency 71 ~ 76 / 81 ~ 86 GHz E-band Radiolink Design

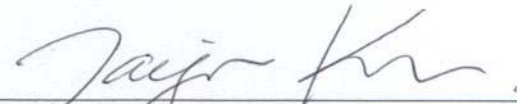
Young Su Kim

This certifies that the dissertation of Young Su Kim is approved

Jun. 17, 2014



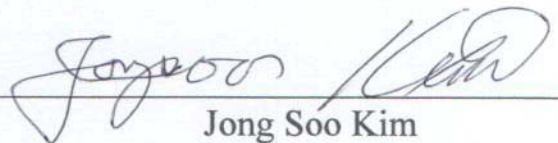
Dissertation Supervisor: Franklin Bien



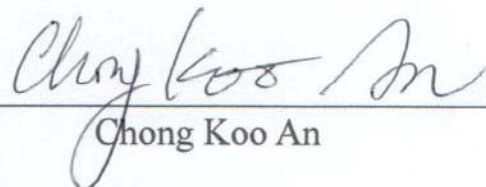
Jae Joon Kim



Ki Jin Han



Jong Soo Kim



Chong Koo An

ABSTRACT

For the special purpose of a time-sensitive system, such as a financial network, banking network, or medical network for real-time access in hospital, a very low latency of several tenths of a nano-second with a 1.25 Gbps transceiver is required. However, most commercial radiolinks are too slow at 5 ~ 350 μ s of latency through the use of Layer-2 topology with higher-level digital modulation. In this work, a unique topology of an ultra low latency transceiver was implemented by using high-speed ASK modulation with the scheme of physical Layer-1 transmission. In order to achieve a range of tenths of a nano-second of ultra-low latency with simple low cost, the direct conversion architecture was tried first. It was simple but still needed to be revised to address several problems. First, it was too difficult to build an ASK modulator directly at a 70/80 GHz millimeter-wave as it was too sensitive at its physical dimension. Secondly, the flatness was important, but it was difficult to secure the required bandwidth. Most of all, the conversion loss was significantly increased when the received power is low. In order to solve these problems, a heterodyne transceiver was considered. The ASK modulation was conducted at the IF stage. By adopting the heterodyne topology, the burdens of building an ultra wideband ASK modulator in 70/80 GHz millimeter-wave range was alleviated. However, building a 1.25 Gbps ASK modulator in the IF stage presented another new challenge. Several wide band design techniques were proposed as well as trial and error. According to the measurement results, the sensitivity was -45 dBm for 1.25 Gbps under BER 10^{-12} , or error free, and one-way latency was measured by 19.1 ns, which is a superior achievement compared to existing commercial radiolinks worldwide. It was field tested at 4.1 km and showed a good match with its link budget. As a field proven solution, this research result has been partially adapted to a financial network in service between Chicago and New York.

KEY WORDS: *E-band Radiolink, Low Latency, mmW Transceiver, Point-to-Point*

CONTENTS

I. Introduction	1
1.1 Latency on Networks	1
1.2 E-band Wide-band Radiolink	5
II. Low Latency E-band Radiolink Design	9
2.1 Proposed E-band Radiolink	9
2.1.1 Introduction to Low Latency Radiolink	9
2.1.2 Scheme of Proposed E-band Transceiver	14
2.2 Previous Work on Direct Conversion ASK Transceiver	15
2.2.1 Frequency plan for E-band Radiolink	16
2.2.2 System Budget	17
2.2.3 Design Review on Previous Work	18
2.2.4 Measurement Result	26
2.2.5 Challenging Issues on Direct Conversion	29
2.3 Proposed Heterodyne mmW ASK Transceiver	30
2.3.1 Frequency Plan for E-band Radiolink	31
2.3.2 Wideband ASK Modulator	32
2.3.3 W/G-to-Microstrip Transition	35
2.3.4 Mounting & Bonding Techniques for MMIC	37
2.3.5 Design of mmW TX Front-End	39
2.3.6 Design of mmW RX Front-End	42
2.3.7 Design of PLO	43

2.3.8 Implementation of Wide-Band IF & Baseband Section	-----	44
2.3.9 AGC Circuit for Temperature Compensation	-----	49
2.3.10 Implementation of E-band Transceiver	-----	52
2.4 mmW Diplexer Design	-----	54
2.4.1 Guide Wavelength of WR12	-----	54
2.4.2 Waveguide Inductive Iris Filter	-----	55
2.4.3 Extraction of K-Inverter Parameter	-----	56
2.4.4 Design of Inductive Iris Filter	-----	59
2.4.5 Design of T-junction	-----	61
2.4.6 Simulation Result	-----	65
2.4.7 Measurement Result	-----	67
2.5 Measurement Results	-----	69
2.5.1 Data Rate & Dynamic Range	-----	69
2.5.2 Latency	-----	74
III. Field Test	-----	79
3.1 Link Budget	-----	79
3.2 Field Test	-----	81
3.3 Availability Analysis	-----	83
3.4 Interference Free Scenario	-----	85
IV. Future Work	-----	88
IV. Conclusion	-----	95

LIST OF FIGURES

- Figure 1.1 Trading on New York Stock Exchange (NYSE)
- Figure 1.2 Attenuation versus frequency due to atmospheric gases
- Figure 1.3 Rain attenuation
- Figure 2.1 Commercial common Layer-2 radiolink
- Figure 2.2 Proposed low latency Layer-1 radiolink
- Figure 2.3 System block diagram
- Figure 2.4 Previous work on direct conversion E-band ASK transceiver
- Figure 2.5 E-band frequency use of previous work
- Figure 2.6 ASK modulator (a) Equivalent symbol (b) Implemented circuit
- Figure 2.7 Design of mmW ASK modulator with Schottky diode
- Figure 2.8 Design of diode mounts
- Figure 2.9 Assembled mmW ASK modulator
- Figure 2.10 Modulation characteristic of (a) 70GHz range (b) 80 GHz range
- Figure 2.11 Characteristic of LNA (a) Gain (b) Return loss
- Figure 2.12 Characteristic of HPA (a) Gain (b) Return loss
- Figure 2.13 Improvement of demodulator design
- Figure 2.14 Improvement of diode mount
- Figure 2.15 Characteristic of demodulator at (a) Lower band path (b) Upper band path
- Figure 2.16 Circuit design of wide bandwidth of 1.1GHz baseband
- Figure 2.17 Implemented baseband board
- Figure 2.18 Implemented ASK Transceiver
- Figure 2.19 Measurement result of sensitivity
- Figure 2.20 Proposed heterodyne E-band ASK transceiver

- Figure 2.21 Frequency use of proposed E-band radiolink
- Figure 2.22 Block diagram of wide-band ASK modulator at 3.7GHz IF band
- Figure 2.23 Implemented 3.7GHz wide-band ASK Modulator
- Figure 2.24 BW of 2.2GHz wide-band ASK spectrum at 3.7GHz IF band
- Figure 2.25 Block diagram of wide-band ASK modulator at 6.3GHz IF band
- Figure 2.26 Implemented 6.3GHz wide-band ASK modulator
- Figure 2.27 BW of 2.2GHz wide-band ASK spectrum at 6.3GHz IF band
- Figure 2.28 WR12-to-microstrip transitions
- Figure 2.29 Measured result of transition loss
- Figure 2.30 Die mounting
- Figure 2.31 Simulation modeling for wire bond
- Figure 2.32 Insertion loss of wire bond
- Figure 2.33 Design of mixer mounts
- Figure 2.34 Design of HPA
- Figure 2.35 Measured result of mmW HPA at 70GHz
- Figure 2.36 Measured result of mmW HPA at 80GHz
- Figure 2.37 Design of RX front-end section
- Figure 2.38 Gain performance of ALH509
- Figure 2.39 Designed 13.096GHz PLO
- Figure 2.40 Block diagram of wide-band 3.7GHz IF & ASK detector
- Figure 2.41 Revised block diagram of wide-band 3.7GHz IF Section
- Figure 2.42 Flatness of 3.7GHz IF section with HFCN2275 and LFCN5000
- Figure 2.43 HPF with lumped device to compensate flatness slope
- Figure 2.44 Simulation result of lumped HPF
- Figure 2.45 Improved flatness result

Figure 2.46 Block diagram of wide-band 6.3 GHz IF & ASK detector

Figure 2.47 ASK spectrum of BPF output at 6.3GHz IF stage

Figure 2.48 Insertion of 50ohm resistor for wide-band matching

Figure 2.49 Revised IF section for upper band

Figure 2.50 Temperature compensated AGC circuit design

Figure 2.51 Implemented RX-IF and baseband section

Figure 2.52 Compensation at low temperature adjusting VVA control current

Figure 2.53 Mechanical design of E-band transceiver

Figure 2.54 Outline of implemented E-band transceiver

Figure 2.55 Wavelength of WR12 waveguide

Figure 2.56 Structure of inductive iris

Figure 2.57 K-inverter coupled inductive iris filter

Figure 2.58 Equivalent circuit of K-inverter

Figure 2.59 Simulation result of K-inverter at lower band

Figure 2.60 Simulation result of K-inverter at upper band

Figure 2.61 Shunt connected diplexer

Figure 2.62 T-junction HFSS modeling

Figure 2.63 Simulation result of T-junction

Figure 2.64 Simulation result of lower band matching

Figure 2.65 Simulation result of upper band matching

Figure 2.66 Designed E-band inductive iris coupled filter

Figure 2.67 Simulation result of lower band filter

Figure 2.68 Simulation result of upper band filter

Figure 2.69 Simulation result of diplexer

Figure 2.70 Outline design of diplexer

- Figure 2.71 Measurement result diplexer (lower)
- Figure 2.72 Measurement result diplexer (upper)
- Figure 2.73 ASK modulation spectrum at lower band
- Figure 2.74 Lower band carrier at 74.875GHz
- Figure 2.75 ASK modulation spectrum at upper band
- Figure 2.76 Upper band carrier at 84.875GHz
- Figure 2.77 Eye pattern of detected 1.25Gbps GbE signal
- Figure 2.78 Measurement setup with temperature chamber
- Figure 2.79 Temperature characteristics
- Figure 2.80 Latency measurement setup
- Figure 2.81 Calibration of power divider output
- Figure 2.82 Loopback of radio unit
- Figure 2.83 Latency test setup
- Figure 2.84 Latency measurement result
- Figure 2.85 Comparisons of latency and data rate
- Figure 3.1 Antenna gain & HPBW
- Figure 3.2 Field test site with 4.1 km distance
- Figure 3.3 Rain attenuation versus frequency
- Figure 3.4 Point-to-point multi-links deployments
- Figure 3.5 Frequency plan for interference free scenarios for 10 GbE
- Figure 4.1 Structure of MCPW transmission line
- Figure 4.2 Field distribution and MCPW simulation result
- Figure 4.3 Schematic of 3-stage LNA
- Figure 4.4 Cadences modeling of 3-stage LNA
- Figure 4.5 Simulation result of designed 3-stage LNA

Figure 4.6 Layout design of 3-stage LNA

Figure 4.7 Schematic of single balanced mixer with buffer

Figure 4.8 Simulation result of mixer

Figure 4.9 Layout design of SBM mixer

Figure 4.10 Microphotograph of implemented CMOS LNA (750 x 520 μm^2)

Figure 4.11 Microphotograph of implemented CMOS Mixer (1,500 x 674 μm^2)

LIST OF TABLES

Table 1.1	Comparison of network latency
Table 1.2	E-band frequency allowance in USA
Table 2.1	Technology comparison of several data links
Table 2.2	System budget for direct conversion
Table 2.3	BER test result
Table 2.4	Measurement result on previous work
Table 2.5	Proposed E-band transceiver
Table 2.6	Measurement result of mixer conversion loss
Table 2.7	Measurement result of HPA P1dB
Table 2.8	Design specifications of E-band diplexer
Table 2.9	Designed K-inverter and iris length of lower band filter
Table 2.10	Designed K-inverter and iris length of upper band filter
Table 2.11	Designed resonator lengths D [mm]
Table 2.12	Measurement result of diplexer
Table 2.13	Test result of dynamic range
Table 2.14	System noise figure
Table 2.15	Comparison of latency among commercial technologies
Table 2.16	Summary of measurement result
Table 3.1	Link budget analysis
Table 3.2	Rain rate worldwide recommended from ITU-R
Table 3.3	Estimated link distance of implemented radiolink
Table 3.4	Deployment case
Table 3.5	Required separations for interference free
Table 3.6	Interference free scenarios for 10GbE

NOMENCLATURE

ASK	Amplitude Shift Keying
AGC	Automatic Gain Control.
BPF	Band Pass Filter
BER	Bit Error Rate
CFR	Code of Federal Regulations
CMOS	Complementary Metal Oxide Semiconductor
DQA	Data Quality Analyzer
EIRP	Equivalent Isotropically Radiated Power
FCC	Federal Communications Commission
FET	Field Effect Transistor
FSO	Free space optic
GbE	Gigabit Ethernet
HPBW	Half Power Beam Width
HFSS	High Frequency Structure Simulator
HFT	High Frequency Trading
HPF	High Pass Filter
HPA	High Power Amplifier
ISM	Industrial Scientific Medical
IP	Internet Protocol
LGA	Linear Gain Amplifier
LOS	Line-of-Site
LO	Local Oscillator
LNA	Low Noise Amplifier

LPF	Low Pass Filter
mmW	Millimeter Wave
MDS	Minimum Detectable Signal
MMIC	Monolithic Microwave Integrated Circuit
MCPW	Multi-layer Coplanar Waveguide
NMOS	N-channel Metal Oxide Semiconductor
NRD	Non-Radiated Dielectric
OOK	On-Off Keying
PIC	Peripheral Interface Controller
PLO	Phase Locked Oscillator
PA	Power Amplifier
PRBS	Pseudo-Random Binary Sequence
QAM	Quadrature Amplitude Modulation
QPSK	Quadrature Phase Shift Keying
RSSI	Received Signal Strength Indicator
RX	Receiver
SNR	Signal to Noise Ratio
SFP	Small Form Factor Pluggable Transceivers
SMA	Sub-Miniature version A
TCP	Transmission Control Protocol
TX	Transmitter
TE	Transverse Electric
UDP	User Datagram Protocol
VCO	Voltage Controlled Oscillator

I. Introduction

1.1 Latency on Networks

In a communication network, latency is an expression of how much time is needed for a stream of data to get from one designated point to another. It is often used as a kind of signal delay in a digital network. Network latency is measured either one-way or round-trip. Round-trip latency is more often quoted, because it can be measured from a single point. By sending a packet of data, the time that is returned to the sender and the round-trip is considered the latency, and it is often used as one of the key parameters to verify network performance [1].

The contributors to network latency include propagation on the channel of air or cable, transmission media like radiolink, signal processing in a router or gateway, and other storage delays in the network pass [2]. One can reduce the latency of artificial network devices by using fast switching equipment, but in case of a wireless radiolink the latency due to the air channel itself is not being reduced.

In the case of an air channel, the latency is largely a function of the speed of light, which is 3×10^8 meters per second, which results in a latency of $3.33 \mu\text{s}$ per every kilometer of the path length. In case of a fiber optic cable, the index of refraction is about 1.5. This means that the light travels about 1.5 times slower in the fiber optic cable than it does in the air [3], and it results in $5 \mu\text{s}$ of latency per every kilometer in the cable. If one needs to have a faster network over quite a long distance, the total network latency would be increased as much as $5 \mu\text{s}$ per each kilometer.

Table 1.1 shows the comparison of total latency among media in the case of a 450 km network from Seoul to Busan. In the case of the fiber optic cable, a total of 22.5 network repeaters are required,

assuming each network repeater covers every 20 km distance. Total latency is the latency by optic cable of 2.25 ms plus the latency by network repeater of 2.25 ms, which results in 4.5 ms total latency. The latency of radio, or air, is 1.5 time faster than that of fiber optic. Note that if the latency of network equipment for fiber optic link per every 20 ~ 40 km in the path are considered, the difference will be increased even more.

Table 1.1 Comparison of network latency

Parameters	Unit	Air/Radio	Fiber Optic	Remark
Velocity	m/s	3×10^8	2×10^8	
Unit Latency	$\mu\text{s}/\text{km}$	3.33	5.0	
Distance	km	450	450	Seoul to Busan
Total Latency	ms	1.5	2.25	

The calculation in Table 1.1 is an example only for Seoul to Busan. What if a network is required from Chicago to New York? The latency would exceed 6 ms over the distance of 1,200 km. If one consider the latency of all network nodes together, it would exceed several tenths of milliseconds. Therefore, the fiber optic cable is not a good solution anymore for an advanced latency-sensitive network or speed critical system. If one can reduce the latency of a device itself, radiolink will be faster than such conventional fiber optic link.

For the special purpose of a time-sensitive system, such as a financial network, banking network, or medical network for real-time access in a hospital, a very low latency of several tenths of a nano-second as well as a higher data rate, or ultra wide bandwidth, from 1.25 Gbps to multi-gigabit up to 10 Gbps is required [4].

Figure 1.1 shows the working hours in New York Stock Exchange (NYSE). In case of the NYSE, trading amount on the market reaches a daily average of US\$3.47 billion, or US\$40.2k per second [5]. Although super-computers are faster for trading, one will lose money unless the network speed is

faster while accessing the data from a local remote site. This is why a fiber optic cable is limitedly used in such time-sensitive financial network, but specially designed wireless radiolink is used to reduce the latency in high frequency trading (HFT). One will make money if they use a faster network, or else they will lose [6].



Figure 1.1 Trading on New York Stock Exchange (NYSE)

HFT uses sophisticated technological tools with very low latency wireless bridges and computer algorithms to trade securities on an extremely fast basis. HFT usually uses proprietary trading strategies that are carried out by computers, and such transactions are increasingly being transmitted over high speed gigabit capacity wireless networks [4], [7].

Unlike regular investing, an investment position in HFT may be held for only seconds, or fractions of a second, with the computer trading in and out of positions of thousands or tens of thousands of times a day. Many high-frequency traders provide liquidity and price discovery to the markets through market-making and arbitrage trading, and high-frequency traders also take liquidity to manage risk or lock in profits [8].

In order to capture a fraction of a penny or currency unit per each trade, HFT traders may move in and out of such short-term positions several times each day. Even it is a little, fractions of a penny accumulate fast to produce significantly positive results by the end of the day. These firms do not employ much leverage, do not accumulate positions, and typically liquidate their entire portfolios on a daily basis. HFT is rapidly growing in popularity and accounted for over 70% of equity trades in the US by 2010 [9] [10].

For safety reasons, medical data in a hospital, including a human body scan, is not compressed when it is transferred to other network terminal, but is transferred as its raw data without signal processing. Thus a very wide bandwidth of data rate of 1.25 Gbps or multi-gigabits is required to access [11] [12]. Also these networks require very low latency too to connect real-time over several remote networks.

A high speed broadband network is required in a campus network too, carrying high speed real-time data between laboratories at remote buildings. A vast amount of simulation data and, scanned 2D/3D image data are a burden for a low speed, narrow bandwidth of conventional IP network [13] [14]. Thus network latency is the key factor for time-sensitive and real-time transmission solutions.

1.2 E-band Wide-band Radiolink

For a WiFi solution at 2.4 GHz, or WiMAX at 5.8 GHz, it is very easy to access but too slow and the data rate is too narrow by 155 Mbps at best. A microwave frequency range of 18 GHz to 38 GHz also has also some band allowance for a fixed point-to-point radiolink, but the allowed bandwidth is too narrow such as 40 MHz to transmit ultra wide bandwidth greater than 1.25 Gbps [15] [16].

Note that at least 250 MHz is required to transmit 1.25 Gbps by using 64QAM, which is considered the maximum modulation level for a commercial radiolink even if higher modulation is available in a laboratory [17]. In order to reduce the required bandwidth for the signal of 1.25 Gbps transmission, an even higher modulation technique of 256QAM or 1024QAM is required, but it is difficult to implement for a practical radiolink. Such higher modulation is available only for a wired network like fiber optic cable transmission, not wireless.

For the accommodation of two key performances of ultra low latency and ultra wideband data transmissions with 1.25 Gbps, a very wide bandwidth of allowed frequency band is required. Even if one can use only 250 MHz bandwidth with higher level of digital modulation like 64QAM for wideband data rate of 1.25 Gbps, the latency would be poor with such higher modulation.

Thus for low latency, a very low level of digital modulation like ASK is required. However, it requires an extremely wide bandwidth of 2.5 GHz for 1.25 Gbps transmission. Considering these in mind to achieve both low latency and very high data rate simultaneously, the E-band millimeter-wave (mmW) frequency range is the best choice. This is why E-band mmW frequency with ASK modulation is chosen in this work.

Table 1.2 E-band frequency allowances in USA

Frequency	Bandwidth	Allowed EIRP	Remark
71 ~ 76 GHz	5 GHz	+55 dBW	
81 ~ 86 GHz	5 GHz	+55 dBW	

*Note: Based on FCC, CFR. Part 101 *CFR: Code of Federal Regulations

Table 1.2 shows E-band frequency allowance in USA [18] and the same regulation is allowed in most countries including South Korea [19] [20]. European E-band regulation is also the same except that the bands are channelized by 20 channels with 250 MHz bandwidth each at both bands [21] [22] [23]. The 71 ~ 76 GHz and 81 ~ 86 GHz allocation allows 5 GHz of transmission bandwidth, which is available to transmit 1.25 Gbps full-duplex gigabit Ethernet signal by the ASK modulation scheme.

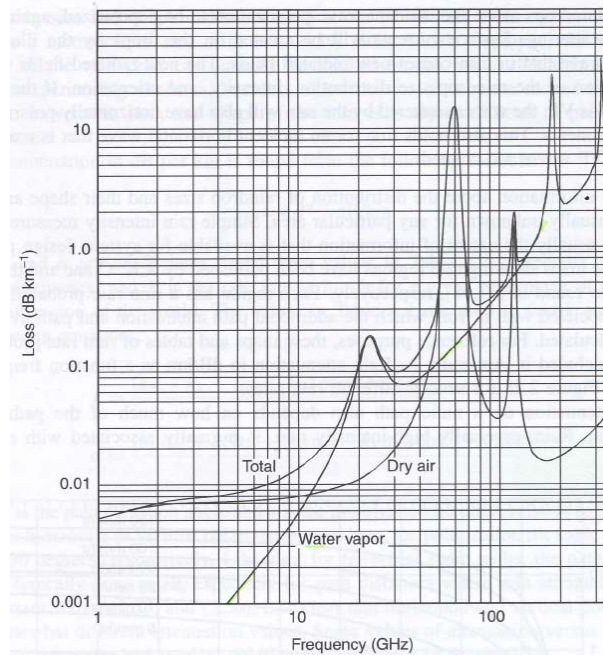


Figure 1.2 Attenuation versus frequency due to atmospheric gases

Figure 1.2 shows the atmospheric attenuation of radio propagation at various frequencies [24]. For lower microwave frequencies up to around 30 GHz, atmospheric attenuation is relatively low by 0.2 dB per kilometer or less. At around 60 GHz, the oxygen absorption shows a large spike in attenuation.

Due to the large increase of oxygen absorption, a radio transmission distance of 60 GHz is seriously limited. However, over 70 GHz to 90 GHz, the attenuation drops back to values around 0.5 dB/km. This lower attenuation range is referred to as the E-band. It is the relatively low atmospheric attenuation window between 70 GHz and 100 GHz, which makes E-band frequencies attractive for higher capacity of point-to-point fixed wireless transmission.

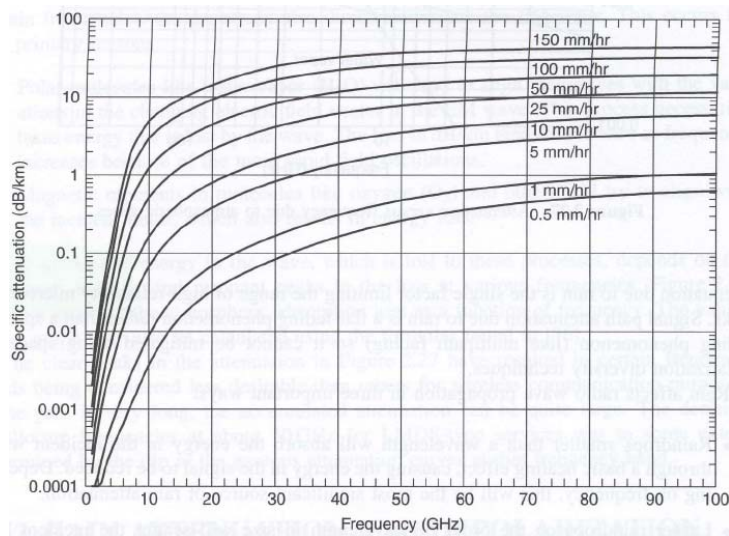


Figure 1.3 Rain attenuation

For higher frequency radio propagation, the practical limit on transmission distance is determined by rain attenuation typically. Figure 1.3 shows rain attenuation of radio at each frequency range [24]. The E-band can be experience large attenuation during rainfall. Fortunately, the most intense rain tends to fall in limited parts of the world, mainly the subtropical and equatorial countries.

In Korea, ITU-R designates the rain region-K [25]. For 99.999% of link availability, which is equivalent to 5.3 minutes per year, the recommended rain rate is 100 mm/hour. This means that in order to guarantee 99.999% of stable link availability at a distance, one need to consider the rainfall rate of 100 mm/hour.

The proposed E-band radiolink can be utilized for a point-to-point connectivity between buildings and/or towers for a high speed Ethernet networks such as HFT applications in stock trading market, real-time military or homeland security applications. These applications are all available in the industry, universities, businesses, government agencies, and hospitals having higher bandwidth needs.

In this work, a unique topology for an ultra low latency transceiver was implemented. The idea suggests a trial to transmit the raw digital bits over physical Layer-1 without any addition of overhead bits. To reduce the system latency, ASK modulation was chosen without using higher symbol modulation of QPSK ~ 64QAM, which has simple structure and low cost as well. The upcoming problem was the securement of required bandwidth (BW) of 2.5 GHz (actually 2.2 GHz in the work) for 1.25 Gbps transmission with ASK. There are no such permitted wide bands of frequency range in the ISM band in 2.4 GHz, 5.8 GHz, 24 GHz, or any other microwave frequency range. Thus 71 ~ 76 GHz and 81 ~ 86 GHz E-band millimeter-wave frequency was chosen, which allows for 5 GHz bandwidth.

In chapter II, a high speed mmW ASK transceiver design is presented with its previous work with wide band E-band diplexer design, showing several key techniques to build ultra wide bandwidth characteristics. In chapter III, link budget and field test results are introduced with several interference free scenarios. A challenging 10 Gbps configuration is introduced by utilizing 8 links of 1.25 Gbps transceiver for practical HFT. Link availability under rainfall is also described. In chapter IV, future work on a CMOS approach will be briefly described as a preliminary trial to reduce the cost, finally followed by the conclusion of this work.

II. Low Latency E-band Radiolink Design

2.1 Proposed E-band Radiolink

2.1.1 Introduction to Low Latency Radiolink

With the wide bandwidth allowance of 71 ~ 76 GHz and 81 ~ 86 GHz E-band frequency range with its lower oxygen absorption characteristic, E-band radiolink is often used for ultra broad bandwidth data transmission as described in the previous section. Figure 2.1 shows the scheme of data transmission and detection of common commercial Layer-2 radiolink. Assume that a stream of digital data needs to be transmitted as combination of ones and zeros from one site to another.

In order to transmit the data correctly by using wireless radiolink, a set of header bits are added at the transmitter at the head or tail of the upper layer data messages at each step before it is transmitted and is removed at receiver after delivery. These header of TCP/UDP, IP, or Layer-2 header include the identification of each data frame to deliver it to each designated destination correctly in a network [26] [27].

In the end, the radiolink delivers the Layer-2 data frame, which includes quite a lot of header bits on both sides of its original data. Note that the transmitter delivers significantly more extra bits together as well as its original data. At the receiver of the radiolink, it detects the delivered Layer-2 frame data, and the data stream still includes the required sets of each layer header. These sets of each layer header need to be removed before the original data is extracted.

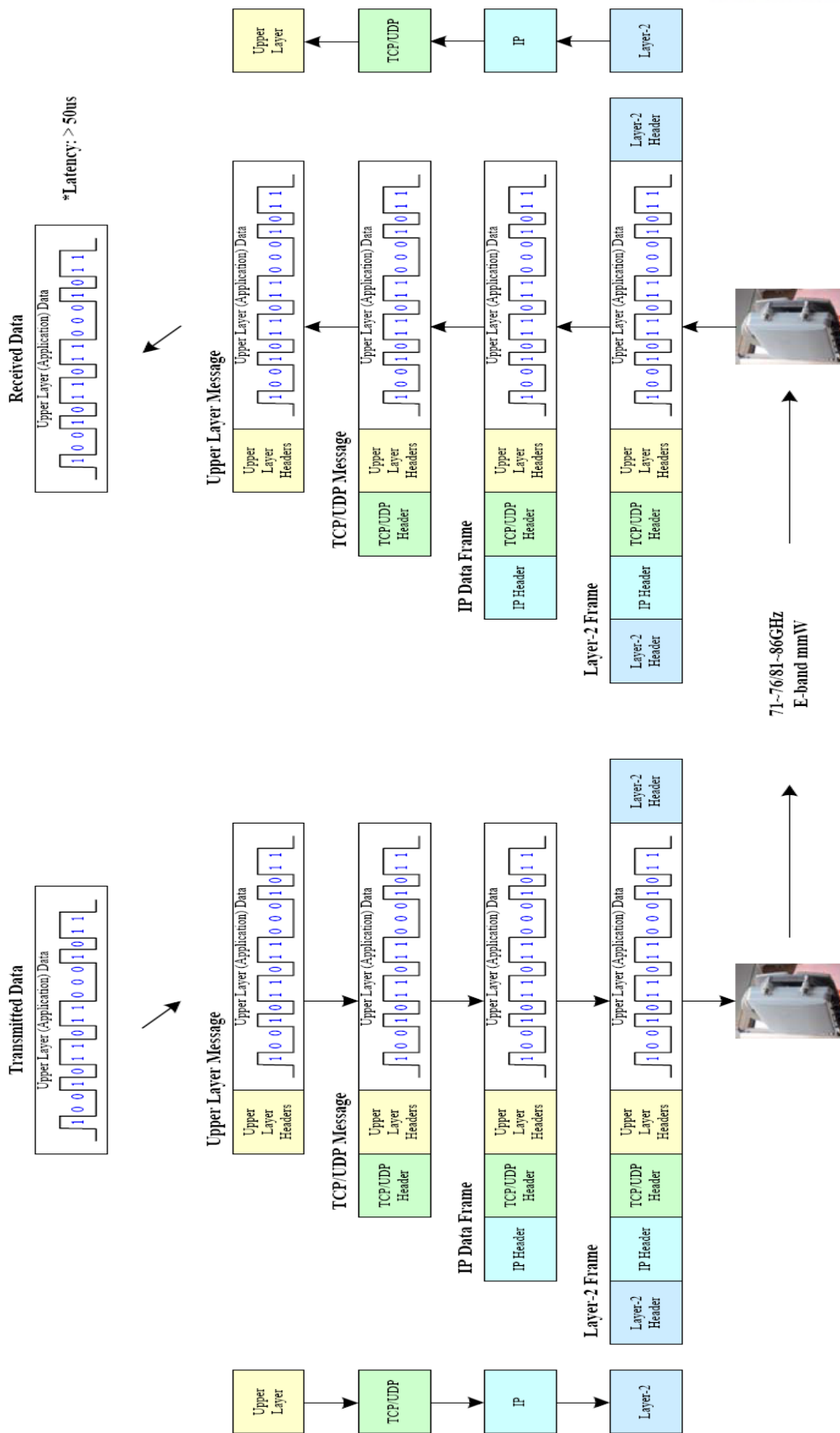


Figure 2.1 Commercial common Layer-2 radiolink

By adding and removing these headers according to an IP protocol, it takes time by signal processing on both sides of transmitter and receiver [26]. This is general scheme of common commercial radiolink lately. It is very good for safely delivering the original data, but it also causes the delay [27]. This delay at each side of radio unit is called the latency of equipment, which is in a range from 5 μ s to 350 μ s with common commercial radiolink [28] ~ [38]. Note this is significantly long when applied to a time-sensitive financial network.

On the contrary, Figure 2.2 shows the scheme of the proposed ultra low latency Layer-1 radiolink. Once the signal senses at the transmitter of the radiolink, the signal is modulated by directly switching into E-band radio frequency and is transmitted to the receiver. At the receiver, the delivered signal is detected at once. Note that there are no extra sets of header bits added or removed at both side of transmitter and receiver, as it does in the common commercial Layer-2 radiolink. By no adding or removing IP protocol headers, the delivery of the signal is very fast without conducting a signal processing. Thus it can be achieve an ultra low latency of only several tenths of nano-second. As there is no error correction or any control bits during delivery, the signal path of the transceiver needs to be controlled very carefully.

In conclusion, guaranteeing low latency does not work with Layer-2 equipment due to the delay. This is why Layer-2 is not chosen, but Layer-1 transmission is chosen in this work. In addition to delivering ultra wide band of 1.25 Gbps without compression, which is commonly done with a symbol transmission like QPSK ~ 64QAM modulation, the simple switching scheme of ASK modulation was chosen. In order to transmit an ultra wide band of 1.25 Gbps with simple ASK modulation, even though the radio bandwidth of 2.5 GHz is required theoretically, only 2.2 GHz BW is actually used in this work.

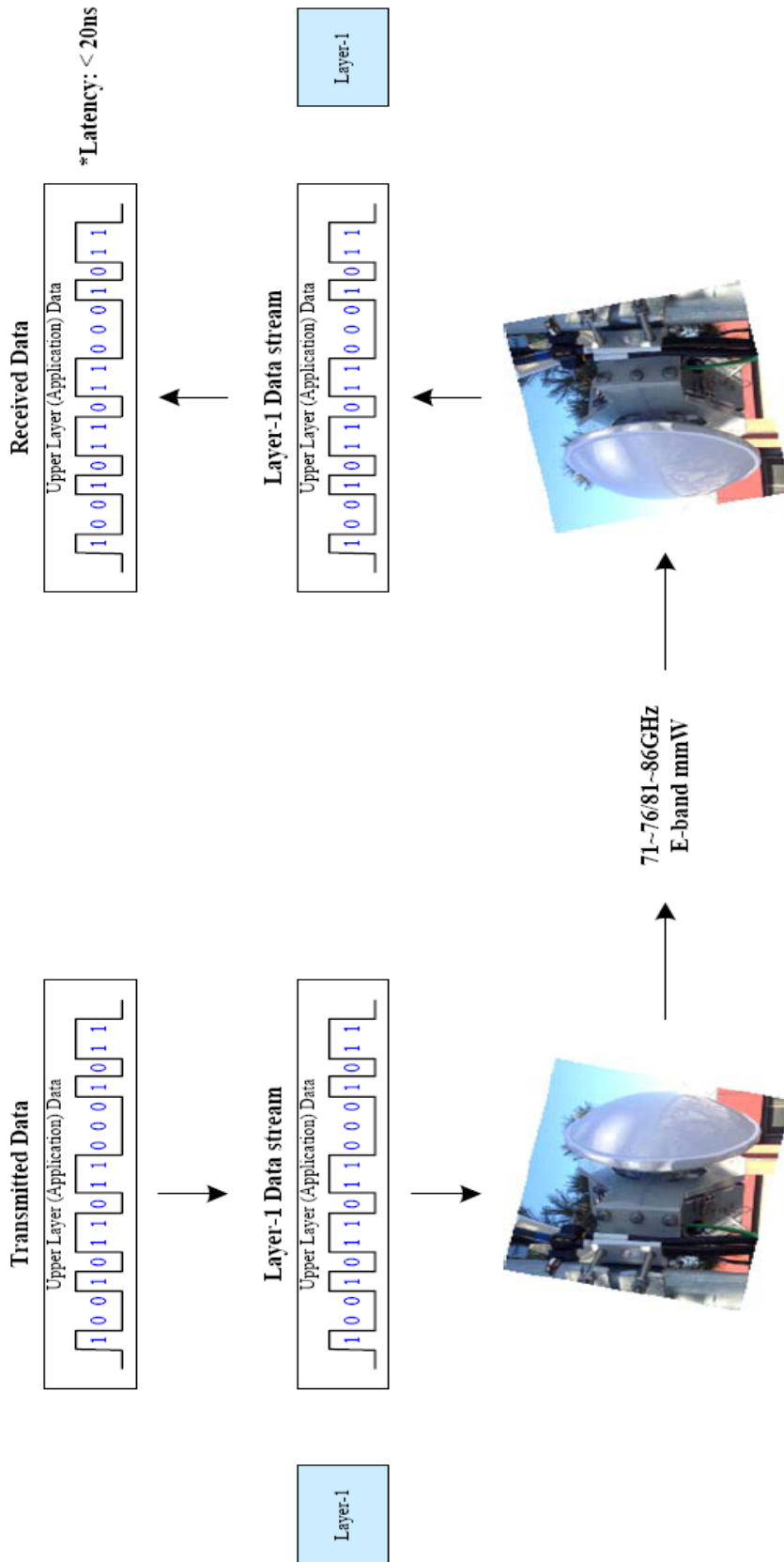


Figure 2.2 Proposed low latency Layer-1 radiolink

Table 2.1 shows the comparison of technology among several data links as well as 71 ~ 76 / 81 ~ 86 GHz E-band mmW. A free space optic (FSO) can be another choice, but note that there are so many restrictions over various weather conditions and environmental issues including rainfall, snowfall, dust, fog, etc. [39]. For these reasons, E-band mmW radiolink is chosen for the ultra broad bandwidth of 1.25 Gbps transmission.

Table 2.1 Technology comparison of several data links

Parameters	18/24 GHz Microwave	Fiber Optic (Cable)	Free Space Optic (FSO)	mmW V-band (57~64GHz)	mmW E-band (71~76/81~86GHz)
99.999% @1km (5.26 min/year)	OK	OK	NO	NO	OK
Deployment Time	Days	Several Months	4~8 Hours	4~8 Hours	4~8 Hours
Expense per Gbps per km	Moderate	High	Low	Moderate	Low
Regulatory Protection	Sometimes	OK	NO	NO	OK
License/ Rental Fee	Sometimes	Need	OK	OK	Need
Fog	OK	OK	NO	OK	OK
Snow	OK	OK	NO	OK	OK
Heavy Rain	Potentially	OK	NO	Potentially	Potentially
Dust/ Smoke	OK	OK	NO	OK	OK
Frequency Reuse efficiency	Low	OK	High	High	Moderate
Data Rate (max)	200 Mbps	10 Gbps	2.5 Gbps	2.5 Gbps	2.5 Gbps

2.1.2 Scheme of Proposed E-band Transceiver

Figure 2.3 shows the system block diagram of proposed E-band radiolink. The 1.25 Gbps Gigabit Ethernet (GbE) signal is plugged by using fiber optic transceiver with SFP connector. The GbE optic signal is converted into electric signal through optic GbE transceiver and transferred to the designed E-band ASK transceiver. The high speed GbE signal is modulated, and the modulated E-band spectrum is band limited at the diplexer filter and radiated through the antenna.

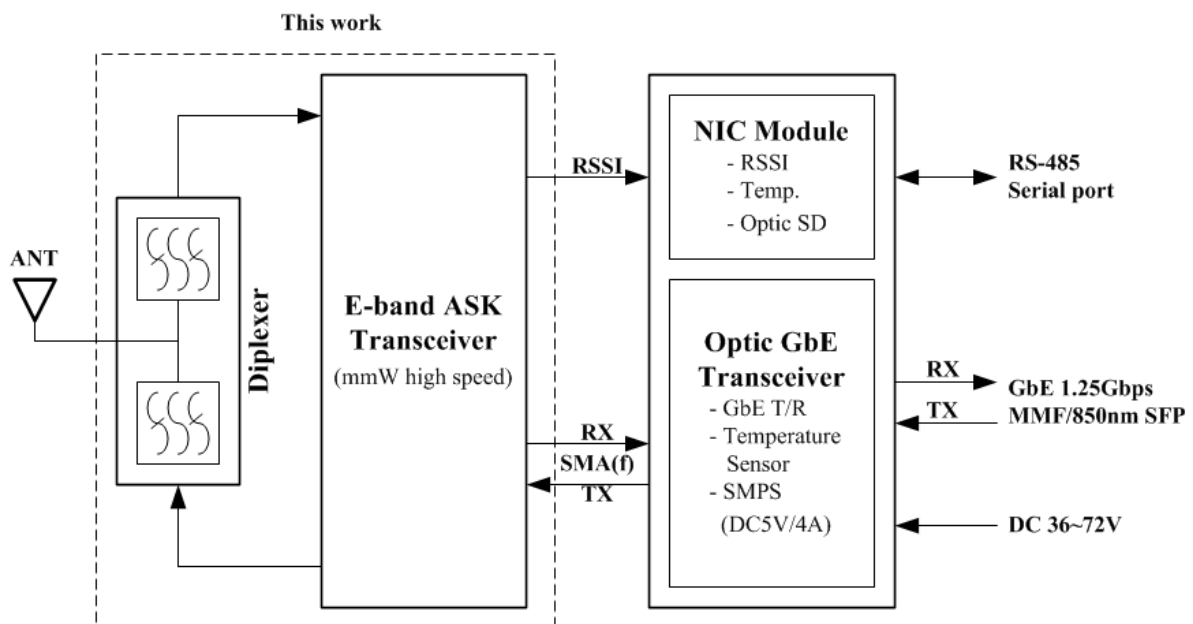


Figure 2.3 System block diagram

In this work, the E-band high speed mmW ASK transceiver and wide-band E-band diplexer are designed for the ultra low latency with ultra wide bandwidth of 1.25 Gbps transmission. Except the E-band front-end of transceiver and diplexer, other parts are utilized by using a commercial shelf-product to build the whole system, aiming of course for low latency with ultra wide band characteristics.

2.2 Previous Work on Direct Conversion ASK Transceiver

Figure 2.4 shows the block diagram of previous work on direct conversion E-band ASK transceiver. In order to achieve the transceiver simple low cost [40], the direct conversion architecture was tried first. The input signals of 1.25Gbps GbE have spectrum distribution from DC to 1.25 GHz. This wide bandwidth of TX signals is band limited before ASK modulation. A 12 GHz range of VCO output was multiplied by 6 and switched by a TX signal, which resulted in direct ASK modulation up to 71 ~ 76 GHz or 81 ~ 86GHz E-band frequency spectrum. The ASK modulated signal is amplified at the HPA stage before radiation through antenna after filtering at diplexer.

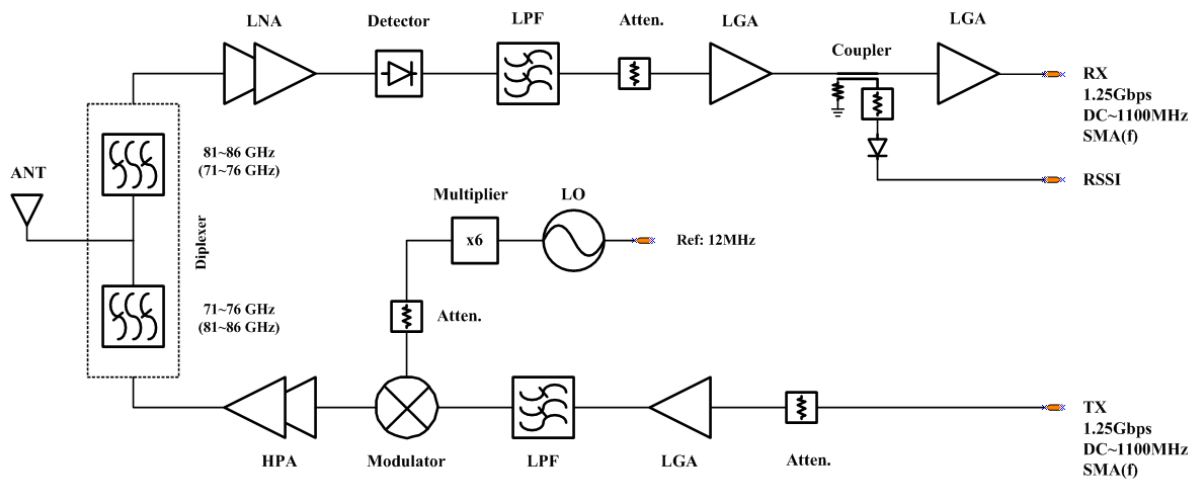


Figure 2.4 Previous work on direct conversion E-band ASK transceiver

At the receiver (RX), the weak received signal is low noise amplified at LNA. At the designed high speed detector, the original signal is extracted by envelop detection with E-band Zero-IF mixer, which is non-coherent detection. The self-detection is available as the received signal spectrum already includes LO carrier as well as the signal. By transmitting the LO carrier from TX signal which is generated by ASK modulator, RX section can be implemented with a simple structure without LO source.

2.2.1 Frequency plan for E-band Radiolink

Figure 2.5 shows the frequency use of proposed E-band radiolink. To transmit the capacity of 1.25 Gbps data rate by using ASK, the required BW theoretically is 2.5 GHz. However, most of the radiated power is concentrated at or near the LO carrier. Thus it does not need to use 100% of the required BW, which means ‘necessary bandwidth’ according to [41]. According to the experiment, 99% of the occupied BW of 1.25 Gbps Ethernet signal was within 62.8%, or 1.57 GHz, of the theoretical BW of 2.5 GHz. In this work, only 88% of them, or 2.2 GHz BW, was chosen for reasonable sensitivity. This will be shown in the following section 2.5 again with its measured spectrum plot.

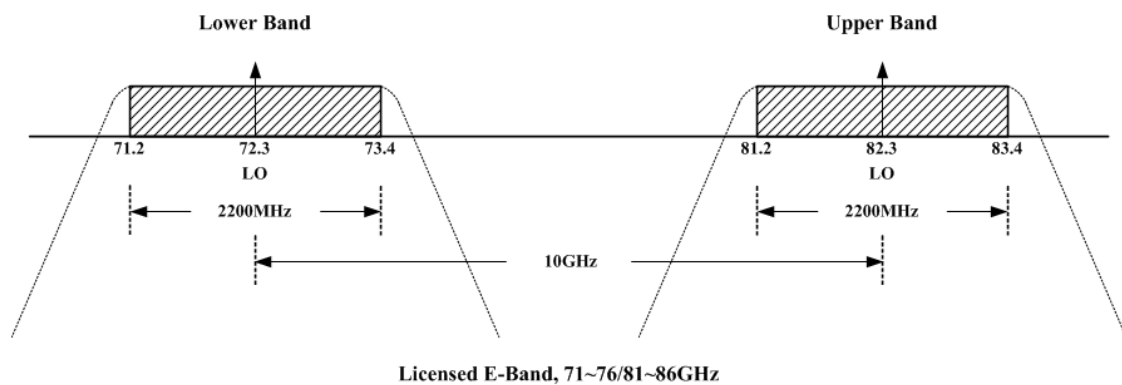


Figure 2.5 E-band frequency use of previous work

For the full-duplex of the radiolink, both of 71 ~ 76 GHz and 81 ~ 86 GHz frequency bands are used with 2.2 GHz BW each. The center frequencies are chosen at 72.3 GHz for the lower band and 82.3 GHz for the upper band. As there is 10 GHz separation between two bands, the burden for building of required isolation of diplexer was relatively easy.

All required parts, including ASK modulator, transition, mixer, LNA, PA, and demodulator (detector) and other any components, should be built with sufficient wideband characteristics than 2.2 GHz. If

any one of mentioned parts has a narrow characteristic, an ultra wide bandwidth of signal will not be transmitted, and the goal of implementation of ultra low latency radiolink will fail. Therefore, the building of wide band characteristics greater than the required 2.2 GHz was the greatest challenging issue in this work. At the IF stage, this issue acts as greater problem and is magnified as frequency decrease to baseband circuit.

For the 72.3 GHz and 82.3 GHz TX carrier, 12.050 GHz and 13.717 GHz of PLO output were multiplied by 6 before being sensed at TX mixer as ASK modulator. The design of PLO is out of scope of the section so it is described briefly in section 2.3.

2.2.2 System Budget

Table 2.2 shows the system budget for direct conversion as previous work. Overall noise figure was estimated by 9.1 dB and total system gain was 52 dB. As the receiver architecture was non-coherent envelop detection, the conversion loss of de-modulator was not a constant, rather it showed a variation in accordance with its input level.

Table 2.2 System budget for direct conversion

Stage	Device	Gain [dB]	Noise Figure [dB]	Power [dBm]	
				Min (-50)	Max (-20)
1	Diplexer	-3	3	-53	-23
2	LNA	30	6	-23	7
3	De-Modulator	-14	4	-37	-7
4	LPF	-1	1	-38	-8
5	LGA	21	5	-17	13
6	Coupler	-1	1	-18	12
7	Limit Amp	20	3	2	15
System Total Gain		52			
Overall Noise Figure			9.1		

2.2.3 Design Review on Previous Work

Figure 2.6 shows the equivalent circuit of designed mmW ASK modulator, which is a key device to implement ultra low latency transceiver. It has the scheme of single balanced type. LO input signal is switched by baseband input and the ASK modulated output is pulled out by using waveguide coupler.

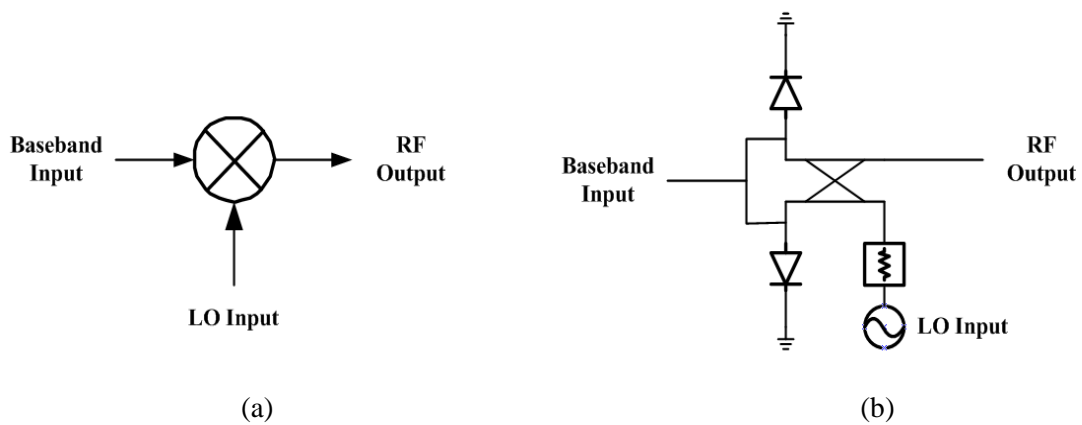


Figure 2.6 ASK modulator (a) Equivalent symbol (b) Implemented circuit

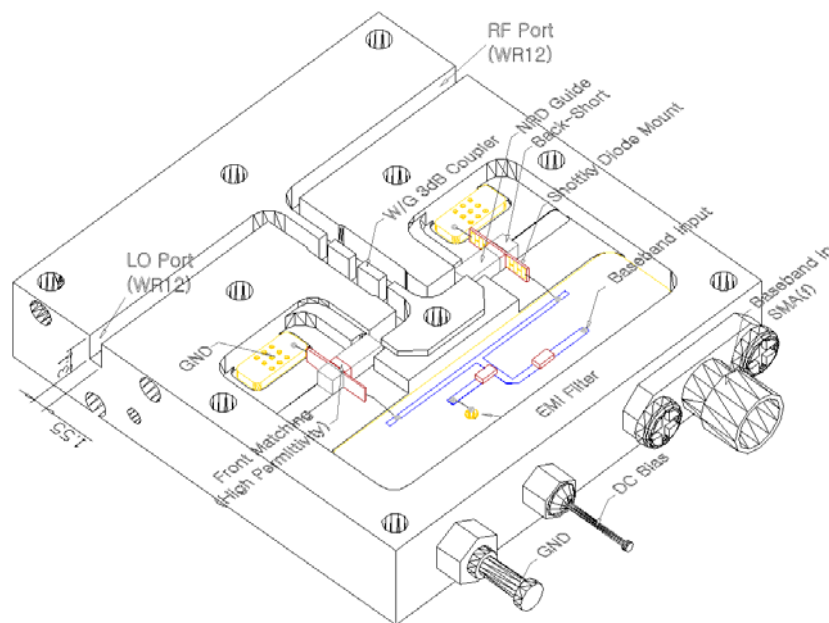


Figure 2.7 Design of mmW ASK modulator with Schottky diode

In order to mount the Schottky diode, non-radiated dielectric (NRD) waveguide was used [42]. The cross section of NRD guide was 2.0 x 1.9 mm. Its dielectric constant is 2.08, as with PTFE (Teflon). The designed optimum back short length was 1.3 mm and it also acts as a protector of the mounted Schottky diode. Figure 2.8 shows the designed diode mount with 7.4 x 1.6 mm TLY-5 substrate with dielectric constant of 2.2 with 15 mil thicknesses.

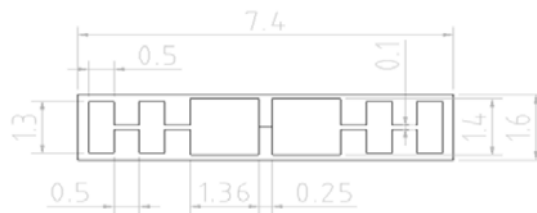


Figure 2.8 Design of diode mounts

Microstrip tee for baseband signaling input with biasing was implemented on FR-4 substrate. For AC coupling, 1 μ F capacitance was used and 33 μ H inductor was used for bias choke.

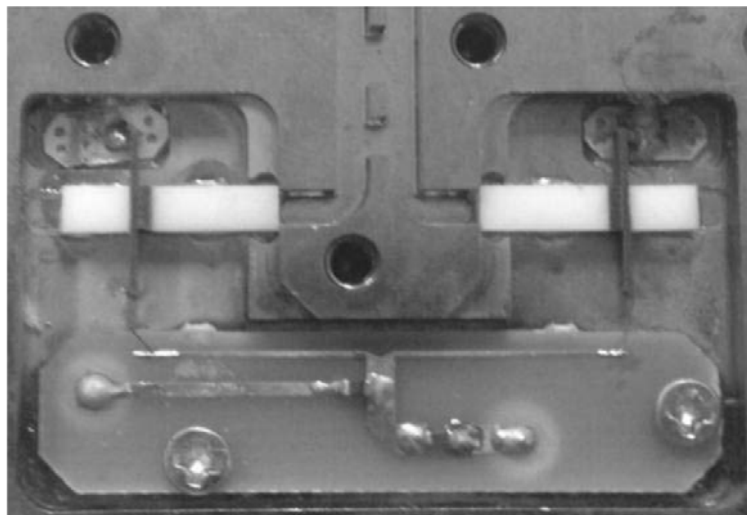


Figure 2.9 Assembled mmW ASK modulator

Figure 2.9 shows the implemented high speed ASK modulator by using Schottky diode as the previous work. The baseband signal input is divided by 3 dB at microstrip tee and sensed at each

diode mount. LO signal is also divided by 3 dB waveguide coupler and is sensed at Schottky diode, which has the characteristic of a 90 degree hybrid. Baseband signal is sensed from bottom layer by using feed through. The LO signal is switched according to its baseband input. The ASK modulated signal, RF, is delivered to the next TX stage of HPA along to the waveguide.

Figure 2.10 (a) shows the ASK modulation characteristic of 70 GHz frequency range. LO input level was +10 dBm, which was generated by multiplier with 6 times multiplication from 12.05 GHz VCO output. The pulse pattern generator with 0.5 V_{p-p} magnitudes was used for baseband signal input. The optimum DC offset voltage of baseband input port was 0.4 ~ 0.5 V. The flatness in the interested frequency band of 71.2 ~ 73.4 GHz was within +/-1 dB, which is good with 2.2 GHz wide bandwidth characteristic. The delta of LO carrier and 1st peak power of baseband was 5 ~ 6 dB in band and measured conversion loss was 10 ~ 12 dB with 10 dBm of LO level.

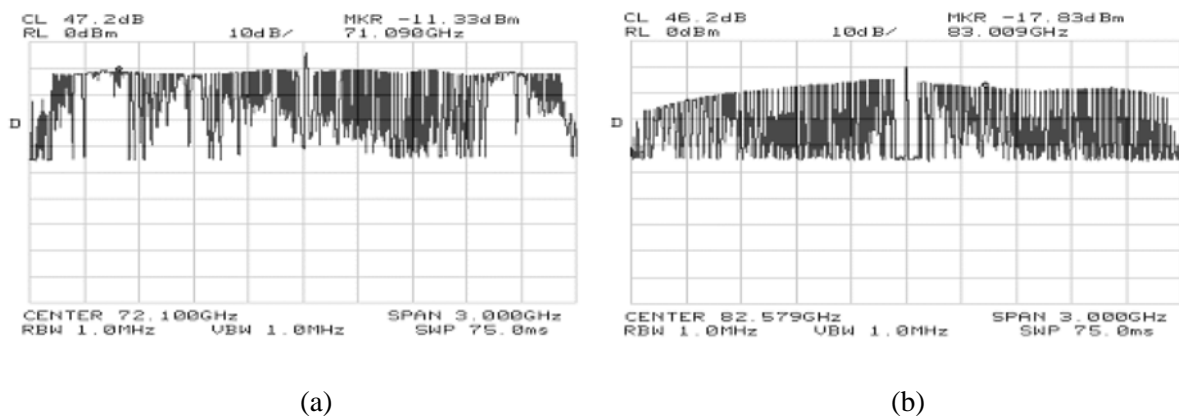


Figure 2.10 Modulation characteristic of (a) 70 GHz range (b) 80 GHz range

Figure 2.10 (b) shows the ASK modulation characteristic of 80 GHz frequency range. The 13.717 GHz VCO output was multiplied by 6 to make 82.3 GHz LO with 5 dBm output level. The flatness of 81.2 ~ 83.4 GHz in-band was +/-3 dB and the measured conversion loss was 15 ~ 21 dB. Note that

especially in 80 GHz, the designed ASK modulator showed greater variations in both flatness and conversion loss, which was 7 dB bigger than that of 70 GHz.

Figure 2.11 shows the characteristics of LNA. Hittite ALH459 and AUH318 bare-type die was packaged by using 1 mil gold wire. MMICs were mounted onto the RO5880 substrate. To overcome the degradation of sensitivity due to direct conversion, the gain of LNA needed to be large enough so that two stages of ALH459 and AUH318 were cascaded. Total gain over the interest band of 71.2 ~ 73.4 GHz was 36 dB typical with +/- 1.8 dB flatness.

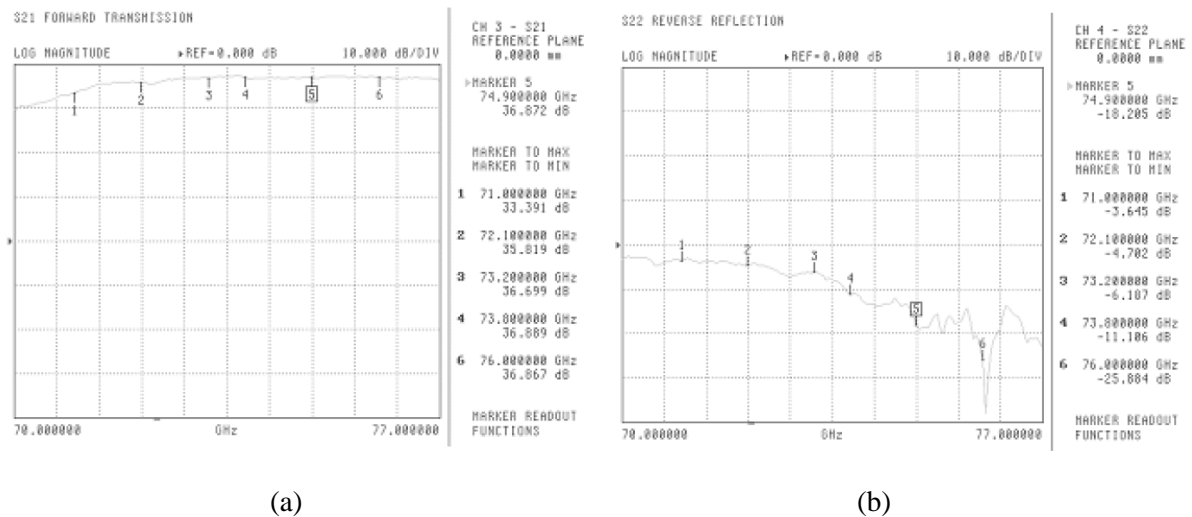


Figure 2.11 Characteristic of LNA (a) Gain (b) Return loss

As P1dB of HPA is high but the gain is low, a driver amplifier (DRA) is required. But in previous work, 2-stage of Hittite AUH318 for 70 GHz band and 2-stage of AUH317 for 80 GHz band were used, one for HPA and the other for DRA. It was possible because the P1dB of MMIC was 18 dBm and the gain was 21 dB, while the required total gain was 33 dB according to the designed system budget.

Over the 2.2 GHz required BW, the performance of flatness is important to increase the link performance. It was challenging work to secure the wide bandwidth characteristic. Figure 2.12 shows the measurement result of the packaged HPA. In the required band of 81.2 ~ 83.4 GHz, the gain was 35 dB +/- 3 dB.

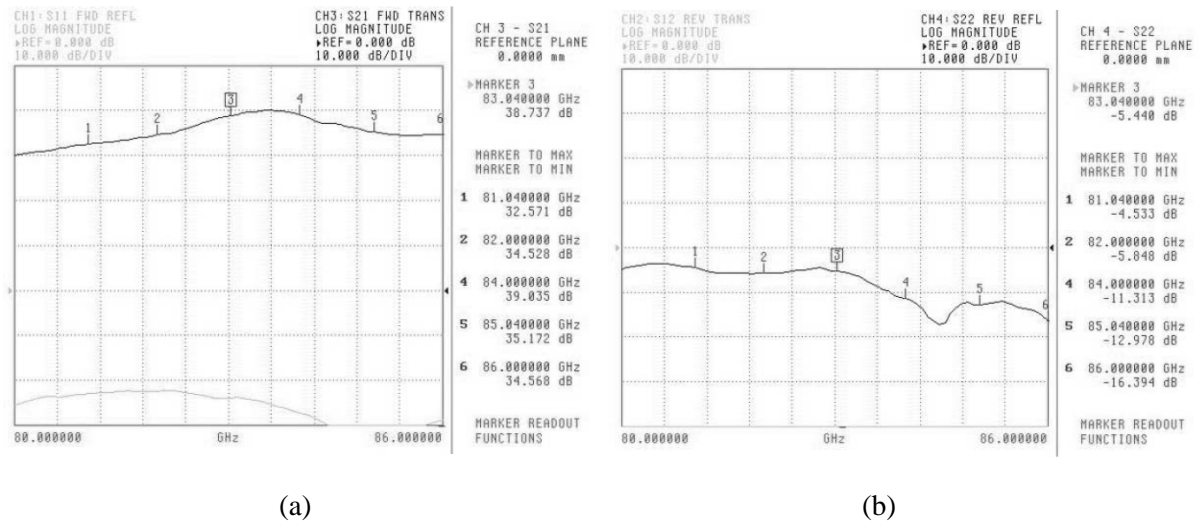


Figure 2.12 Characteristic of HPA (a) Gain (b) Return loss

To detect the signal at the receiver, a single ended type of envelope detector was designed by using fin-line transition. Figure 2.13 shows the implemented demodulator. By inserting via holes at each side of pattern edge, the harmonic generation was significantly reduced, which causes a signal distortion and increased conversion loss.

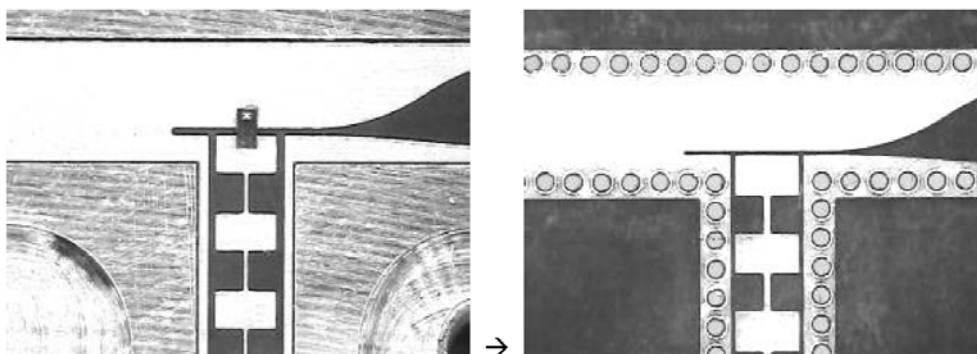


Figure 2.13 Improvement of demodulator design

Figure 2.14 shows the improvement of diode mount and feed thru. By extending diode mount with low pass filter pattern to the center of feed thru, the matched 50 Ω line was able to directly attach to feed thru. A long lead line causes significant bandwidth reduction [43]. With this mechanical modification, unwanted inductance element was effectively removed and the aimed 2.2 GHz of wide bandwidth characteristic was sustained.

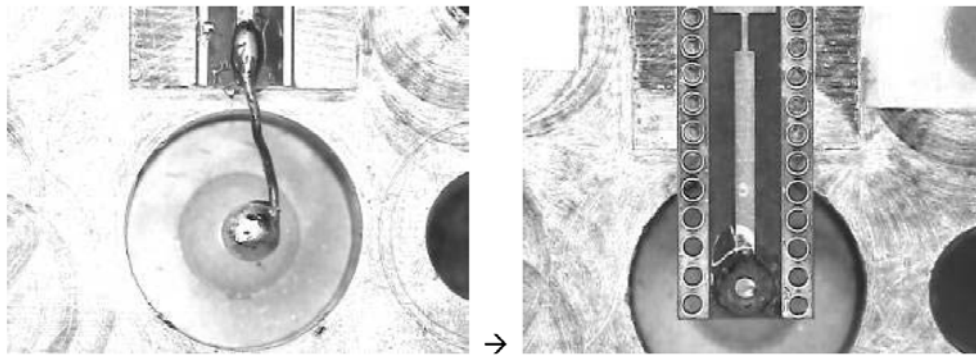


Figure 2.14 Improvement of diode mount

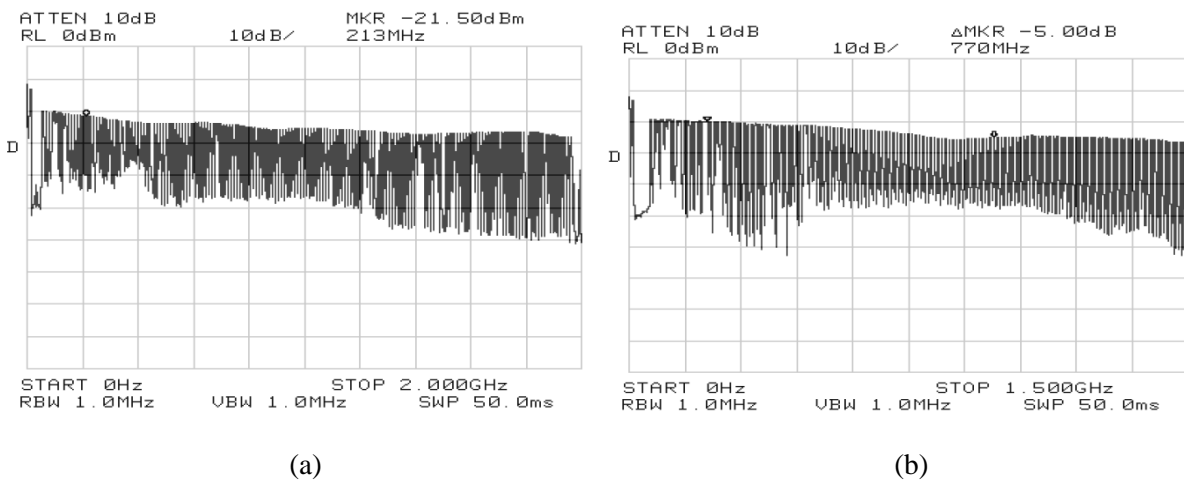


Figure 2.15 Characteristic of demodulator at (a) Lower band path (b) Upper band path

Figure 2.15 shows the measured results of characteristic of designed demodulator of lower and upper band respectively. As RF signal input, each transmitter output of 70 GHz and 80 GHz band were used. The output power was set to -30 dBm by using waveguide variable attenuator. According to the

measurement result, conversion loss was 14dB typically with the flatness of ± 3 dB over the required BW of 1.1 GHz from DC to 1.1 GHz baseband. Figure 2.15 (a) shows the result of lower band characteristics. Figure 2.15 (b) shows the result of upper band characteristics. Note that there can be a maximum 6 dB (± 3 dB) difference in conversion loss of detected signal spectrum between DC to required BW up to 1.1 GHz. These in-band flatness mismatches cause sensitivity reduction for the whole radiolink. This is why the flatness characteristic is important.

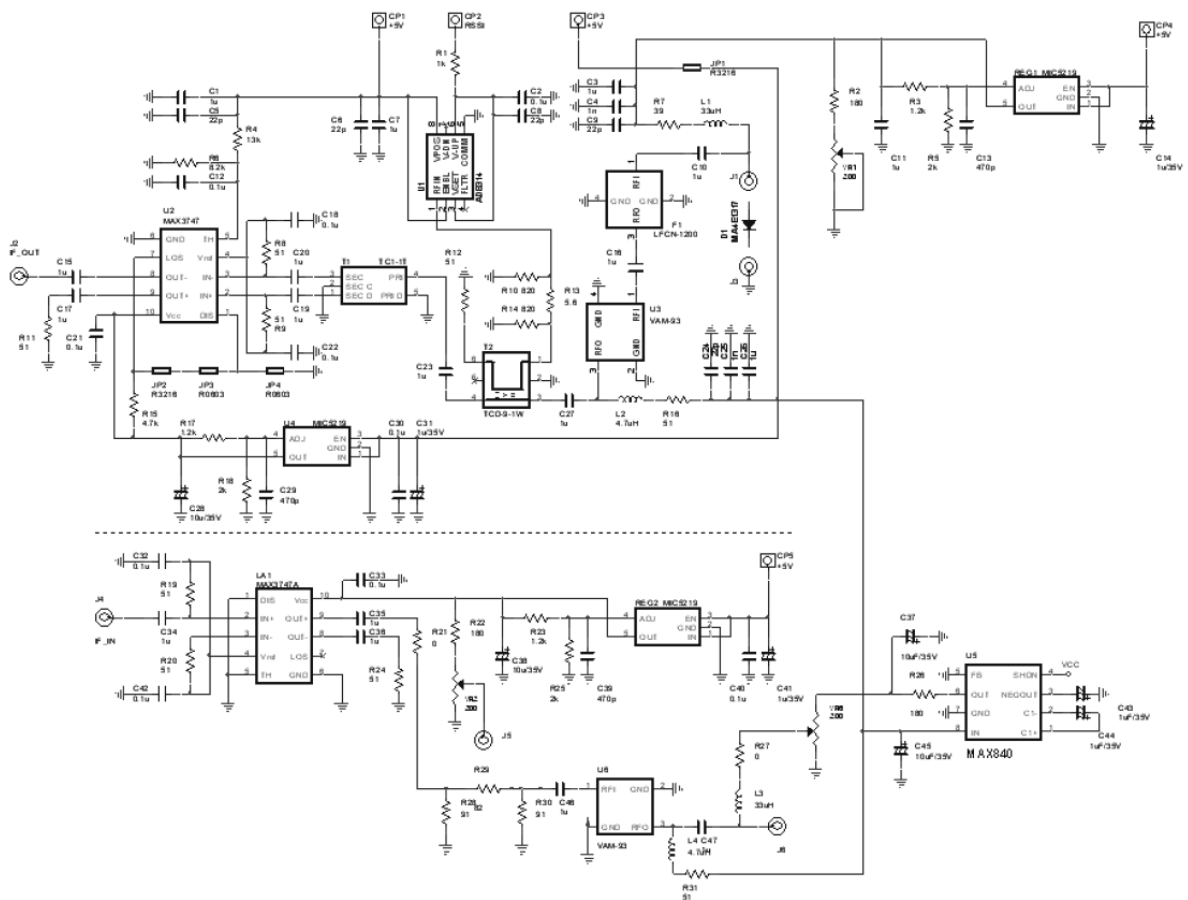


Figure 2.16 Circuit design of wide bandwidth of 1.1GHz baseband

Figure 2.16 shows the designed baseband circuit. As the building of wide bandwidth over DC to 1.1 GHz was the main issues, all parts were carefully chosen to secure sufficient wide bandwidth characteristics. The upper section is the RX circuit in the picture. Low pass filter was used to cut out a

spurious and harmonic elements from envelop detected signal. After LGA for linear gain, a wide bandwidth coupler was used to extract a voltage for received signal strength indicator (RSSI). A 1:1 transformer was used to make a differential signal for the differential input of limit amplifier at final stage. Note that capacitance of 1 μF was used as the AC couple at each stage for its wide bandwidth characteristics.

In order to pull out a constant level at RX, or to sense a constant input power level at TX, MAX3747, a limit amplifier was used. In TX circuit, the output of limit amplifier of 1.25 Gbps GbE signal was input to the designed E-band ASK modulator through π -type attenuator and LGA of VAM-93.

Figure 2.17 shows the implemented baseband circuit board. To reduce unwanted noise coupling on signal path, all circuit were designed by using CPW locating GND pad near signal path. According to the measurement result, the dynamic range was -65 dBm to -30 dBm, which was sufficient to cover the sensitivity of designed ASK demodulator with 1.1 GHz bandwidth.

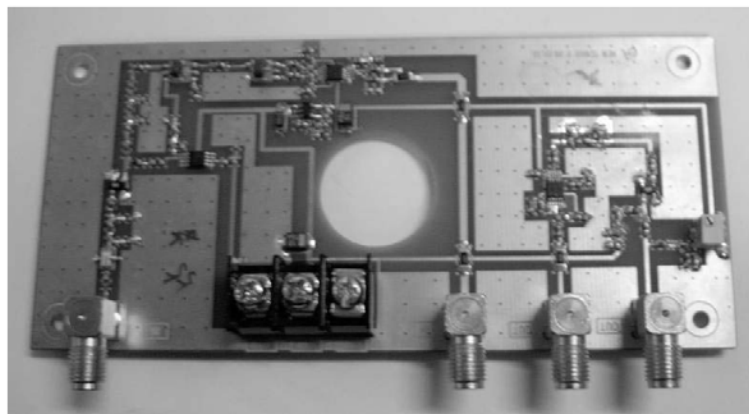


Figure 2.17 Implemented baseband board

2.2.4 Measurement Result

Figure 2.18 shows the implemented E-band ASK transceiver using 71 ~ 76 / 81 ~ 86 GHz mmW. Both of TX and RX section are placed in the same layer of aluminum housing. Both of TX and RX ports were designed with WR-12 standard rectangular waveguide flange. The baseband signal interface was designed by SMA(f). The implemented dimension was 100 x 80 x 25 mm³.

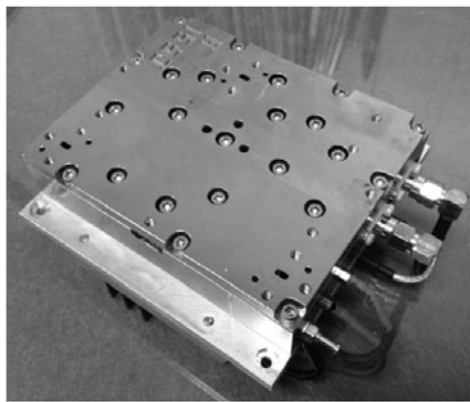


Figure 2.18 Implemented ASK transceiver

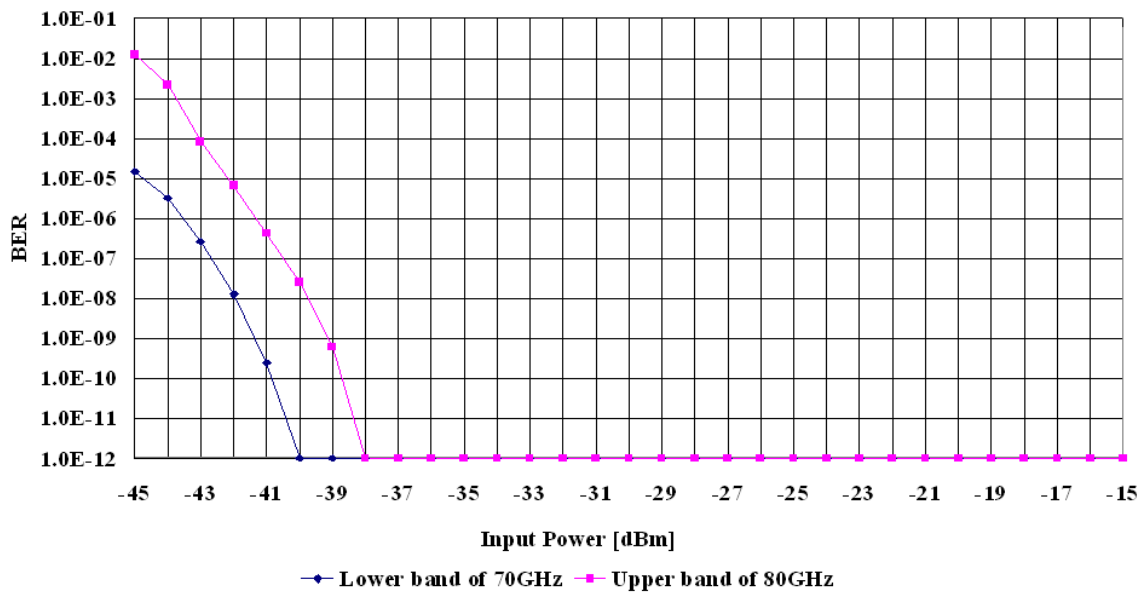


Figure 2.19 Measurement result of sensitivity

Table 2.3 BER test result

Attenuation [dB]	Input Power [dBm]	Lower Band (70GHz)	Upper Band (80GHz)
-60	-45	1.48E-05	1.25E-02
-59	-44	3.21E-06	2.21E-03
-58	-43	2.62E-07	8.21E-05
-57	-42	1.27E-08	6.50E-06
-56	-41	2.45E-10	4.24E-07
-55	-40	0	2.51E-08
-54	-39	0	6.04E-10
-53	-38	0	0
-52	-37	0	0
-51	-36	0	0
-50	-35	0	0
-49	-34	0	0
-48	-33	0	0
-47	-32	0	0
-46	-31	0	0
-45	-30	0	0
-44	-29	0	0
-43	-28	0	0
-42	-27	0	0
-41	-26	0	0
-40	-25	0	0
-39	-24	0	0
-38	-23	0	0
-37	-22	0	0
-36	-21	0	0
-35	-20	0	0
-34	-19	0	0
-33	-18	0	0
-32	-17	0	0
-31	-16	0	0
-30	-15	0	0

*Test Conditions: 1250 Mbps, PRBS 2⁹-1, Data 500 mV

Table 2.3 shows BER test result of the implemented wide bandwidth ASK transceiver at E-band for previous work on direct conversion. For the measurement, a 30 dB fixed attenuator and a 30 dB variable attenuator were inserted between unit-A and unit-B. TX output power at the antenna port of diplexer was +15 dBm , which is 2 dB lower from its original +17 dBm due to diplexer loss.

By increasing the variable attenuator with 1 dB step, the readout of BER was recorded from the other side of receiver. According to the test result, BER was error free or less than 10^{-12} at -40 dBm of input power for the lower band path. For the upper band, the minimum input level for BER 10^{-12} or error free was -38 dBm, which was 2 dB worse than that of lower band path.

Figure 2.19 shows the sensitivity of implemented ASK transceiver. The sensitivity of designed radiolink was limited to -38 dBm of upper band performance. In Table 2.4, the measurement results were summarized.

Table 2.4 Measurement result on previous work

Parameters		Unit-A	Unit-B	Remark
Tx	Frequency	71.2~73.4 GHz	81.2~83.4 GHz	
	BW	2200 MHz		
	Output Power	+15 dBm		typical
	VSWR	2.0:1		
Rx	Frequency	81.2~83.4 GHz	71.2~73.4 GHz	
	BW	2200 MHz		
	Dynamic Range	-38 ~ -15 dBm @BER 10^{-12}		PRBS 2^9-1
	Noise Figure	9.1 dB		estimated
	VSWR	1.8:1		
Common	Modulation	ASK		
	Data Rate	1.25 Gbps		
	Latency	23 ns		

2.2.5 Challenging Issues on Direct Conversion

With the topology of direct conversion, the dynamic range was measured by 23 dB from -38 ~ -15 dBm under the BER 10^{-12} or error free with PRBS pattern of 2^9-1 . The whole performance was not significant, but it was still meaningful, leaves as future task three challenging issues as follows.

First, it was difficult to build an ASK modulator directly at 70/80 GHz mmW range of E-band. As the wavelength at these frequency range is too short by only 5.57 mm at 72.3 GHz and 4.50 mm at 82.3 GHz, the performance of the designed modulator was too sensitive and significantly affected with by small variations of physical dimensions.

Secondly, it was difficult to secure the required 2.2 GHz wide BW characteristics. As the required BW was too wide by 2.2 GHz, the securement of flatness in E-band mmW frequency range was difficult.

Finally, the conversion loss of the designed demodulator was significantly increased when the received power level is low approaching down to its minimum detectable level. This resulted in lower sensitivity, showing that the variation of conversion loss was a function of input power level.

In conclusion, the approach with direct conversion has a simple structure, but it also has several issues that make the performance worse. In order to solve these problems, a new topology of heterodyne structure was attempted.

2.3 Proposed Heterodyne mmW ASK Transceiver

In order to improve the sensitivity of the direct conversion type transceiver, new IF stage modulated heterodyne type wide band ASK transceiver is proposed. Figure 2.20 shows the block diagram of the new topology. The basic concept of the new scheme is to use a heterodyne up/down converter type with IF frequency band. Differently from previous work, ASK modulation is conducted at IF stage and demodulation is also conducted at IF frequency band. By using up/down converter, the burden of building wide band ASK modulator and demodulator at mmW is removed. However, it is still critical to secure the requirement of wide band characteristic at both baseband and IF band range.

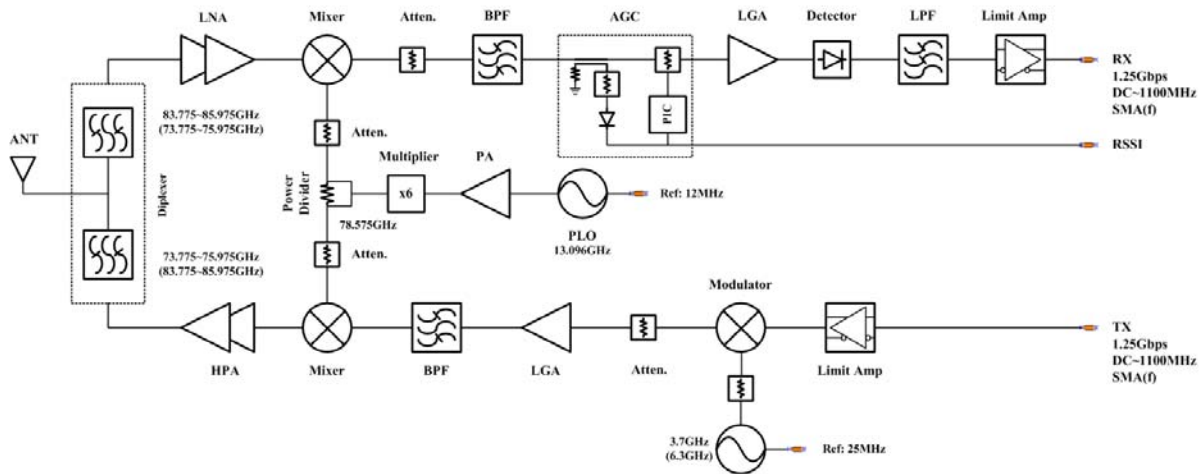


Figure 2.20 Proposed heterodyne E-band ASK transceiver

Table 2.5 Proposed E-band transceiver

Item	Previous Work	Proposed Work
Topology	Direct conversion	Heterodyne, Non-coherent
IF	Zero-IF	IF (3.7 GHz / 6.3 GHz)
Modulation	ASK @ mmW	ASK @ IF
Detection	Envelop detection @ mmW	Envelop detection @ IF
AGC	None	AGC @IF

Table 2.5 shows the difference of new proposed work with heterodyne topology. Note that IF frequency of 3.7 GHz and 6.3 GHz are defined, and modulation and demodulation are conducted at IF stage to increase sensitivity. To obtain a more dynamic range, AGC circuit is added at IF stage.

2.3.1 Frequency plan for E-band Radiolink

Figure 2.21 shows the frequency use of proposed E-band radiolink. As mentioned in a previous section, the required BW theoretically is 2.5 GHz to transmit the capacity of 1.25 Gbps data rate by using ASK, but only 2.2GHz was used [41].

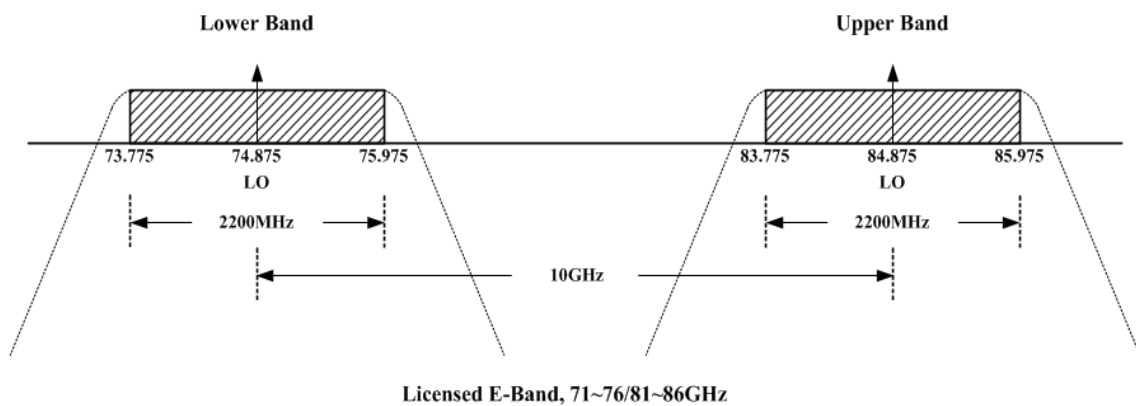


Figure 2.21 Frequency use of proposed E-band radiolink

The center frequency was shifted slightly from previous work to meet one of the European regulation of 250 MHz designated center frequency for each band [21], [22], [23]. For the full-duplex, both of 71 ~ 76 GHz and 81 ~ 86 GHz frequency band with 2.2 GHz BW are used. As there is 10 GHz separation between two bands, the burden of building required isolation criteria of the specifications of diplexer was relatively easy.

For the ultra low latency with high capacity of data rate, all required parts including ASK modulator, transition, mixer, LNA, PA, and demodulator (detector) and other components should be designed to have wideband characteristic. Any one of the devices with narrow band characteristic can cause significant performance degradation in terms of sensitivity.

2.3.2 Wideband ASK Modulator

Figure 2.22 shows designed block diagram of wide band ASK modulator at 3.7 GHz IF band for unit-A. As the required BW is 2.2 GHz, the in-band is 2.6 ~ 4.8 GHz. The challenging issue is wide band implementation at low frequency range. Its relative bandwidth exceeds 59.5%, which is an ultra wide band, while the only 10% of relative BW is commonly considered as a wide bandwidth. For example, BW of only 370 MHz at 3.7 GHz carrier frequency is considered as a wide band.

For this work, BW of 2.2 GHz at 3.7 GHz IF carrier frequencies has to be implemented successfully for the aimed radiolink. Hittite HMC213 packaged mixer is used as ASK modulator switching 3.7 GHz LO with 1.25 Gbps baseband signal. ASK modulated IF signal is amplified by linear amplifier.

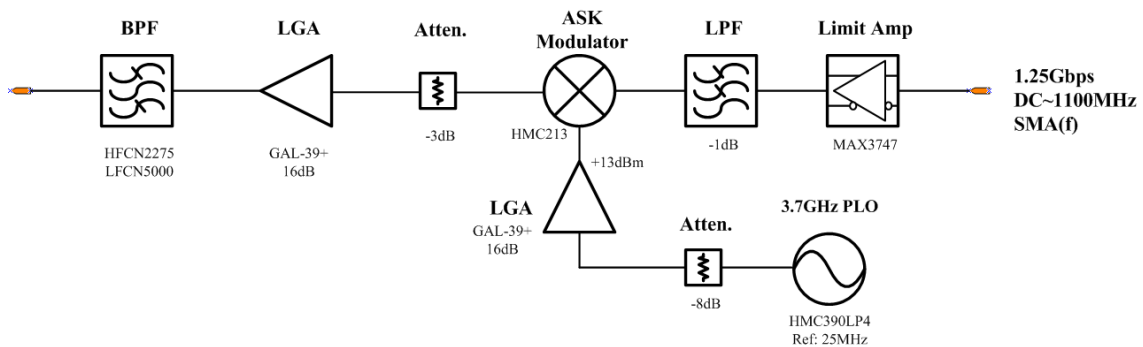


Figure 2.22 Block diagram of wide-band ASK modulator at 3.7 GHz IF band

To remove harmonic elements from ASK modulated spectrum at 3.7 GHz, a band pass filter is required in front of the following stage of mmW mixer. As there is no choice to make such wide band pass filter, it was solved by combining high pass filter with 2.275 GHz cutoff and low pass filter with 5 GHz cutoff. Figure 2.23 shows the implemented 3.7 GHz wide band ASK modulator and Figure 2.24 shows modulated spectrum. Note that 1.25 GbE signal spectrum is spread over BW of 2.5 GHz over right and left side of center frequency at 3.7 GHz.

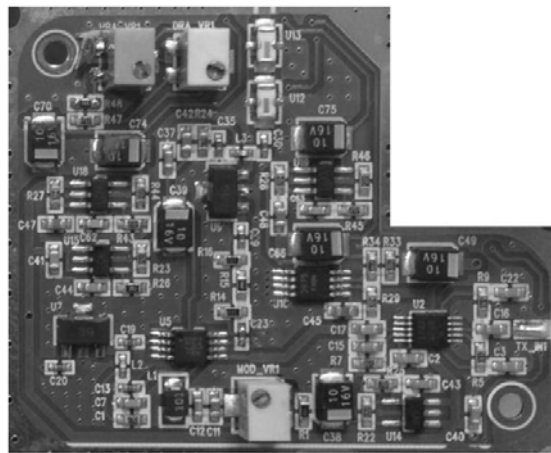


Figure 2.23 Implemented 3.7 GHz wide-band ASK modulator

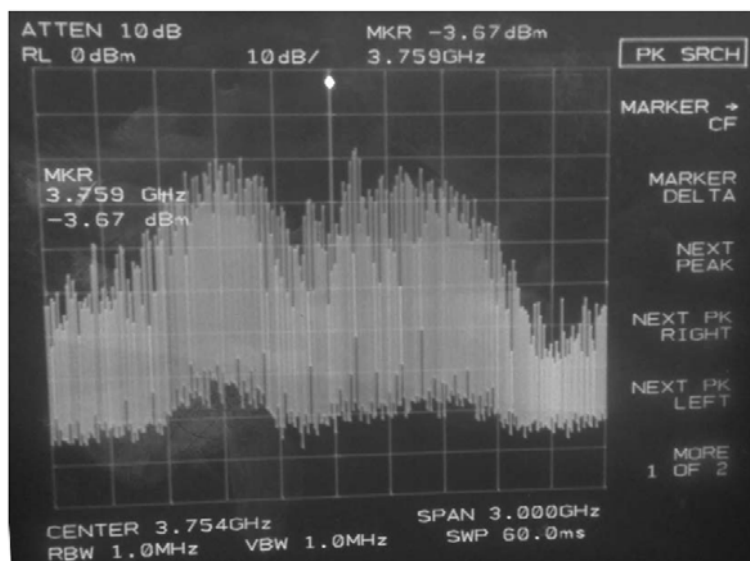


Figure 2.24 BW of 2.2 GHz wide-band ASK spectrum at 3.7 GHz IF band

Figure 2.25 shows the designed wide band ASK modulator at 6.3 GHz IF band for unit-B. Except the IF LO frequency and pass band, it is the same with IF section for unit-A. For the ASK modulator, the HMC219 packaged IC was used as IF mixer.

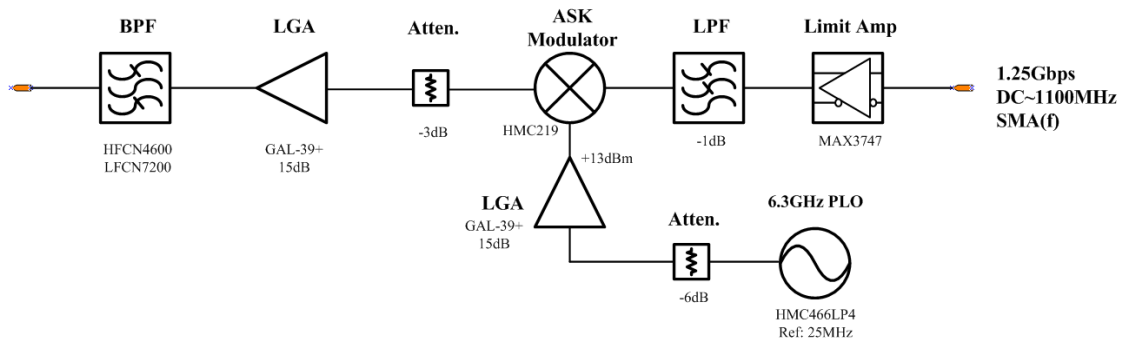


Figure 2.25 Block diagram of wide-band ASK modulator at 6.3 GHz IF band

To build a BPF, a high pass filter with 4.6 GHz cutoff and low pass filter with 7.2 GHz cutoff are used. The required IF pass band is exactly 5.2 ~ 7.4 GHz, but these lumped filters with a ceramic filter has quite a few variations for its cutoff frequency. For this work, a pass band matched filter was carefully selected after measurement with VNA and applied on the circuit board. Figure 2.26 shows the implemented 6.3 GHz wide band ASK modulator. Figure 2.27 shows the ASK modulated spectrum.

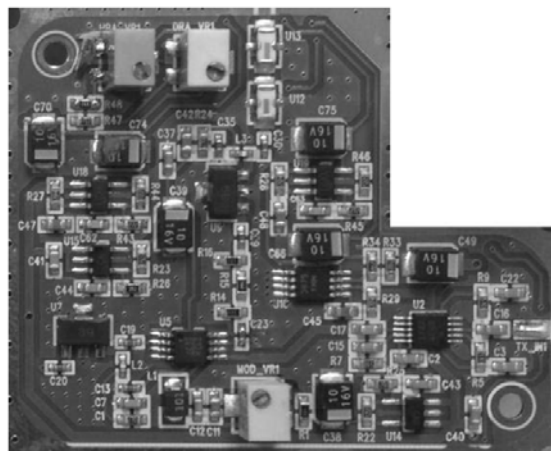


Figure 2.26 Implemented 6.3 GHz wide-band ASK modulator

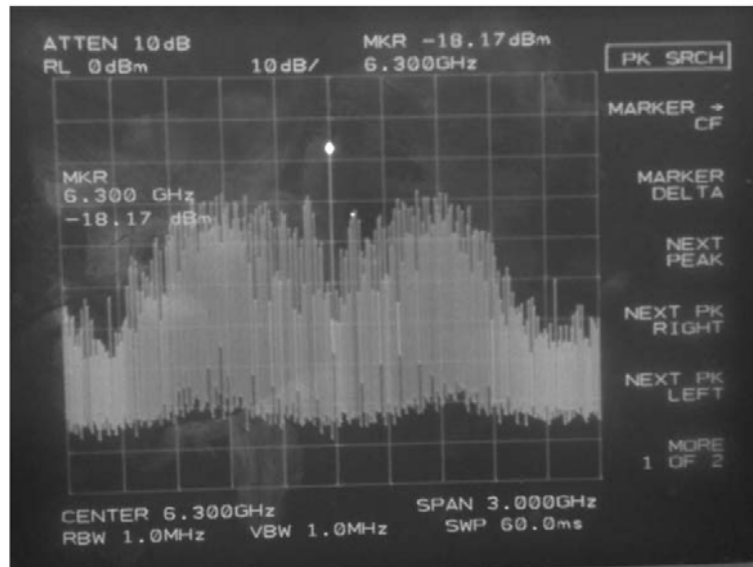


Figure 2.27 BW of 2.2 GHz wide-band ASK spectrum at 6.3 GHz IF band

2.3.3 W/G-to-Microstrip Transition

In order to connect in/out of MMICs to standard waveguide of WR12, waveguide-to-microstrip transition is required. Figure 2.28 shows the designed WR12-to_microstrip transition with back-to-back HFSS modeling for electromagnetic field simulation. For the assembly efficiency considering mass production, it is designed in a simple way so that microstrip line is mounted on mechanical housing adjusting its center to WR12 center of cross section.

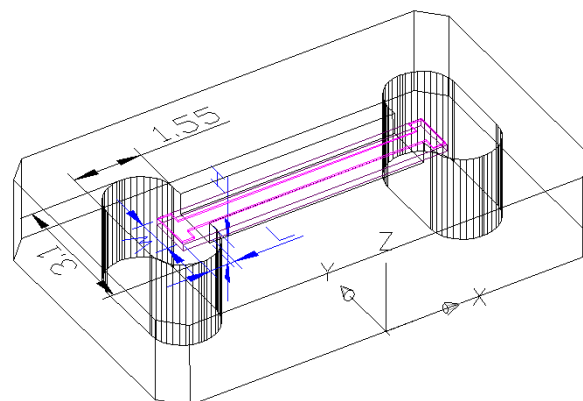


Figure 2.28 WR12-to-microstrip transitions

Design parameters are line width W , length L and height H . By using HFSS simulation, the optimum dimensions were chosen as W of 0.9 mm, L of 0.58 mm and height H is 0.5 mm. Figure 2.29 shows back-to-back measurement result. The transition loss was typical 1.2dB at both of lower and upper band. Return loss was less than -15 dB, which is sufficient to be adapted for the work.

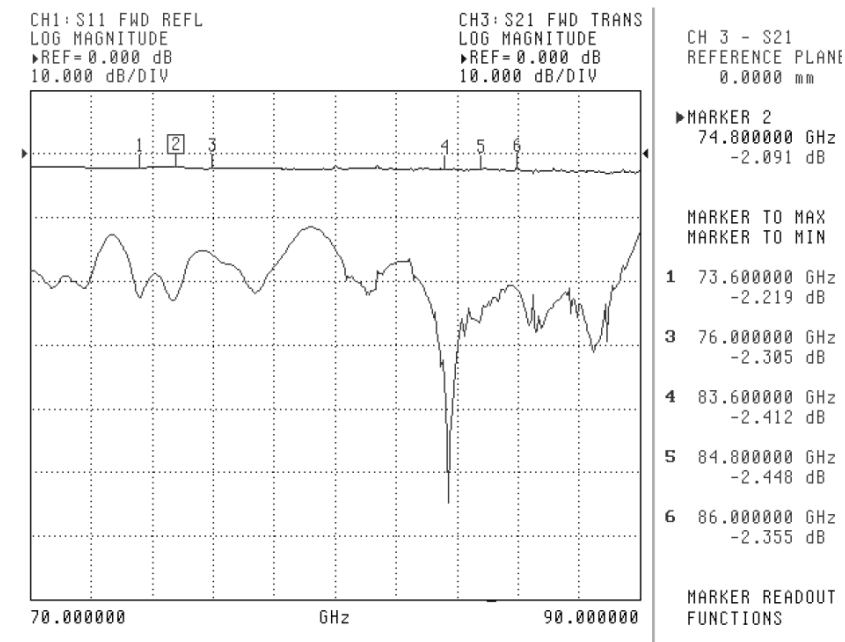


Figure 2.29 Measured result of transition loss

2.3.4 Mounting & Bonding Techniques for MMIC

The die should be attached directly to the ground plane of the Aluminum housing by using conductive epoxy. A 50 Ω microstrip transmission line on 0.127 mm (5 mil) thickness of Teflon film substrates are used to match RF to and from the chip (Figure 2.30). If 0.254 mm (10 mil) thick of film substrates is used, the die should be raised so that the surface of the die is coplanar with the surface of the substrate. Microstrip substrates should be placed as close to the die as possible in order to minimize bond wire length. By using VNA, typical die-to-substrate spacing was chosen by 0.1 ~ 0.15 mm.

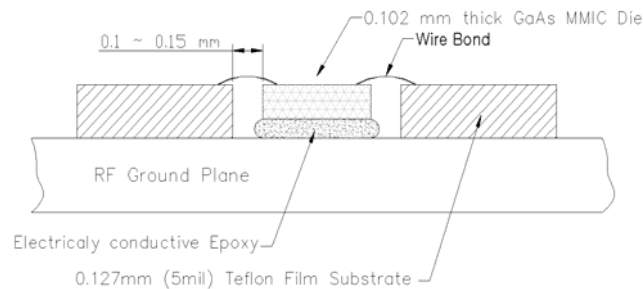


Figure 2.30 Die mounting

The MMIC chip is back-metalized and can be mounted with electrically conductive epoxy. The mounting surface should be clean and flat. To mount the die, a minimum amount of epoxy should be applied to the mounting surface so that a thin epoxy fillet is observed around the perimeter of the chip once it is placed into proper position. To cure epoxy, the mounted die on the metallic housing need to be placed on 135 degree of hot plate for 1 hour and 30 minutes or per manufacturer's recommendation.

Wire bonds were made with 1 mil diameter of gold wire. These bonds should be thermosonically bonded with a force of 40 ~ 60 grams. All bonds should be made with a nominal stage temperature of 150 °C. A minimum amount of ultrasonic energy should be applied to achieve reliable bonds [43]. All bondings should be done in as short a time as possible.

Figure 2.31 shows the electromagnetic simulation modeling for wire bond to figure out the insertion loss and return loss in accordance with wire length or number of wires. The influence due to the height variation was relatively small less than 0.01 dB losses with 0.02 mm variation. Figure 2.32 shows the insertion loss of wire bond. At a length of 0.1 ~ 0.15 mm with the number of 3 ~ 4 wires, it showed the optimum matching showing less than 0.2 dB loss. For the mount of all MMICs in the work, 3 wires of 1 mil gold wire were applied according to the test result.

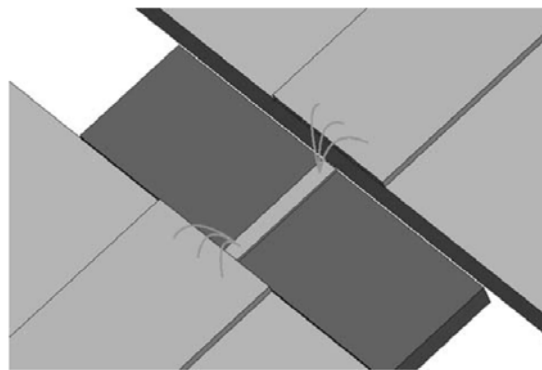


Figure 2.31 Simulation modeling for wire bond

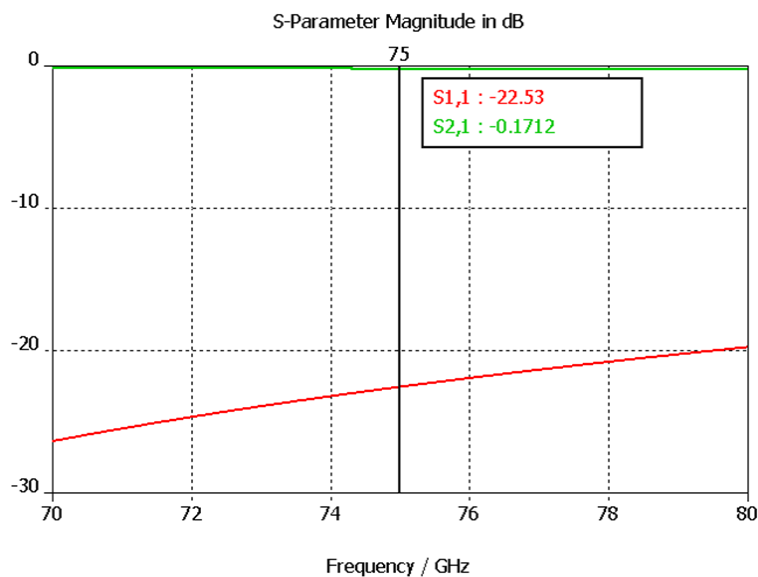


Figure 2.32 Insertion loss of wire bond

2.3.5 Design of mmW TX Front-End

Different to previous work on direct conversion, a packaged MMIC die of mixer is used for up and down converter. The MDB277 is a passive double balanced MMIC mixer which utilizes GaAs Hetero-junction bipolar transistor (HBT) Schottky diode technology and can be used as either an upconverter or a downconverter. This compact MMIC is more consistent alternative for hybrid style double balanced mixer assemblies.

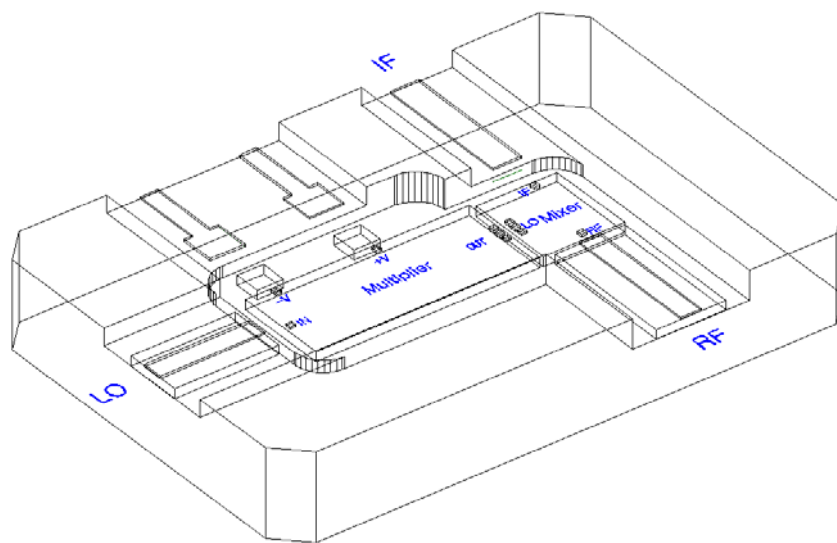


Figure 2.33 Design of mixer mounts

Figure 2.33 shows up conversion mixer design with die mount on Aluminum housing. The CHU3377 6 times multiplier is used to generate 78.575 GHz mmW carrier from 13.096 GHz LO output. In order to switch the MDB277, the output power of 14 dBm from CHU3377 multiplier is sufficient for up conversion, but it is not for down conversion operation, which result in 5 ~ 6 dB more loss.

To reduce the loss of down conversion, IF input of mixer is sensed with 0.3 V bias offset so that mixer conversion loss does not influenced by LO power fluctuation. Table 2.6 shows the measured result of mixer conversion loss of both up conversion and down conversion. The nominal conversion loss is 12

dB from makers, but it shows some variation according to frequency. Note that it shows around 2 dB more loss at 80 GHz range compared to 70 GHz. There is no way further improve this, as it is the characteristic of the chip itself related to higher frequency loss.

Table 2.6 Measurement result of mixer conversion loss

Parameter	Up Conversion		Down Conversion	
	70 GHz	80 GHz	70 GHz	80 GHz
Conversion Loss [dB]	11.0	13.2	16.6	18.5

For 71 ~ 76 GHz high power amplifier (HPA), AUH318 medium power amplifier and APH633 higher power amplifiers from Velocium are used. As even the output power of APH633 is higher by +20 dBm but gain is low, a driver amplifier is required to have sufficient gain. For the work, AUH318 medium power amplifier was chosen. For 81 ~ 86 GHz HPA, the pair of AUH317 and APH634 was used. Figure 2.34 shows the layout design of HPA. The up-converted ASK modulated signal get a gain at DRA stage and are amplified at HPA.

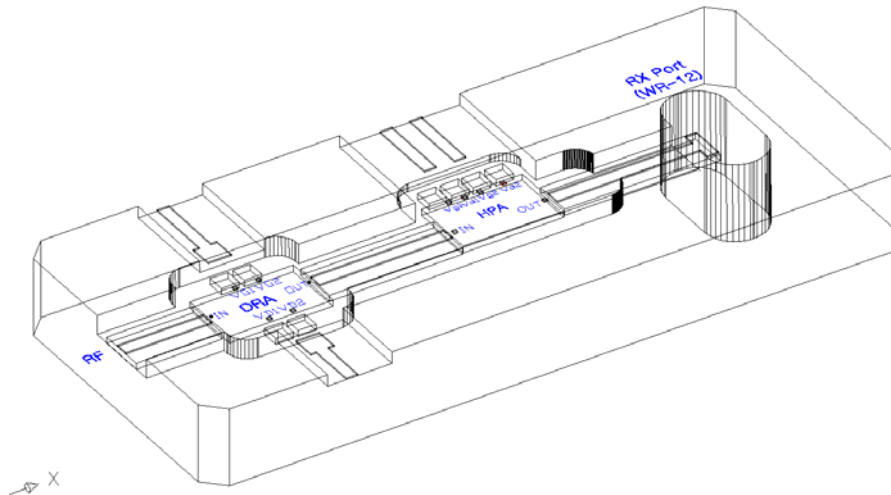


Figure 2.34 Design of HPA

Figure 2.35 and Figure 2.36 shows the measurement result of mmW HPA at both 70 GHz and 80 GHz range. At the interest frequency of 84.875 GHz, it shows around 5 dB less gain than that of 74.875

GHz. To compensate for the gain differences, IF amplifier gain for 80 GHz was tuned to have 5 dB more. Table 2.7 shows P1dB measurement result of deigned HPA. At both bands, it shows a typical 20 dBm.

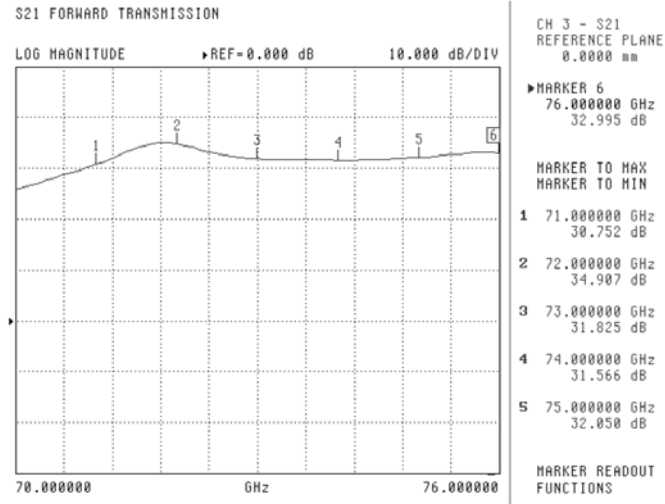


Figure 2.35 Measured result of mmW HPA at 70 GHz

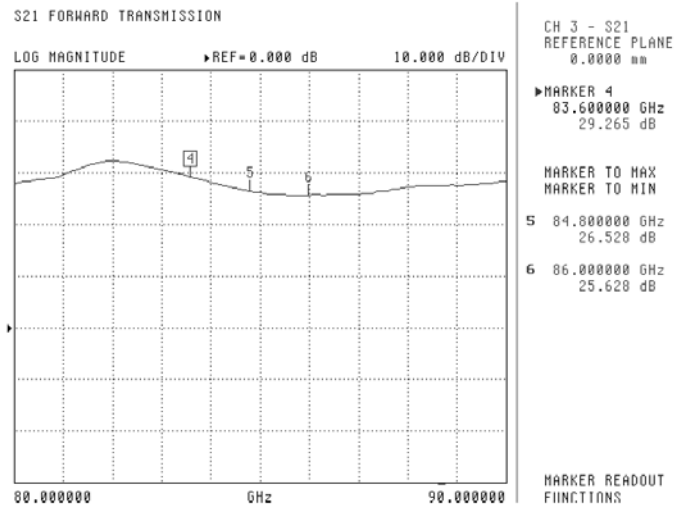


Figure 2.36 Measured result of mmW HPA at 80 GHz

Table 2.7 Measurement result of P1dB

Freq.[GHz]	Lower Band			Upper Band		
	73	74	75	83	84	85
P1dB [dBm]	19.8	21.0	20.0	20.0	20.5	20.2

2.3.6 Design of mmW RX Front-End

Figure 2.37 shows the layout design of RX front-end section. ALH509 and AUH318 are cascaded to have more gain reducing the noise figure of whole receiver. AUH318 is a medium power amplifier with 24dB gain. ALH509 is a 3-stage GaAs HEMT MMIC LNA which operates between 71 and 86 GHz. It features a 14 dB of small signal gain, 5 dB of NF and P1dB of +7 dBm at +2 V supply voltage. Figure 2.38 shows the gain performance of single chip offered from maker. The gain at 80 GHz range is 2 ~ 3 dB lower than 70 GHz, which results in less sensitivity of transceiver at 80 GHz. Note that the lower gain at 80 GHz is one of the causes of lower performance at 80 GHz upper path.

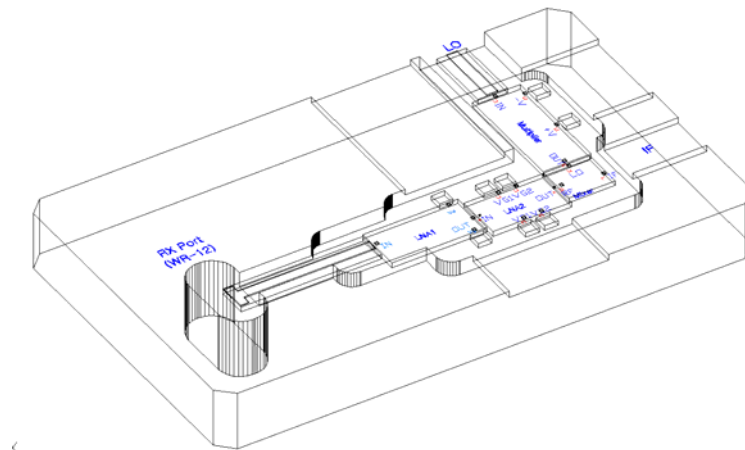


Figure 2.37 Design of RX front-end section

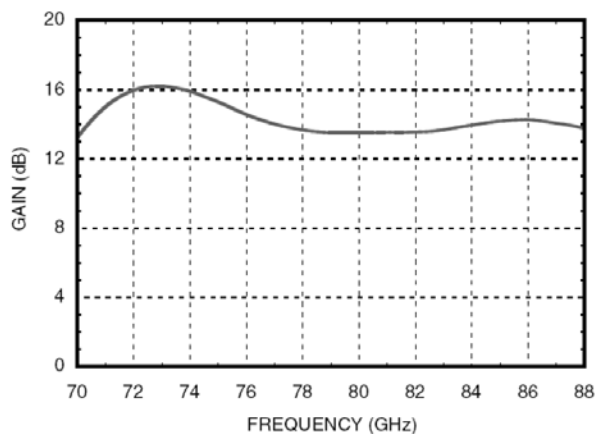


Figure 2.38 Gain performance of ALH509

2.3.7 Design of PLO

Figure 2.39 shows the designed 13.096 GHz PLO [44]. HMC531, GaAs hetero-junction bipolar transistor (HBT) is used as VCO. It is available to use half frequency or divided by 4 in recommended range of 13.6 ~ 14.9 GHz. Half frequency output is used for PLL loop with 6.1 GHz range of fractional-N frequency synthesizer, ADF4159. To increase the output power of 13.096 GHz PLO output for the following mixer driving, HMC441 medium power amplifier was used, which is an efficient GaAs PHEMT MMIC that operates between 6 ~ 18 GHz. The amplifier provides 15.5 dB of gain and +22 dBm of saturated power. To remove half LO, an HPF with 8.4 GHz cut-off was inserted at the final stage.

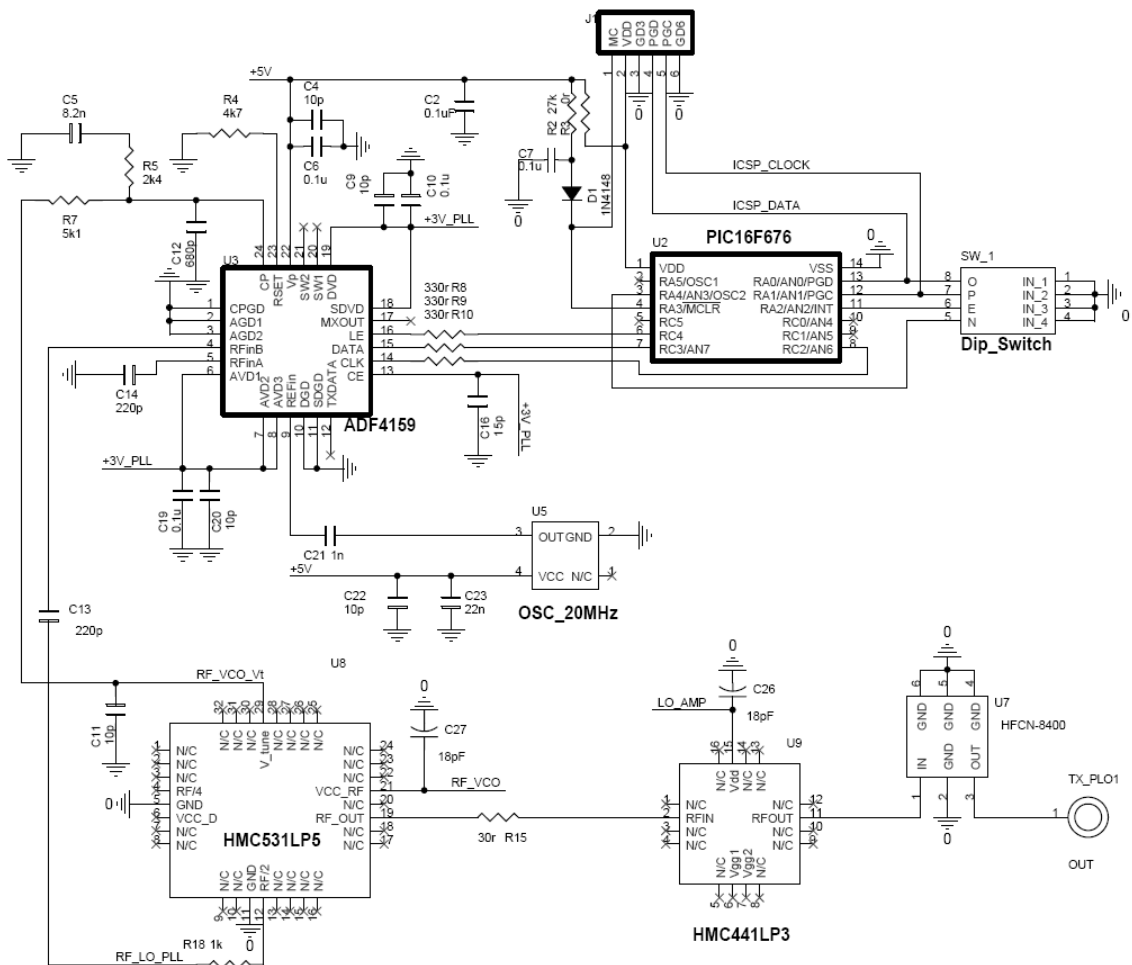


Figure 2.39 Designed 13.096 GHz PLO

2.3.8 Implementation of Wide-Band IF & Baseband Section

Different from previous work, detection of the signal is conducted at IF stage. Thus the 2.2 GHz ultra wide band of IF & baseband section should be successfully implemented. This is the most challenging task to build the radiolink of the work.

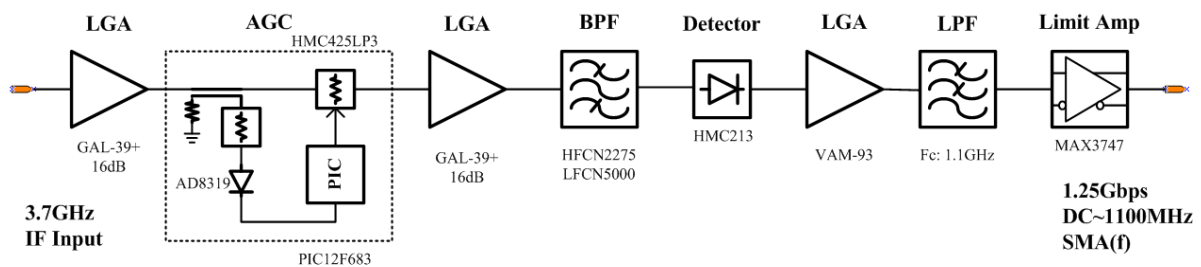


Figure 2.40 Block diagram of wide-band 3.7 GHz IF & ASK detector

Figure 2.40 shows the block diagram of designed wide-band 3.7 GHz IF and baseband section. To detect signal from IF, HMC213, GaAs MMIC SMT packaged type of double balanced mixer for 1.5 ~ 4.5 GHz is used as Zero-IF detector.

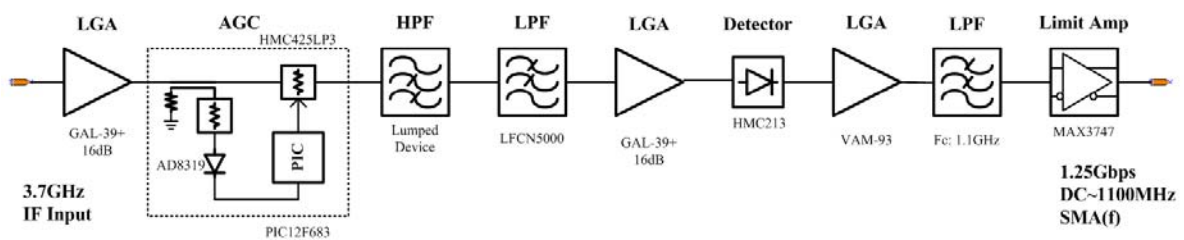


Figure 2.41 Revised block diagram of wide-band 3.7 GHz IF section

At the first trial, to obtain more dynamic range, series of LGA and attenuator set were used, but the flatness characteristic was getting worse in the wide range of the required band. Thus, one of LGA

was removed and BPF and the last stage of LGA were switched in order. By doing so, unwanted harmonics were effectively removed before conducting detection (Figure 2.41).

For the BPF, in order to make ultra wide bandwidth of 2.2 GHz at only 3.7 GHz IF frequencies, a set of high pass filter and low pass filter of HFCN2275 and LFCN5000 were used. Figure 2.42 shows the measurement result. Over the frequency range of interest of 2.6 ~ 4.8 GHz, the difference of loss at each edge of band exceeds by 12 dB.

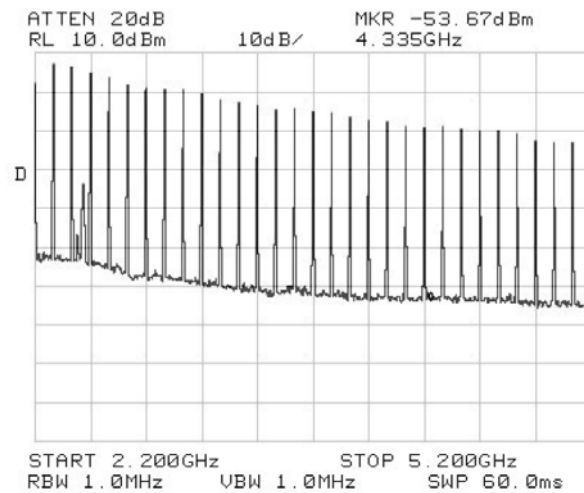


Figure 2.42 Flatness of 3.7 GHz IF section with HFCN2275 and LFCN5000

To compensate the steep slope of the conversion loss, a ceramic HPF of HFCN2275 was switched by lumped type of HPF. Figure 2.43 shows the designed lumped HPF and Figure 2.44 shows the simulation result. Note that the insertion loss of S_{21} has a slope at the interest band of 2.6 ~ 4.8 GHz range. The loss at 2.6 GHz is large but is reduced as frequency increase up to 4.8 GHz. This slope is opposite direction with the measured result of Figure 2.42. Figure 2.45 shows the compensated conversion loss plot. Finally achieved flatness was ± 3 dB, which was 5 ~ 6 dB improved.

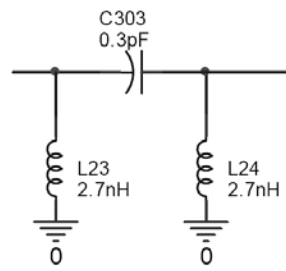


Figure 2.43 HPF with lumped device to compensate flatness slope

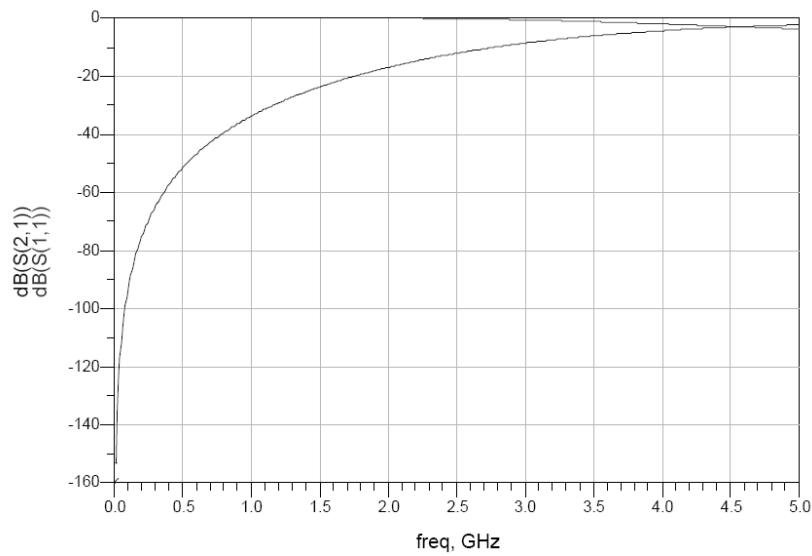


Figure 2.44 Simulation result of lumped HPF

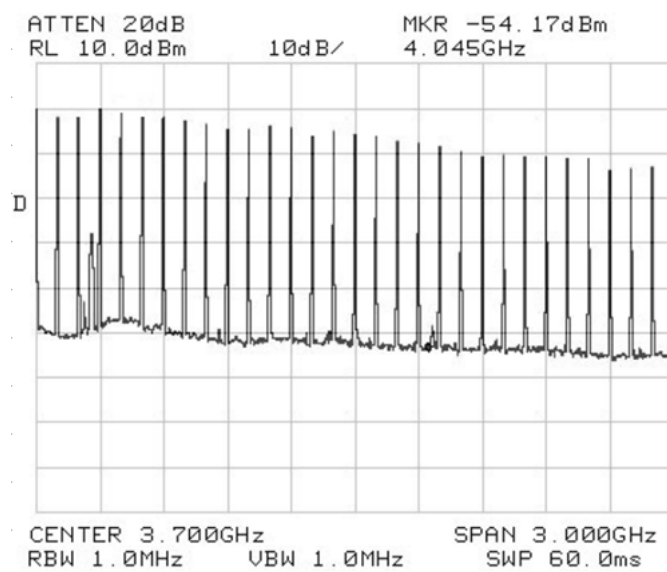


Figure 2.45 Improved flatness result

Figure 2.46 shows the designed block diagram of wide band of upper 6.3 GHz RX-IF and baseband section. With the same reason mentioned in 3.7 GHz lower band design, to obtain more dynamic range, one stage of LGA was removed and BPF and the last stage of LGA were switched with each other.

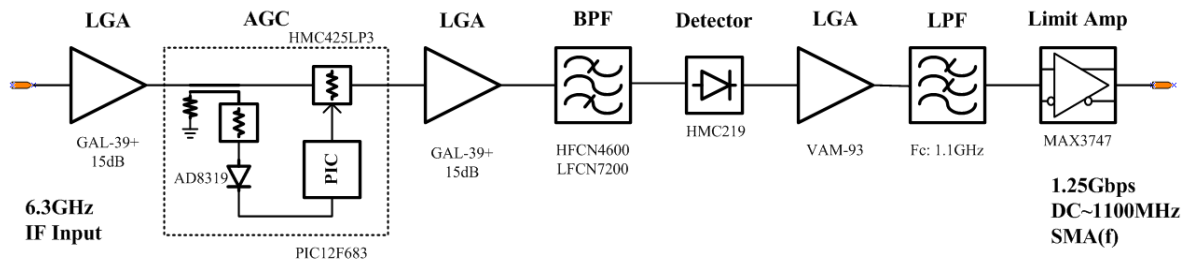


Figure 2.46 Block diagram of wide-band 6.3 GHz IF & ASK detector

Figure 2.47 shows the ASK spectrum of BPF output at 6.3 GHz IF stage. Note that 1.25 Gbps digital signal is occupied in 2.2 GHz band of frequency spectrum.

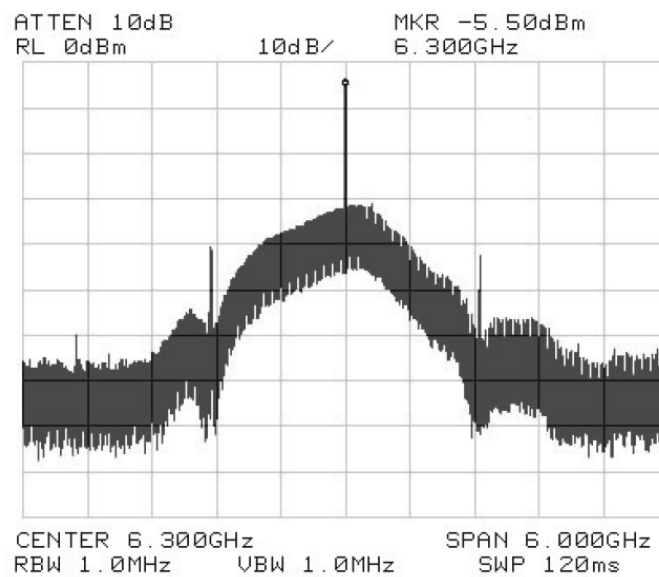


Figure 2.47 ASK spectrum of BPF output at 6.3 GHz IF stage

To build the challenging ultra wide band of 2.2 GHz at 6.3 GHz, which exceeds 35% relative bandwidth, BPF was initially implemented with the combination of HPF and LPF of HFCN4600 and LFCN7200 respectively, while the required BW of 2.2 GHz is 5.2 ~ 7.4 GHz. Due to the characteristics of LPF of LFCN7200 with 7.2 GHz cut-off frequency, the conversion loss near 7.4 GHz was increased. Thus the LPF was also finally removed.

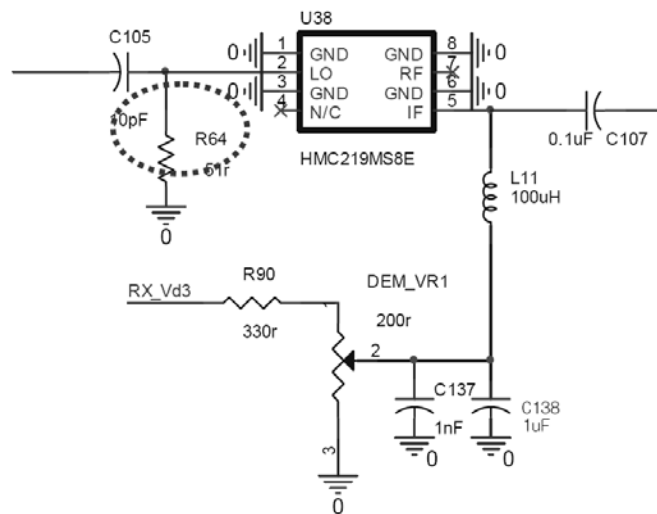


Figure 2.48 Insertion of 50 Ω resistor for wide-band matching

For the wide band matching for IF detector, shunt 50 Ω resistor was inserted (Figure 2.48). On the IF output, DC offset of 0.3 ~ 0.4 V was applied for optimum matching of detector. Figure 2.49 shows the revised block diagram of wide-band matched 6.3 GHz IF Section.

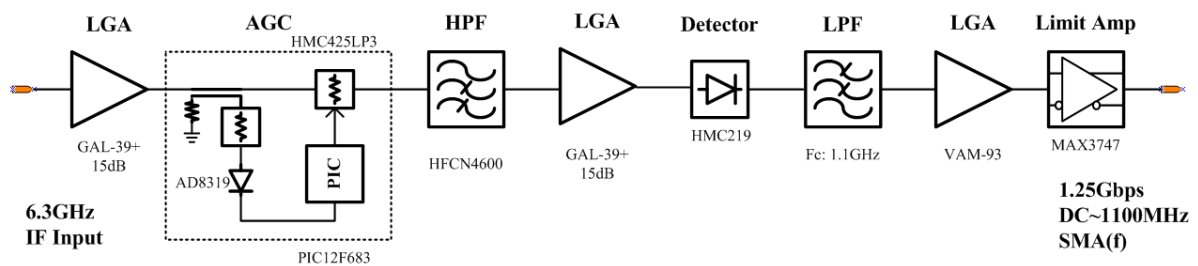


Figure 2.49 Revised IF section for upper band

2.3.9 AGC Circuit for Temperature Compensation

To solve the signal distortion due to temperature variation, AGC circuit was inserted (Figure 2.50). HMC425LP3 was used for voltage variable attenuator (VVA). It is a 6 bit digital attenuator, but for the work only 4 bits were used by using 2 dB, 4 dB, 8 dB, and 16 dB steps.

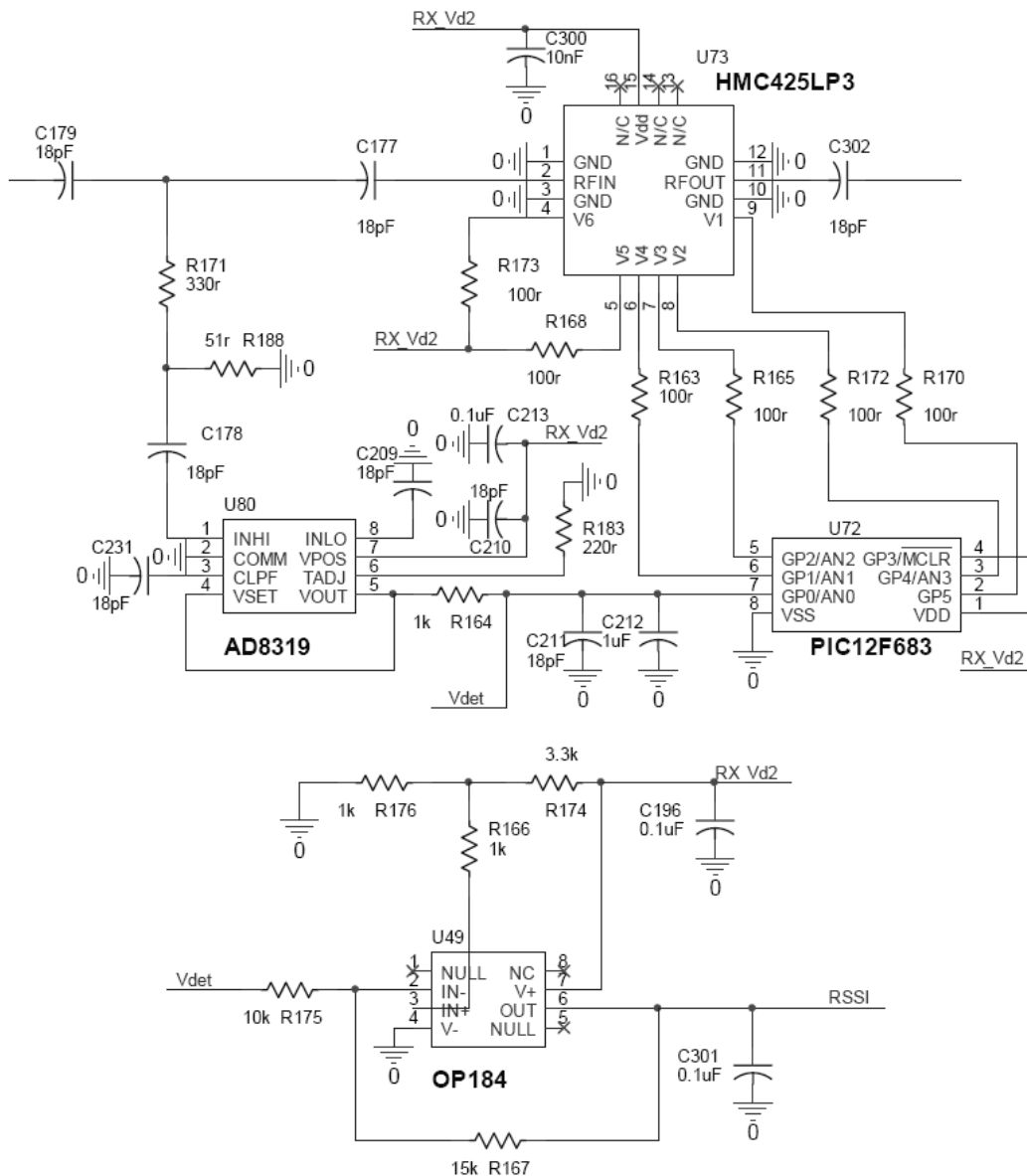


Figure 2.50 Temperature compensated AGC circuit design

For the VVA control, resistor of $330\ \Omega$ path was used as the input of AD8319 detector. AD8319 generate a control voltage in accordance with the level of input power. This analog voltage is converted to digital bits by ADC and was used to control the VVA in accordance with the preset voltage table in PIC register.

The output voltage of the detector AD8319 varies in reverse proportional with its input level. As these opposite action can cause confusion for indoor tests or even in field, its output level was reversed by inserting an OP-amp at the final stage. Figure 2.51 shows the implemented RX-IF and baseband section.

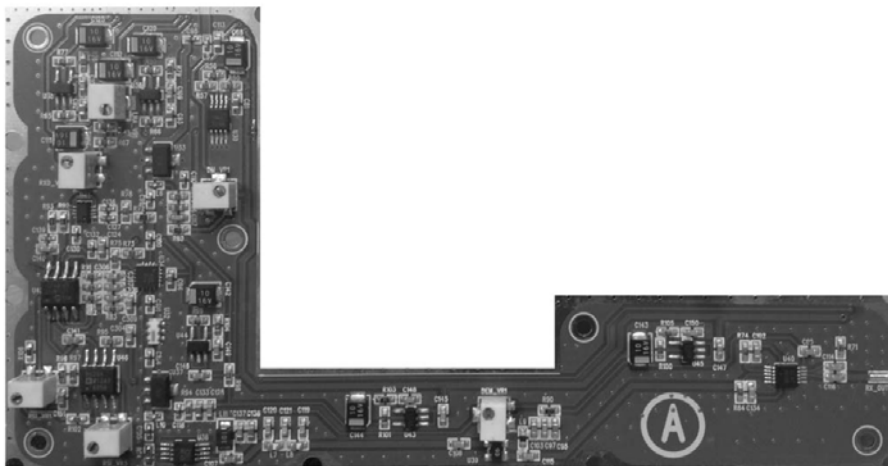


Figure 2.51 Implemented RX-IF and baseband section

With the implemented RX section, it generally showed stable operation on wide band sensitivity test, but it showed two minor issues. Firstly, an error occurred near $-20\ \text{dBm}$ input level with Unit-B under -10°C temperature. Inspection result of waveform with oscilloscope, the signal was saturated at that level of power. From this, it was figured out that the LGA has $1 \sim 2\ \text{dB}$ more gain in accordance with temperature goes down. This issue was cleared by adjusting (increasing) the AGC attenuation mapping values in PIC controller.

Secondly, when VVA changes its attenuation level as temperature decrease under zero level, an instant error occurred occasionally. Similarly to the solution at room temperature, this problem was solved by the restriction of PIC control current replacing the resistance of 200 kΩ to 910 kΩ between VVA and PIC chip. Figure 2.52 shows the low temperature compensated VVA control circuit for IF AGC.

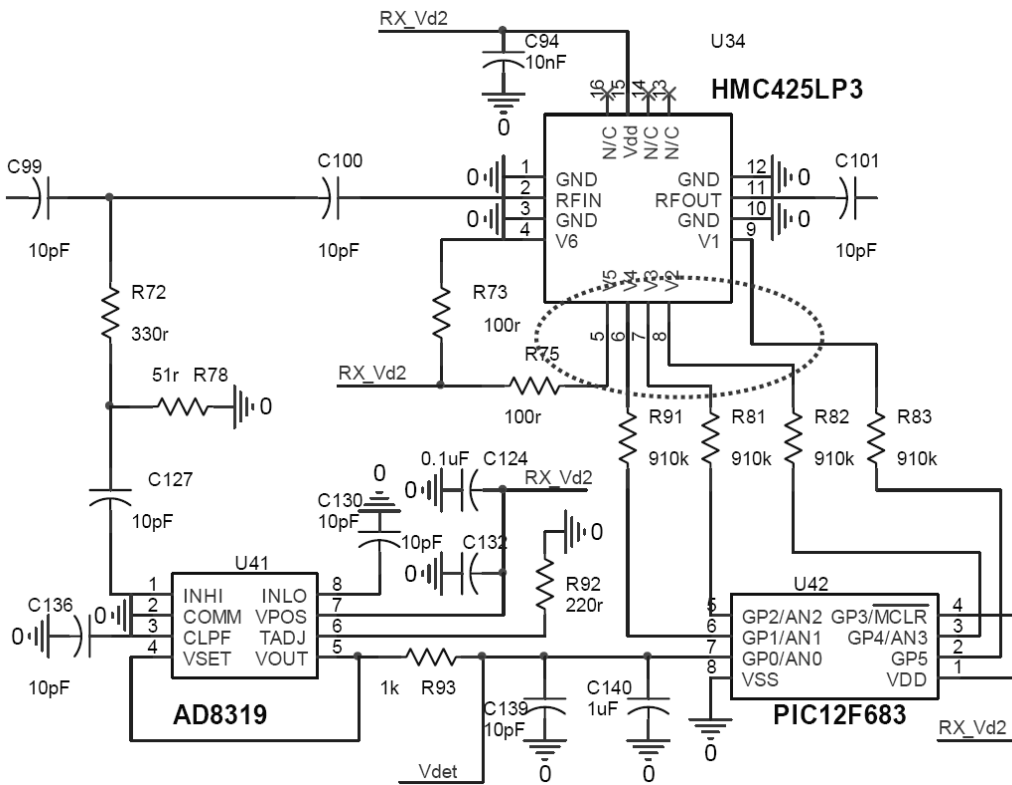


Figure 2.52 Compensation at low temperature adjusting VVA control current

2.3.10 Implementation of E-band Transceiver

Figure 2.53 shows the mechanical design of housing for E-band transceiver. The main body was designed to have proper isolation so as to not interfere with each other by inserting metal walls between TX and RX path. Two SMA(f) connectors for in/out of 1.25 Gbps GbE signal are located at the side wall of right end. The designed IF and baseband circuits are all surface mounted on RO4350, 20 mil substrate with permittivity of 4.35. RO4350 high frequency substrate is a glass reinforced hydrocarbon/ceramic laminates, not PTFE, which is designed for performance sensitive, high volume commercial applications to offer superior high frequency performance and low cost circuit fabrication like standard epoxy/glass (FR4).

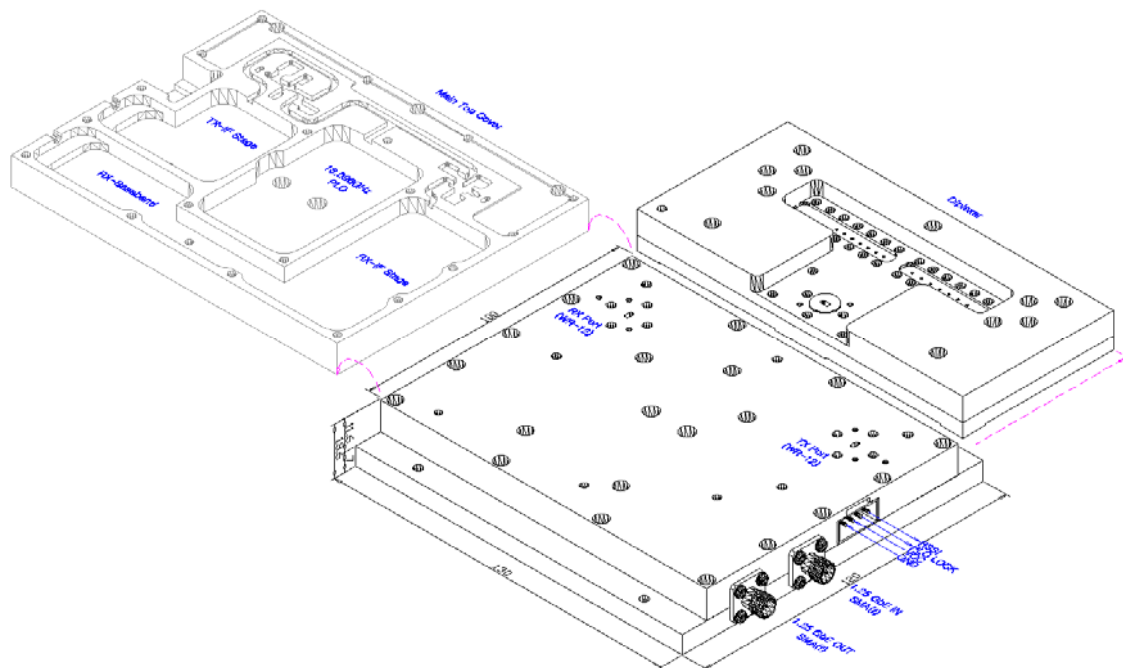


Figure 2.53 Mechanical design of E-band transceiver

The implemented PCB was mounted on the surface of the bottom cover of the aluminum plate. By using top cover with metal walls, these circuits are electromagnetically shielded. TX and RX port are located at each end side of top cover with standard WR-12 flange.

By using the designed E-band diplexer, these two ports are combined as a single common interface of antenna port. At the same side of SMA connector, 4-pins of interfaces is located, which include the single bias of 5 V / 1.2 A power supply for VCC and GND, phase locked indicator, and RSSI. Figure 2.54 shows the outline design of implemented E-band transceiver. The dimension of designed transceivers is 130 mm x 120 mm x 18.6 mm. The total height is 33.1 mm, which includes the diplexer.

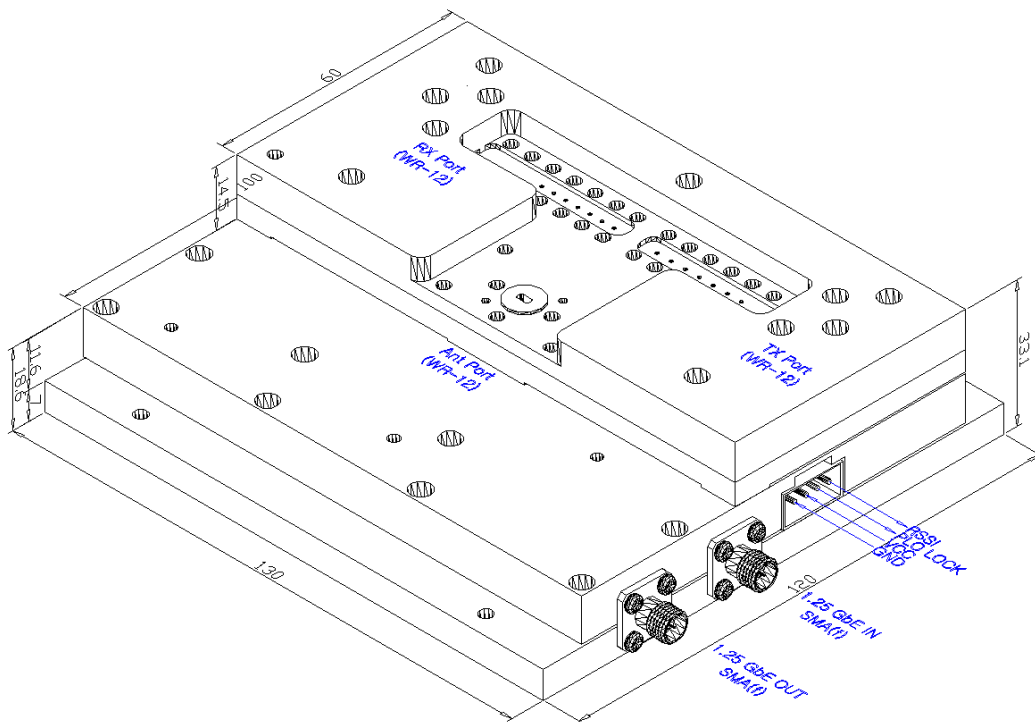


Figure 2.54 Outline of implemented E-band transceiver

2.4 mmW Diplexer Design

2.4.1 Guide Wavelength of WR12

For the implemented E-band transceiver with ultra wide bandwidth of 2.2 GHz, waveguide cavity type of diplexer was designed to use a single antenna for the TX and RX of radiolink. For the design, standard E-band WR12 waveguide with cross-section of 3.1 mm x 1.55 mm was used. The cutoff frequency of WR12 waveguide with given dimension is 48.35 GHz at TE_{10} mode.

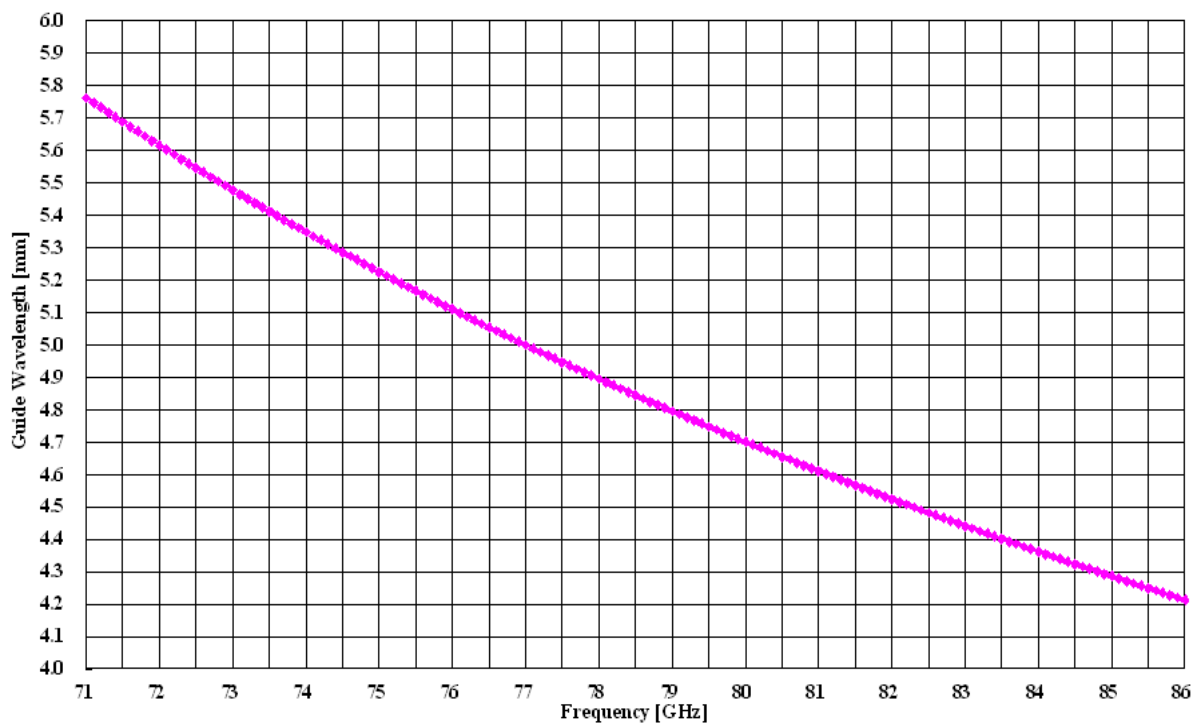


Figure 2.55 Wavelength of WR12 waveguide

Figure 2.55 shows the calculated guide wavelength of WR12 waveguide. The guide wavelength is 5.240 mm at 74.875 GHz, which is the center frequency of lower band, and 4.296 mm at 84.875 GHz, which is the center of upper band.

2.4.2 Waveguide Inductive Iris Filter

At mmW frequency range, to reduce the insertion loss, a waveguide cavity resonator coupled filter is commonly used. Considering mechanical processing by using an endmill machine, productivity should have considered from the design stage in advance [45], [46]. No matter what design shows good performance, it would be of no use if it has a structure that is not easy actually built in production.

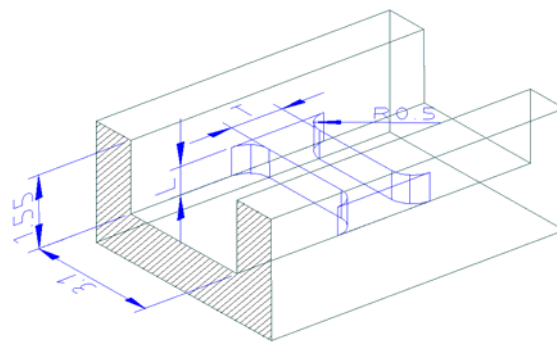


Figure 2.56 Structure of inductive iris

Figure 2.56 shows the HFSS modeling of the designed waveguide inductive iris filter. As rectangular block is located across at H-plane of WR12 waveguide. This metal block acts as inductance element with TE_{10} mode of electromagnetic propagation in WR12 waveguide [45] [46]. E-field is set vertically, or in the direction of the height L .

By adjusting the width T and height L , the coupling amount between resonators is controlled in accordance with its design value. Note that the round corner of $R0.5$ mm was already considered for the radius of endmill tool kit. As the frequency is very high, the wavelength is very short, which means the designed performance of filter is sensitive with the mechanical tolerance. Thus in order to make the filter design accurate, these practical machining situations needs to be fully considered from its early stage of design. The material is aluminum, silver plated for better insertion loss performance.

2.4.3 Extraction of K-Inverter Parameter

Figure 2.57 shows K-inverter coupled inductive iris filter. The K-inverter is chosen so as to have optimal coupling between each stage of resonators having impedance matching at designing frequency with the required number of poles in the designing filter network.

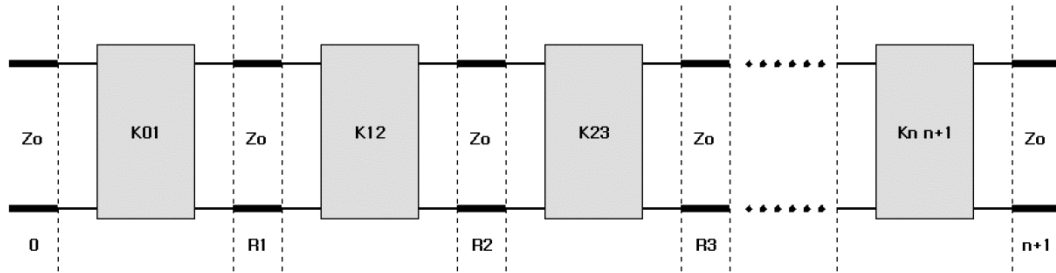


Figure 2.57 K-inverter coupled inductive iris filter

The total filter network can be presented by ABCD matrix in equation (2.4.1). By converting the calculated ABCD matrix of (2.4.1) to S-parameter, insertion loss and return loss can be calculated.

Equation (2.4.2) shows the insertion loss of the filter [47].

$$\begin{bmatrix} A & jB \\ jC & D \end{bmatrix} = \begin{bmatrix} 0 & jK_0 \\ \frac{j}{K_0} & 0 \end{bmatrix} \cdot \begin{bmatrix} \cosh \gamma_1 & Z_0 \sinh \gamma_1 \\ \frac{\sinh \gamma_1}{Z_0} & \cosh \gamma_1 \end{bmatrix} \cdots \begin{bmatrix} \cosh \gamma_n & Z_0 \sinh \gamma_n \\ \frac{\sinh \gamma_n}{Z_0} & \cosh \gamma_n \end{bmatrix} \begin{bmatrix} 0 & jK_{n+1} \\ \frac{j}{K_{n+1}} & 0 \end{bmatrix} \quad (2.4.1)$$

$$|S_{21}|^2 = \frac{1}{1 + \epsilon^2 T_n^2 \left[\frac{\alpha \lambda_g}{\lambda_{g0}} \sin \left(\frac{\pi \lambda_{g0}}{\lambda_g} \right) \right]} \quad (2.4.2)$$

where, $T_n(x)$ is Chebyshev polynomial with n poles and ϵ defines the pass band ripple level.

$$T_n(x) = \cosh[n \cosh^{-1}(x)] \quad \text{for } |x| > 1 \quad (2.4.3)$$

$$T_n(x) = \cos[n \cos^{-1}(x)] \quad \text{for } 0 \leq x \leq 1 \quad (2.4.4)$$

Butterworth polynomial has better in-band flatness, but the group delay is bigger than that of Chebyshev for a given number of poles. Thus Chebyshev polynomial was chosen for the lower group delay as well as the better skirt characteristics [48] [49].

Figure 2.58 shows the T-equivalent circuit of K-inverter. For a cavity filter, a K factor has to be chosen so that each stage of resonators are optimally impedance matched. The K-inverter and electrical length ϕ are calculated by (2.4.5) and (2.4.6) [50].

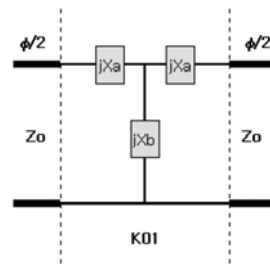


Figure 2.58 Equivalent circuit of K-inverter

$$\phi = -\tan^{-1}(2Xb + Xa) - \tan^{-1}(Xa) \quad (2.4.5)$$

$$\tan(2 \tan^{-1} K) = \frac{2Xb}{1 + 2XbXa + Xa^2} \quad (2.4.6)$$

K-inverter of designed inductive iris filter was extracted by using Ansoft HFSS. Figure 2.59 and Figure 2.60 shows the simulation result of K-Inverter and electrical length ϕ of lower band of 74.875 GHz and upper band of 84.875 GHz respectively. By increasing the height L of iris with 0.01 mm step, the K-inverter and electrical length parameters were extracted. As L increase, the K-inverter value reduces, which means the coupling with next resonator is being weakened.

The metal iris width T of 1.0 mm and R of 0.5 mm were chosen to have optimum K-inverter slope in accordance with height L. If the width T is narrow (thin), K-inverter varies steeply. In this case, the total length of filter can be short, but the performance is too sensitive on mechanical tolerance. On the

contrary if the width is too wide, K-inverter varies slowly so the mechanical tolerance can be slow, but the filter size increase. According to the required K-inverter, the iris heights were chosen.

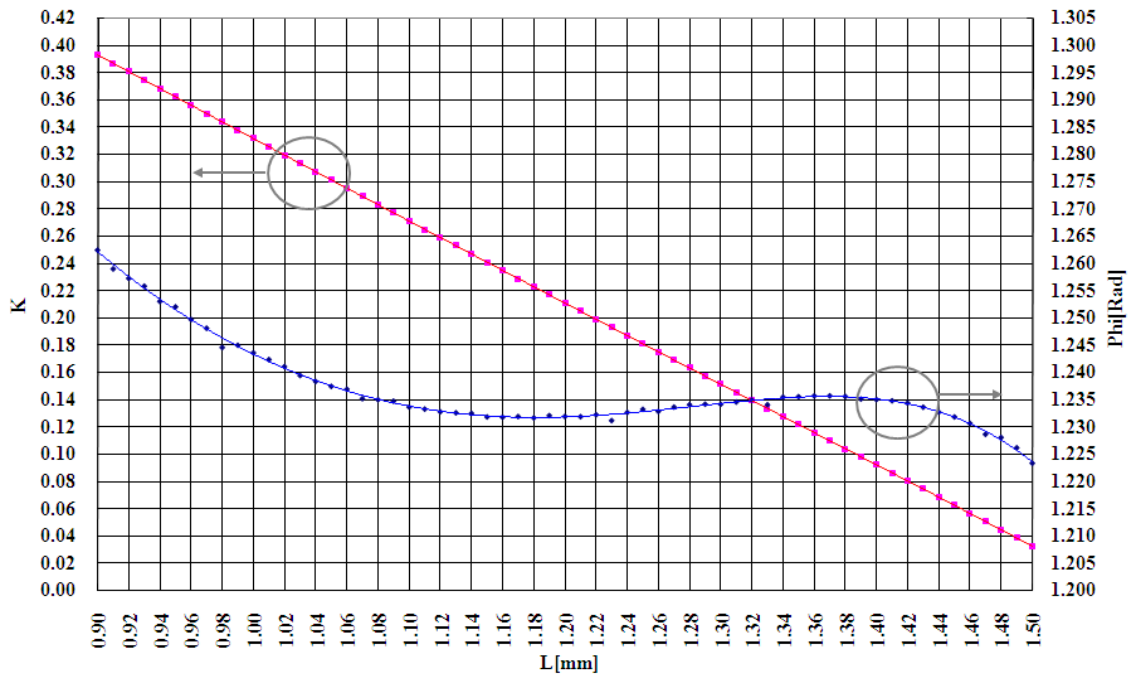


Figure 2.59 Simulation result of K-inverter at lower band

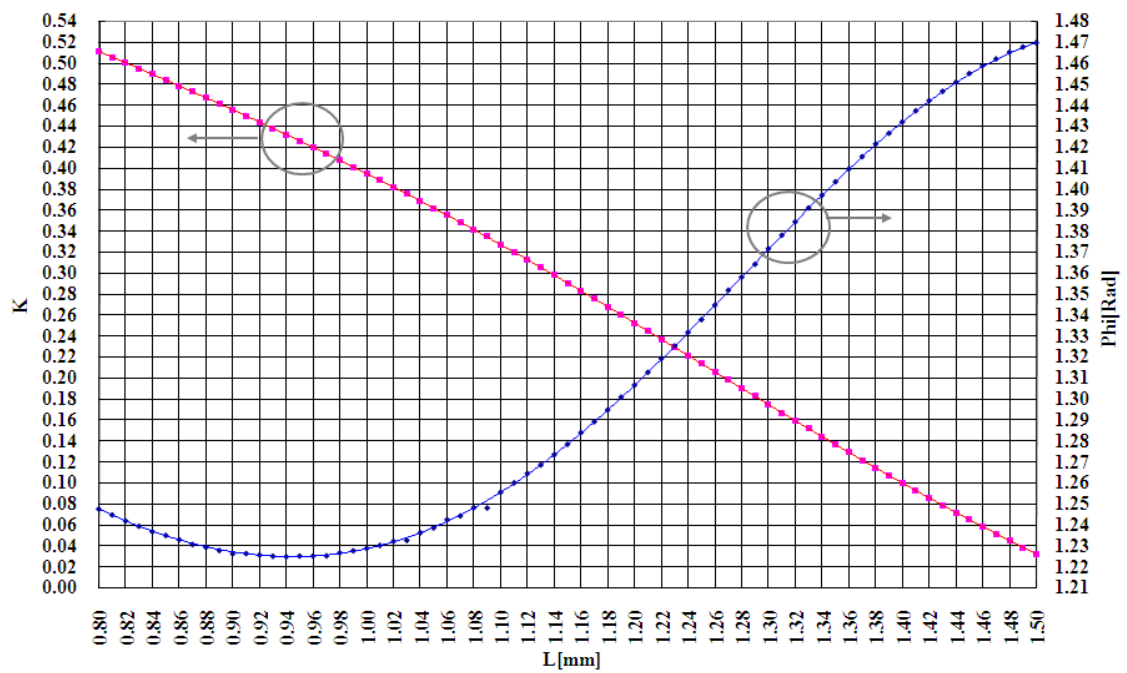


Figure 2.60 Simulation result of K-inverter at upper band

2.4.4 Design of Inductive Iris Filter

The impedance of each stage of the filter are defined in (2.4.7) and K-inverter values are calculated by (2.4.8) [51].

$$Z_k = \frac{2\alpha}{y} \sin\left[\frac{(2k-1)\pi}{2n}\right] - \frac{1}{4\alpha y} \left[\frac{y^2 + \sin^2\left(\frac{k\pi}{n}\right)}{\sin\frac{(2k+1)\pi}{2n}} \right] - \frac{1}{4\alpha y} \left[\frac{y^2 + \sin^2\frac{(k-1)\pi}{n}}{\sin\frac{(2k-3)\pi}{2n}} \right] \quad (2.4.7)$$

where, $k=1,2,3, \dots, n$

$$K'_{r,r+1} = \frac{\sqrt{y^2 + \sin^2\left(\frac{r\pi}{n}\right)}}{y} \quad r=0,1,2, \dots, n \quad (2.4.8)$$

where,

$$y = \sinh\left(\frac{1}{n} \sinh^{-1} \frac{1}{\epsilon}\right) \quad (2.4.9)$$

As the actual waveguide impedance at each stage is the same, equation (2.4.8) can be modified by (2.4.10).

$$K_{r,r+1} = \frac{K'_{r,r+1}}{\sqrt{Z_r Z_{r+1}}} \quad r=0,1,2, \dots, n \quad (2.4.10)$$

The resonator lengths of each stage are $\lambda/2$, and it is compensated by each stage of electrical length ϕ with the extracted parameter in Figure 2.59 and Figure 2.60.

Table 2.8 shows the design specifications. The center frequency of lower band filter is 74.875 GHz with 2.2 GHz of bandwidth. The upper band filter has center frequency of 84.875 GHz with the same 2.2 GHz bandwidth. The guard band between each bands are 7.8 GHz. To achieve the requirement of

rejection of less than 90 dBc, the number of resonators was decided by 7 poles. If the number of poles increases, the group delays increase. Thus, it was decided to achieve the minimal rejection considering low latency. The designed K-inverter and height of each stage of iris are shown in Table 2.9 and Table 2.10. In Table 2.11, the calculated resonator lengths are summarized.

Table 2.8 Design specifications of E-band diplexer

Parameters	Lower	Upper	Remark
Center Frequency	74.875 GHz	84.875 GHz	
Band Width	2.2 GHz	2.2 GHz	
Pass band ripple	0.03 dB	0.03 dB	
Poles	7	7	minimal
Isolation	90 dBc	90 dBc	

Table 2.9 Designed K-inverter and iris L of lower band filter

Parameters	K01	K12	K23	K34	K45	K56	K67	K78
$K_{n,n+1}$	0.3358	0.0818	0.0534	0.04864	0.04864	0.0534	0.08184	0.33584
L [mm]	0.9923	1.4168	1.4647	1.4727	1.4727	1.4647	1.4168	0.9923
ϕ [Rad]	1.2444	1.2342	1.2298	1.2287	1.2287	1.2298	1.2342	1.2444

Table 2.10 Designed K-inverter and iris length of upper band filter

Parameters	K01	K12	K23	K34	K45	K56	K67	K78
$K_{n,n+1}$	0.3349	0.0758	0.0460	0.0407	0.0407	0.0460	0.0758	0.3349
L [mm]	1.0884	1.4335	1.4782	1.4865	1.4865	1.4782	1.4335	1.0884
ϕ [Rad]	1.2514	1.4484	1.4641	1.4661	1.4661	1.4641	1.4484	1.2514

Table 2.11 Designed resonator length D [mm]

Resonator	D1	D2	D3	D4	D5	D6	D7
Lower	3.6572	3.6511	3.6489	3.6484	3.6489	3.6511	3.6572
Upper	3.0722	3.1449	3.1510	3.1517	3.1510	3.1449	3.0722

2.4.5 Design of T-Junction

To implement diplexer, both of the designed lower and upper band pass filters need to be connected by using T-junction. Figure 2.61 shows the equivalent model of shunt connected diplexer. Lower and upper band pass filters are connected at each end of sub-arm of T-junction. The length between junction plane and each filter of L_1 and L_2 are chosen to obtain optimum impedance matching [52].

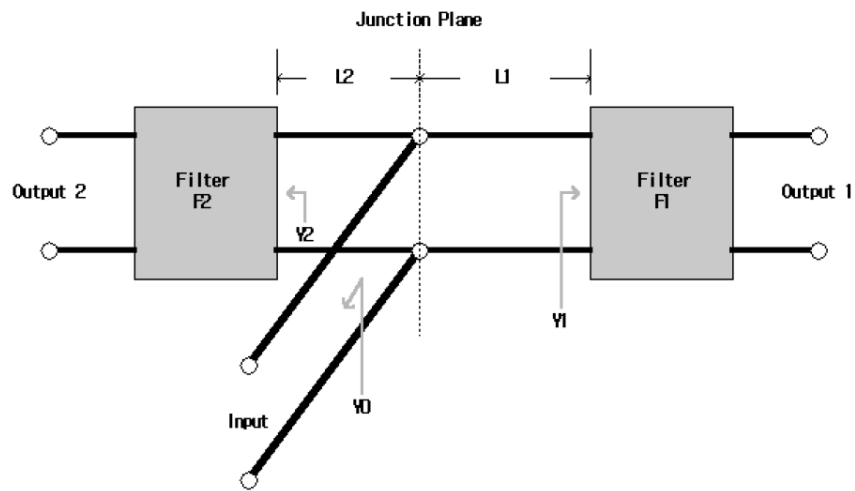


Figure 2.61 Shunt connected diplexer

Figure 2.62 shows the T-junction for HFSS modeling with its design parameters. Differently from a general T-junction for power divider, if the return loss of common port is too perfect, the isolation characteristic between two attached filters is worse [53]. Thus there need to be some trade-off.

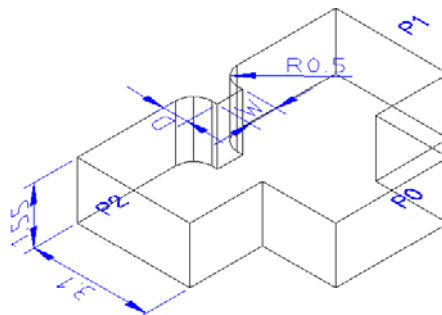


Figure 2.62 T-junction HFSS modeling

According to [54], the recommended return loss at each port is about -9 dB. Design factors are width W and length D with round radius of 0.5 mm considering the endmill machine. According to the simulation result, D of 0.65 mm was chosen with W of 0.7 mm optimally. Figure 2.63 shows the simulation result of designed T-junction finally. Over the whole wide band of interest 71 ~ 76 GHz, 81 ~86 GHz, the return loss shows the flat -9.5 dB typical as expected.

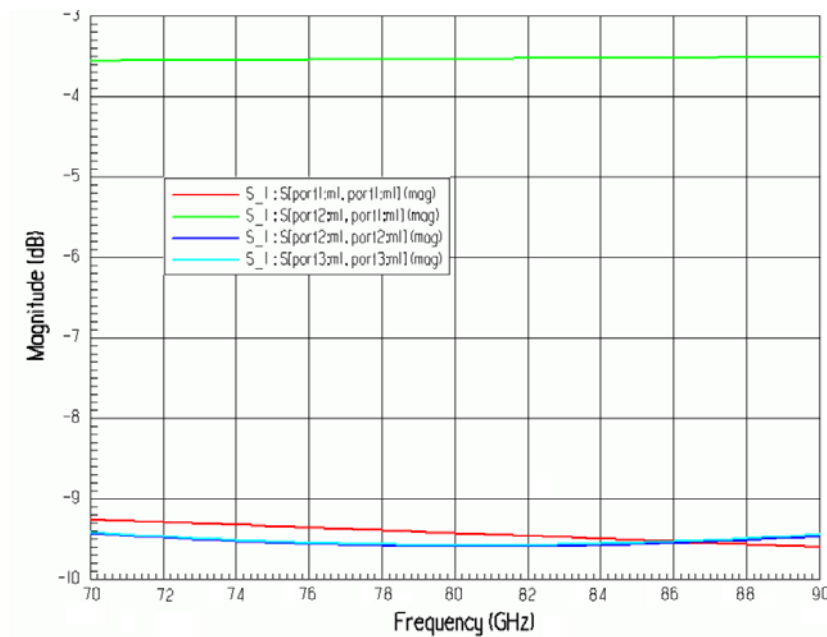


Figure 2.63 Simulation result of T-junction

In the case of two band pass filters connected to build diplexer by using T-junction, as shown in Figure 2.61, signal spectrums of F_1 frequency range from input port easily pass through F_1 filter, but is reflected at F_2 and return back to F_1 or input port again. On the contrary, if F_2 signal spectrum is inputted from input port, F_2 filter passes as well, but is reflected at F_1 filter. Thus if these length of L_1 and L_2 were not matched properly, the reflected signal degrades or attenuates its original traveling signal, which results in increased insertion loss.

For these reasons, L_1 is set as $\lambda/4$ at the center frequency of F_2 , and L_2 is set as $\lambda/4$ at the center frequency of F_1 . By matching the junction length this way, the required wide band of 2.2 GHz diplexer was achieved successfully.

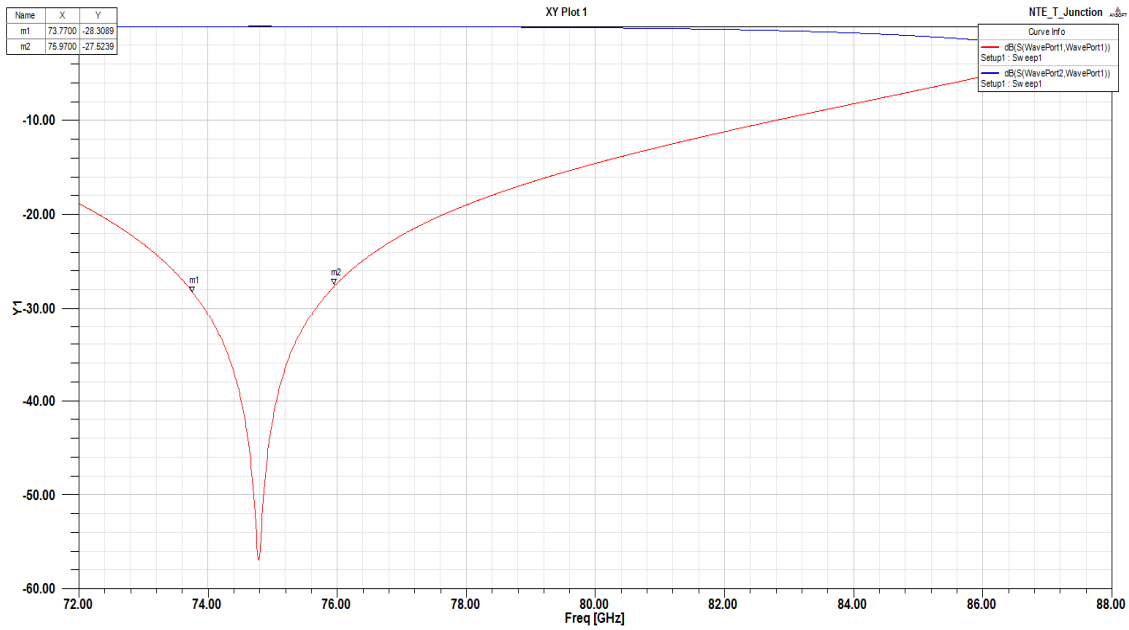


Figure 2.64 Simulation result of lower band matching

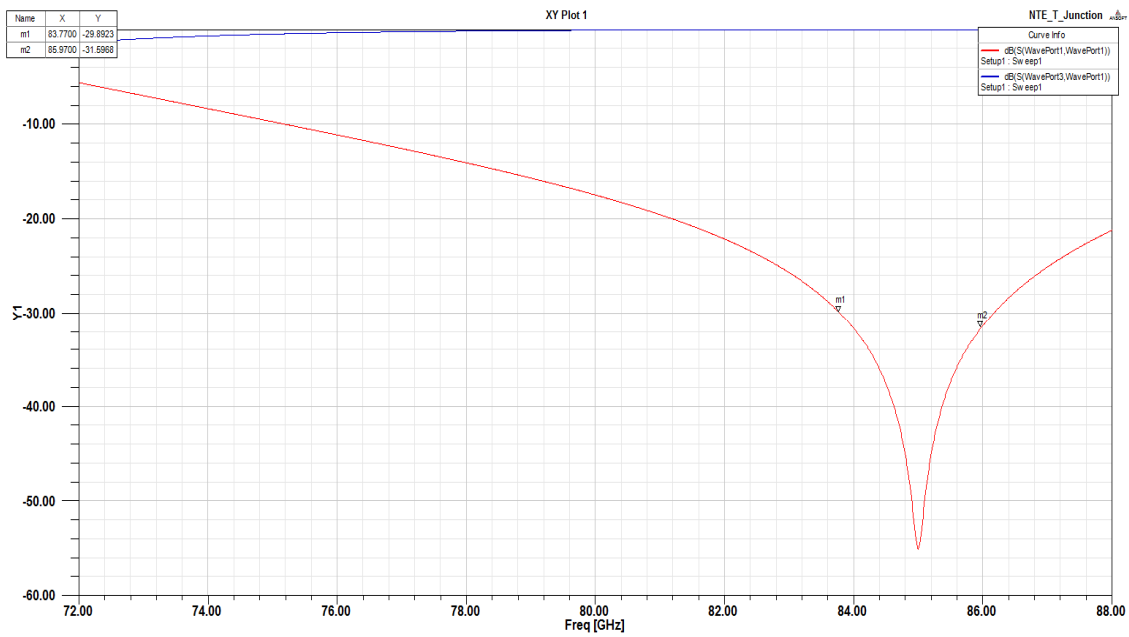


Figure 2.65 Simulation result of upper band matching

Figure 2.64 and Figure 2.65 shows the simulation result of lower band and upper band matching. The matched lengths of each band filter were decided by de-embedding of the wave ports so that the input impedance is open (∞) at the center frequency of each rejection band. The designed matched length of L_1 (lower band arm) and L_2 (upper band arm) are 3.76 mm and 4.15 mm respectively at each rejection band of 84.875 GHz and 74.875 GHz.

According to the simulation result, it shows good matching at both bands as expected with return loss of less than -27 dB. The band width matched by -20 dB is 5 ~ 6 GHz, which is sufficient to accommodate the 2.2 GHz BW for 1.25 Gbps GbE signal transmission. The design of T-junction and matched length are one of the key important procedures on diplexer design because the return loss of each band pass filter depends on T-junction matching status.

Figure 2.66 shows the final design of the E-band inductive iris coupled diplexer. All resonators are coupled with 1 mm thickness of iris. These irises have 0.5 mm round corner so it can be machined easily by using the endmill machine.

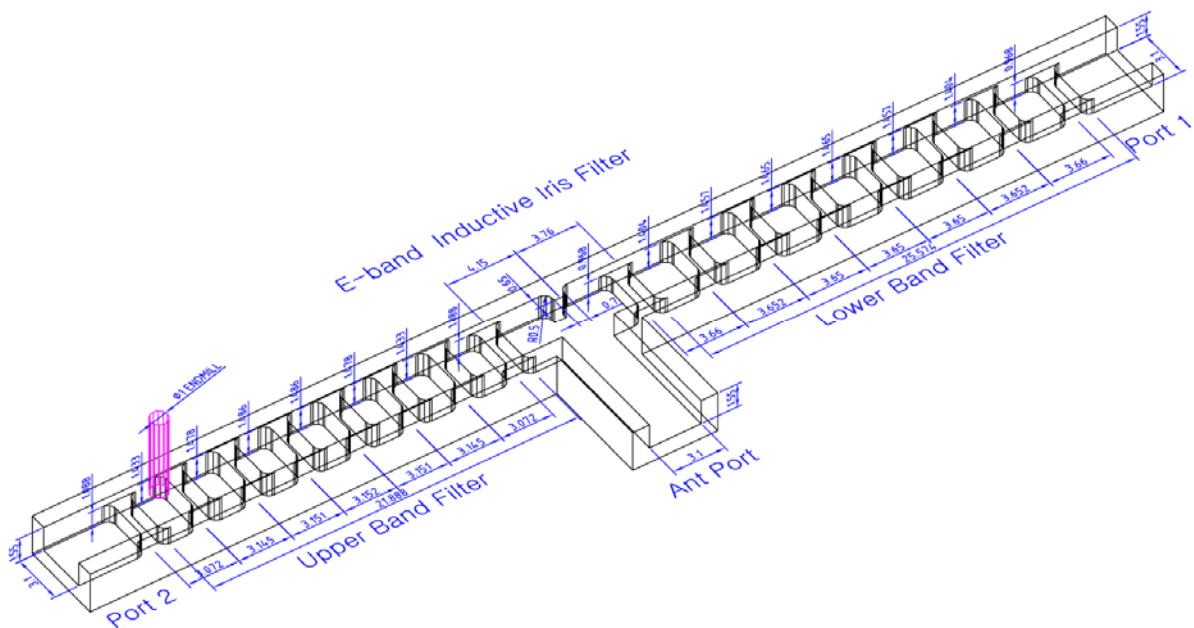


Figure 2.66 Designed E-band inductive iris coupled filter

2.4.6 Simulation Result

Figure 2.67 and Figure 2.68 shows the simulation result of designed lower and upper band pass filter respectively. For the simulation, Ansoft HFSS was used. As can be seen, insertion loss is less than 1.0 dB, and return loss is less than -15 dB.



Figure 2.67 Simulation result of lower band filter

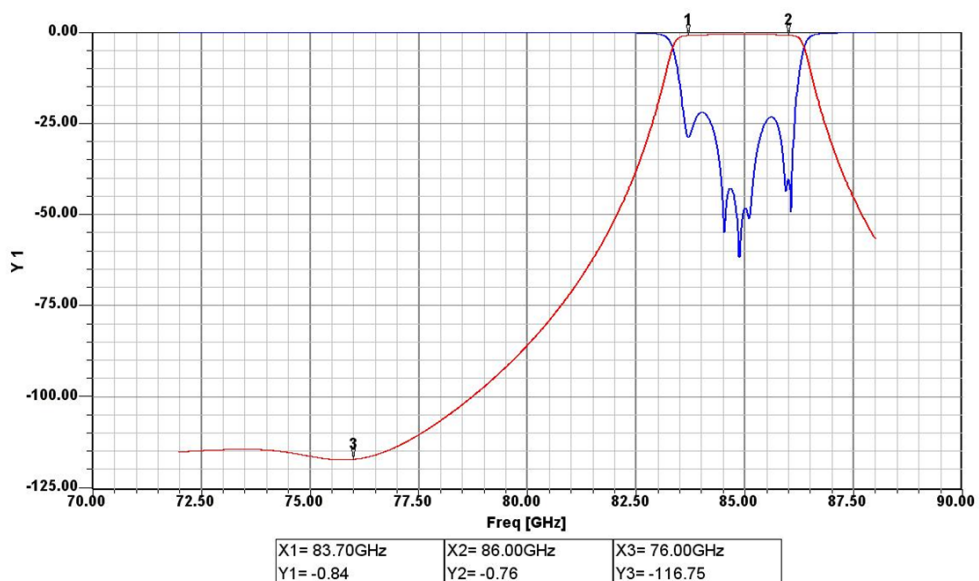


Figure 2.68 Simulation result of upper band filter

Figure 2.69 shows the diplexer simulation result. By using 3-port analyses with ADS, designed lower and upper band filter are coupled with the designed T-junction and analyzed. Note that after combined with T-junction, the insertion loss was slightly increased. The band rejection at each other band is less than -100 dBc. This designed performance becomes degraded after actual implementation. Figure 2.70 shows the outline of designed E-band diplexer.

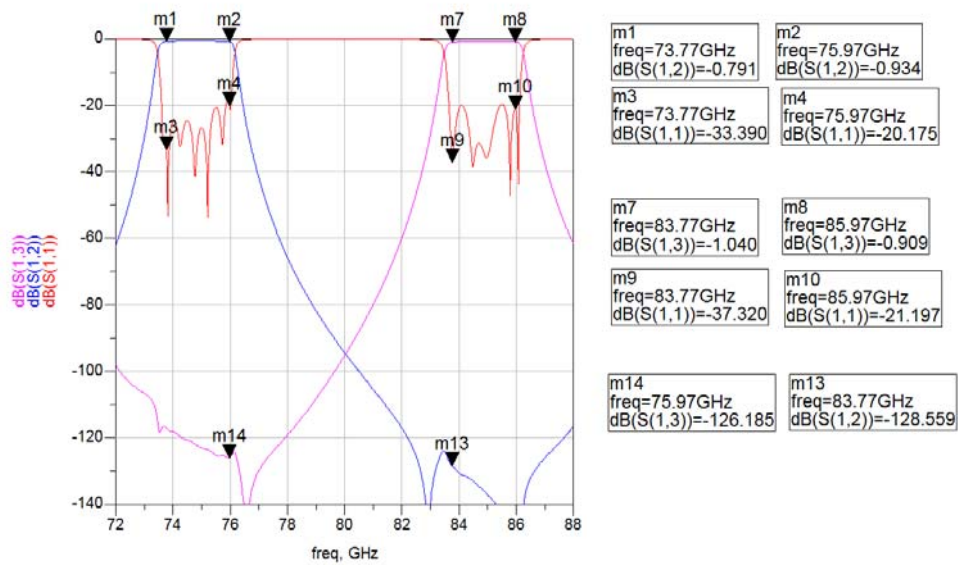


Figure 2.69 Simulation result of diplexer

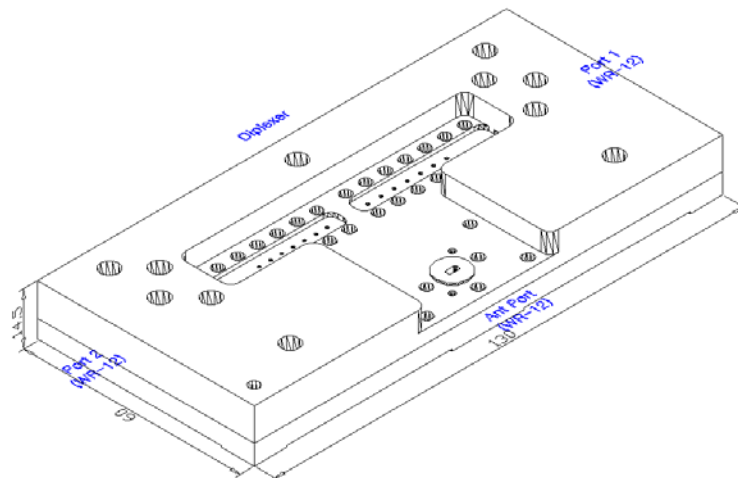


Figure 2.70 Outline design of diplexer

2.4.7 Measurement Result

Figure 2.71 and Figure 2.72 shows the measurement results of implemented diplexer. According to the results, it shows a lower band of 73.775 ~ 75.975 GHz, upper band of 83.775 ~ 85.975 GHz with 2.2 GHz BW. The measured insertion loss is less than 2.2 dB and return loss is less than -15 dB. The measured isolation is -85 dBc. Measurement results are summarized in Table 2.12.

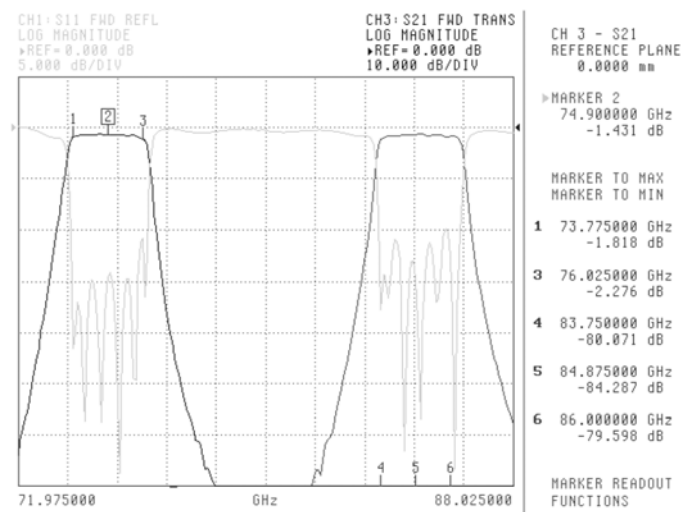


Figure 2.71 Measurement result diplexer (lower)

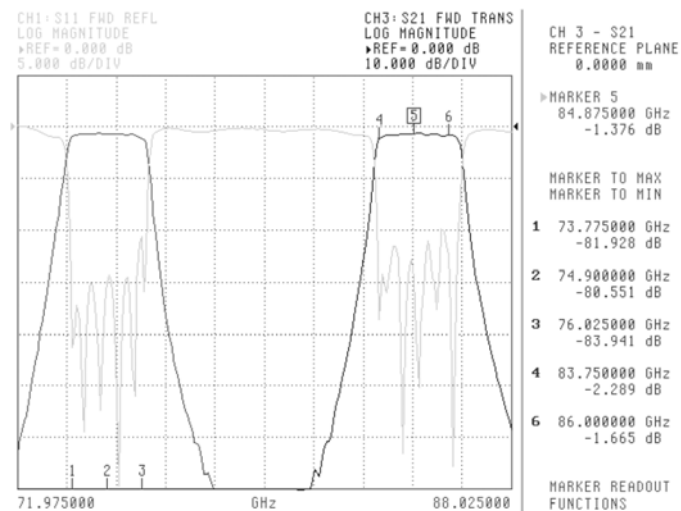


Figure 2.72 Measurement result diplexer (upper)

Table 2.12 Measurement result of diplexer

Parameters		Measurement Result
Lower	Pass Band	73.775 ~ 75.975 GHz
	Bandwidth	2200 MHz
	Insertion Loss	1.8 ~ 2.3 dB
	Return Loss	-15 dB
Upper	Pass Band	83.775 ~ 85.975 GHz
	Bandwidth	2200 MHz
	Insertion Loss	1.4 ~ 2.3 dB
	Return Loss	-15 dB
Tx/Rx Isolation		85 dBc
Interface		WR-12
Dimensions [LxWxH]		130 mm x 60 mm x 14.5 mm

2.5 Measurement Results

2.5.1 Data Rate & Dynamic Range

Figure 2.73 and Figure 2.75 show ASK modulation spectrum of lower and upper band respectively for the designed E-band transceiver at antenna port of diplexer. For the measurement, a 20 dB fixed attenuator was used at the input port of spectrum analyzer to clear power saturation issue.

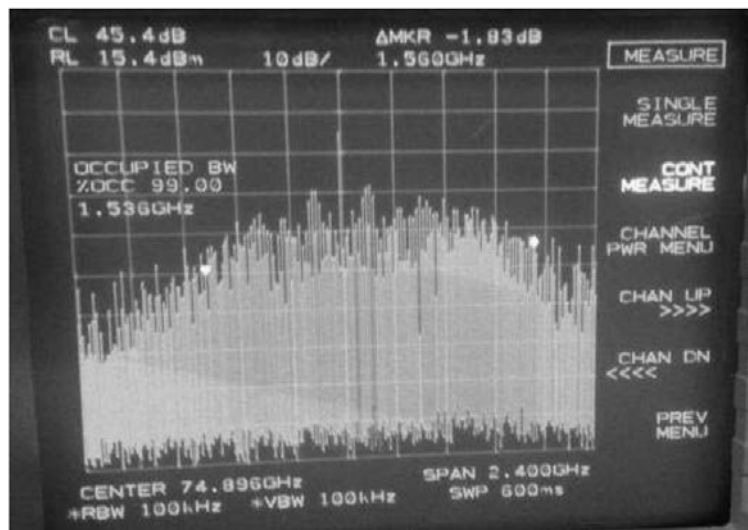


Figure 2.73 ASK modulation spectrum at lower band

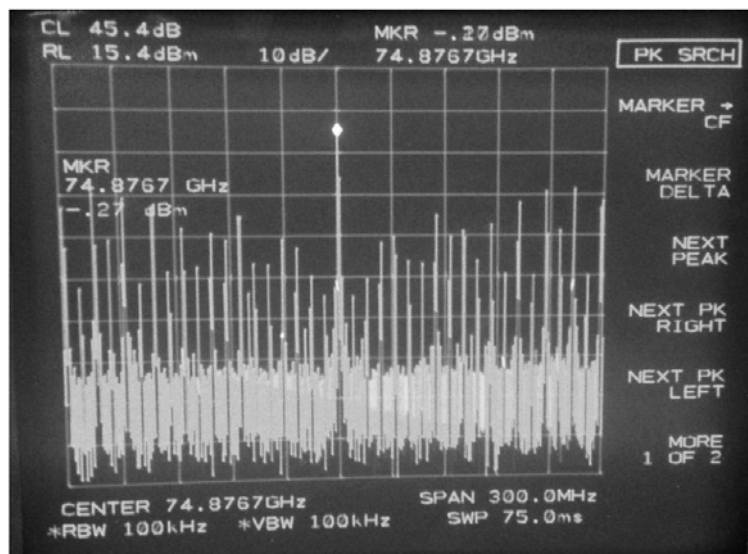


Figure 2.74 Lower band carrier at 74.875 GHz

The power of 99% occupied BW is about 1.53 ~ 1.57 GHz with 1.25 Gbps Ethernet signal input. Figure 2.74 and Figure 2.76 show the lower band carrier at 74.875 GHz and 84.875 GHz respectively.

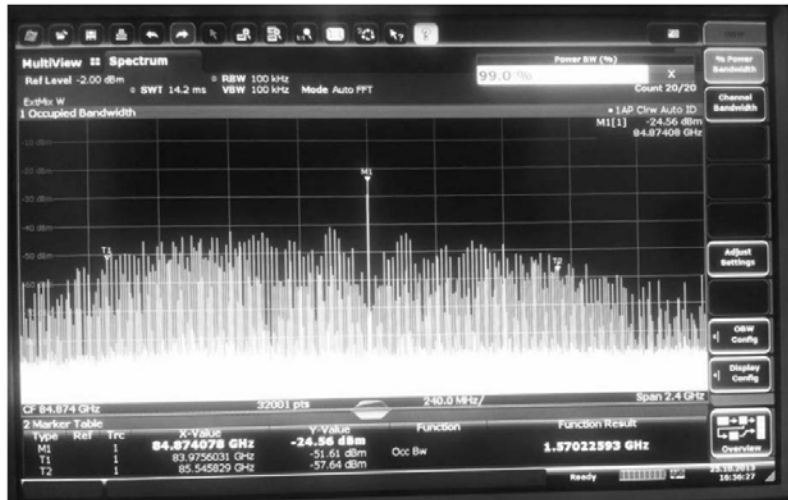


Figure 2.75 ASK modulation spectrum at upper band

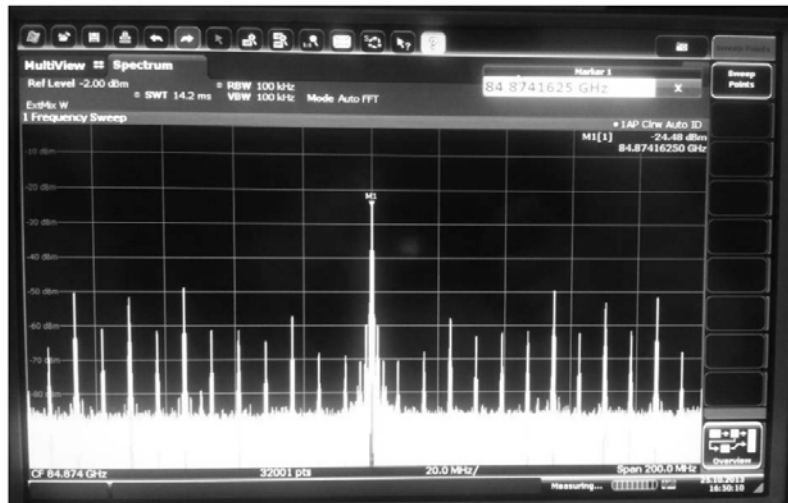


Figure 2.76 Upper band carrier at 84.875 GHz

The high speed 1.25 Gbps GbE signals modulated at each LO carrier are transmitted to the receiver and de-modulated as described in section 2.3. Figure 2.77 shows the eye pattern of the detected signal. According to the measured result, the timing jitter is about 0.25 ns. For this work, the specification of

phase noise of LO carrier is relatively loose, as ASK modulation is used, allowing for a range of several hundred pico-seconds. This is one of the merits for saving on costs. For 16QAM or 64QAM, it is strictly limited by several tenths of pico-seconds.



Figure 2.77 Eye pattern of detected 1.25 Gbps GbE signal

Figure 2.78 shows the measurement setup with data quality analyzer (DQA) for implemented E-band transceiver. To reduce the TX power and not to make spectrum analyzer saturation, E-band variable attenuator was used to measure the sensitivity. The test signal from DQA with 1.25 Gbps Ethernet is plugged in the designed transceiver Unit-A, and it is detected at the other end of transceiver Unit-B.

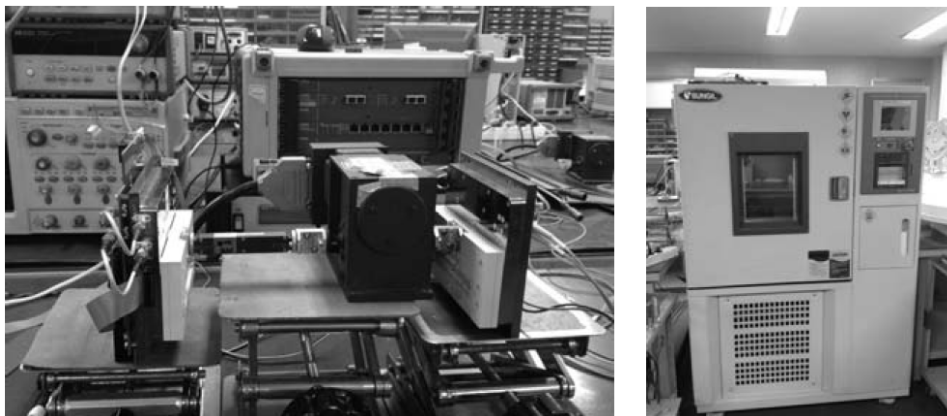


Figure 2.78 Measurement setup with temperature chamber

TX output power is +20 dBm and +18 dBm at 74.875 GHz and 84.875 GHz respectively. By reducing the TX power by using attenuator with 1 dB step, BER was checked and recorded. At room temperature of 25 degree, sensitivity is measured by -45 dBm for Unit-A and -46 dBm for Unit-B. Note that the performance of lower band of 74.875 GHz is better than that of 84.875 GHz upper band.

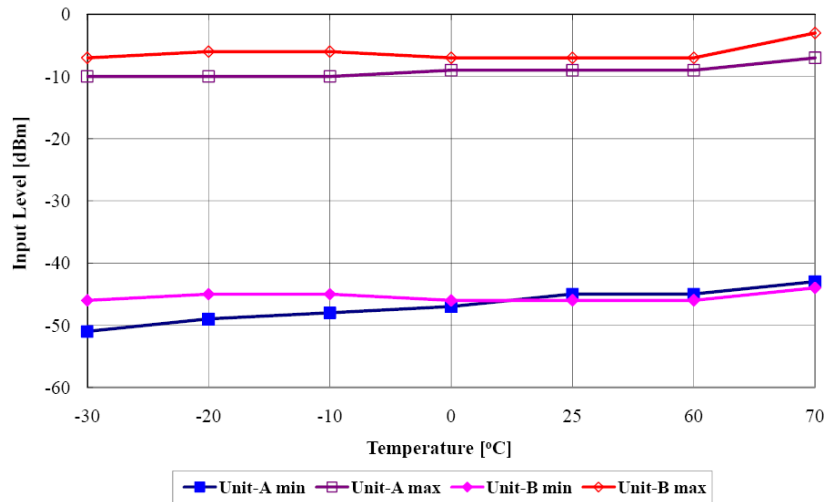


Figure 2.79 Temperature characteristics

Table 2.13 Test result of dynamic range

Temp [°C]	Unit-A		Unit-B	
	min	max	min	max
-30	-51	-10	-46	-7
-20	-49	-10	-45	-6
-10	-48	-10	-45	-6
0	-47	-9	-46	-7
25	-45	-9	-46	-7
60	-45	-9	-46	-7
70	-43	-7	-44	-3

As temperature decreases below zero to -30 °C, the sensitivity increased by 3 ~ 5 dB compared to room temperature. This is because the gain of MMIC chips is increased as temperature decrease.

Figure 2.79 shows the temperature characteristics in operating range for outdoor environment.

Dynamic range is generally defined as the ratio, or difference in dB, of the maximum input level that

the system can tolerate to the minimum input level at which the system provides a reasonable signal quality. In Table 2.13, the test result of dynamic range is summarized with BER 10^{-12} or error free criteria.

Noise figure is a measure of how much the SNR degrades as the signal passes through a system. For a cascade of stages, the overall noise figure can be obtained in terms of the NF and gain of each stage.

For n-stages, NF is calculated by Friis equation (2.5.1) [40].

$$NF_{tot} = 1 + (NF_1 - 1) + \frac{NF_2 - 1}{G_1} + \dots + \frac{NF_n - 1}{G_1 \cdot G_2 \cdots G_{n-1}} \quad (2.5.1)$$

The Friis equation indicates that the noise contributed at each stage degrades as the gain preceding the stage increases, implying that the first few stages in a cascade are the most critical. The overall NF of the implemented E-band transceiver is 9.4 dB as shown in Table 2.14.

Table 2.14 System noise figure

Parameters		Total	Diplexer	LNA	Mixer	Attenuator	BPF	AGC	LGA
Gain	dB	31.0	-3.0	26.0	-20.0	-1.0	-1.0	20.0	10.0
	Dec	1.259E+03	0.501	398.107	0.010	0.794	0.794	100.000	10.000
NF	dB	9.4	3.0	6.0	4.0	1.0	5.0	-20.0	3.0
	Dec	8.67	1.995	3.981	2.512	1.259	3.162	0.010	1.995
Power	max	-20	-23.0	3.0	-17.0	-18.0	-19.0	-9.0	1.0
	min	-50	-53.0	-27.0	-47.0	-48.0	-49.0	-29.0	-19.0

2.5.2 Latency

Figure 2.80 shows the latency measurement setup. A digital signal of 128 bits with 625 MHz from pulse pattern generator was divided by two paths. One thing was plugged directly into to the oscilloscope as CH1. The other path was loop backed through implemented E-band transceiver as round trip and plugged into the same oscilloscope as CH2. By comparing the signal delay, the latency was measured. The used oscilloscope was Hewlett Packard Infineon 1.5 GHz BW with 8 Gs/s, or 0.125 ns of sampling resolution.

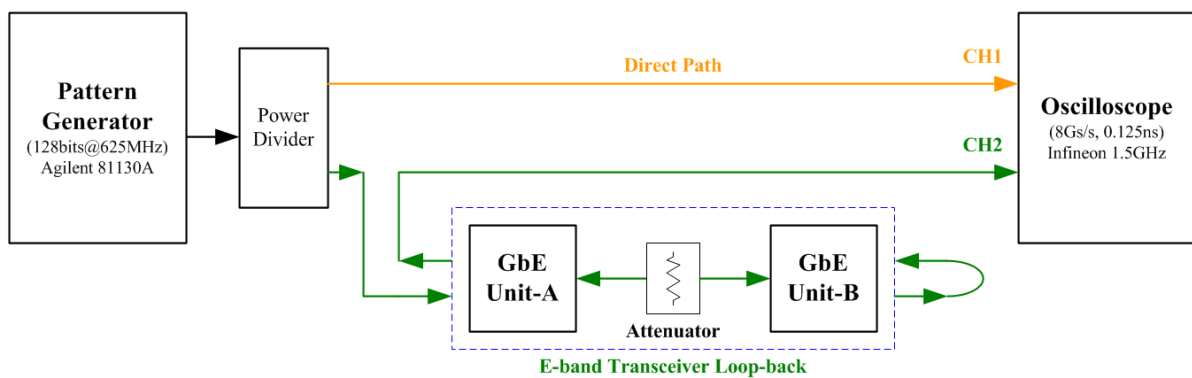


Figure 2.80 Latency measurement setup

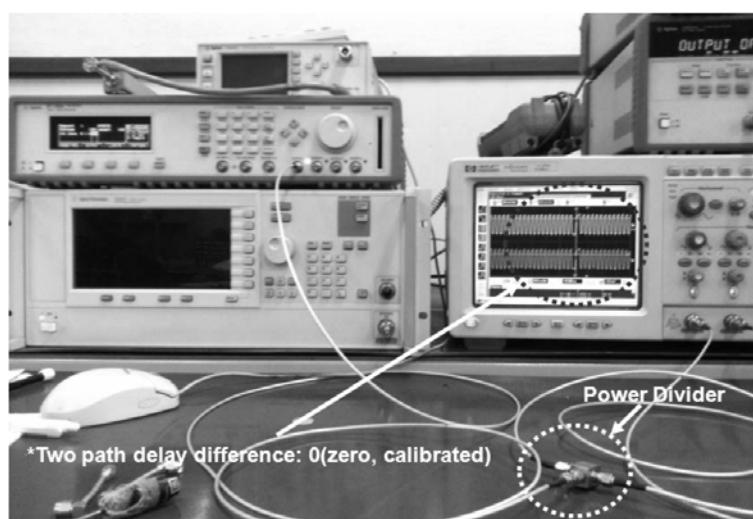


Figure 2.81 Calibration of power divider output

Figure 2.81 shows the signal calibration of power divider output. The signal outputs of power divider were calibrated by using the oscilloscope. Note that the reference of waveform readout of oscilloscope is the same. Figure 2.82 shows the loopback setup with implemented two radio units. Between two radio units, E-band variable attenuator was attached to attenuate the TX power properly.

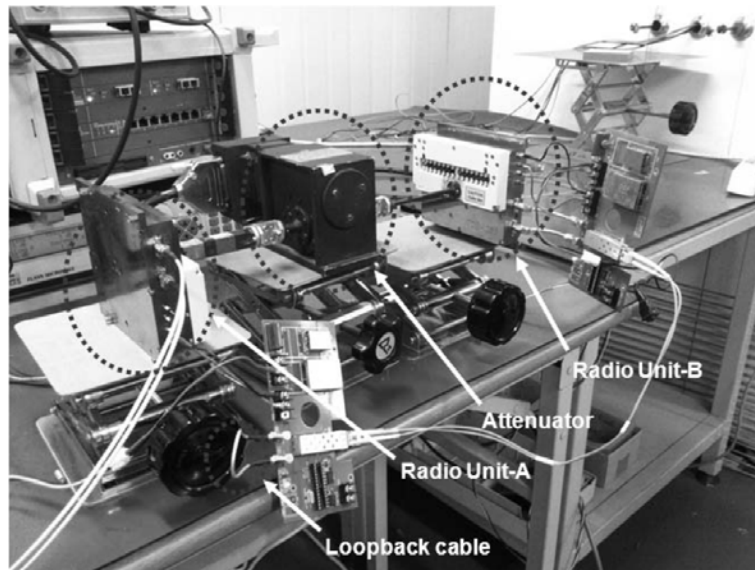


Figure 2.82 Loopback of implemented radio unit

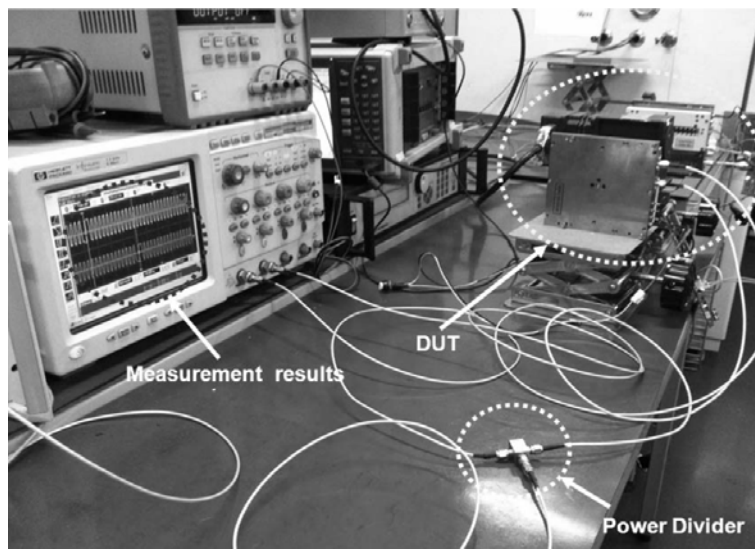


Figure 2.83 Latency test setup

Figure 2.83 shows the latency test setup. For the loop-back, to reform the received test signal at the other end of radio unit, an optic interface board was used that has a SFP fiber optic module. The function of optic interface board is the signal conversion between electrical and fiber optic signal with clock data recovery. A fiber optic cable was connected as a loop-back to return back the test signal.

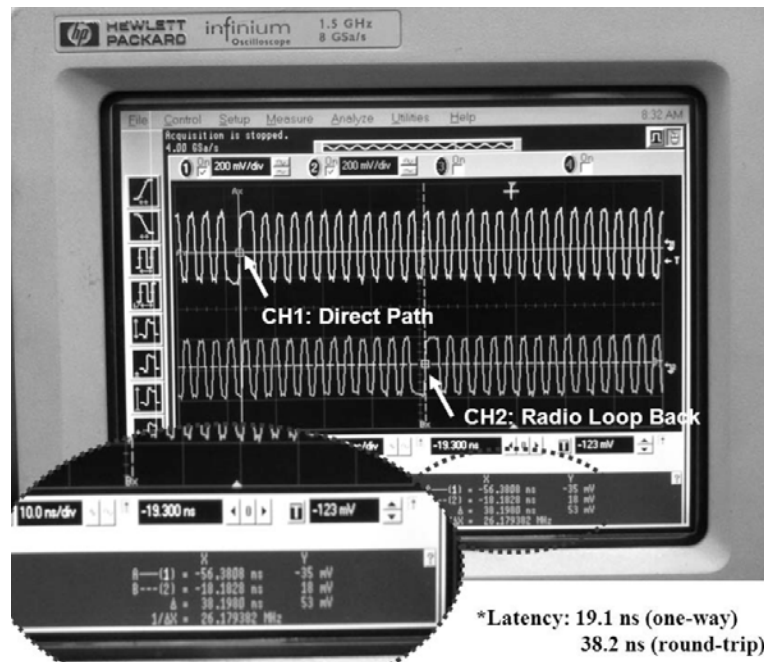


Figure 2.84 Latency measurement result

Figure 2.84 shows the latency measurement result. The signal tagged CH1 is from direct path and CH2 shows the signal through the implemented E-band radio unit of loop-back path. The time difference is 38.2 ns, which is the round-trip latency of the radio unit. It is equivalent to 19.1 ns of one-way latency for the implemented transceiver.

Table 2.15 shows the comparison of latency among current existing commercial technologies. Most of commercial makers provide greater than 50 μ s of latency up to 350 μ s in case of Siklu. E-band and SIAE achieved quite good latency of less than 5 μ s, but this is still large compared to 19.1 ns achieved in this work.

Figure 2.85 shows a relative comparison with its available data rate. The implemented radio shows ultra-low latency and wide bandwidth of 1.25 Gbps high speed.

Table 2.15 Comparison of latency among commercial technologies

Maker	Model	Data Rate [Gbps]	Modulation	BW [MHz]	Latency [μ s]
This Work	n/a	1.25	ASK	2,200	0.019
SIAE [28]	ALFOplus80	2.50	64QAM	500	5
E-band ¹⁾ [29]	E-Link 1000Q	1.25	QPSK	1,000	5
E-band ¹⁾ [30]	E-Link 2500	2.50	QPSK	1,000	5
Sub10 [31]	Liberator-E1000c	1.25	DBPSK	1,500	8
Huawei [32]	RTN380	1.25	64QAM	250	50
Elva-1 ³⁾ [33]	PPC-1000-E	1.25	QPSK	1,000	50
BridgeWave ²⁾ [34]	AR80	1.25	BFSK	1,400	50
BridgeWave ²⁾ [35]	FlexPort80-3000	2.50	QPSK	1,000	65
Fujitsu [36]	GX4000	3.00	ASK	5,000	75
Sub10 [37]	Liberator-E1000e	1.25	8-PSK	500	200
Siklu [38]	EtherHaul-1200	1.25	64QAM	500	350

*Note

- 1) Mosley merged and acquired with E-band in mid of 2013
- 2) REMEC merged and acquired with BridgeWave in the end of 2013
- 3) DOK has sales right of Elva-1 product exclusively

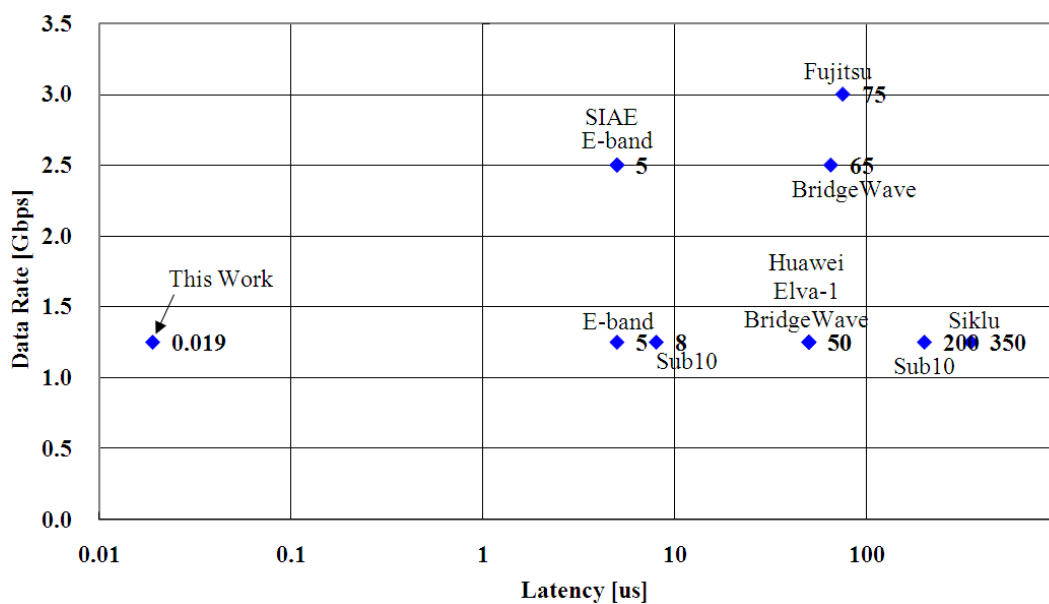


Figure 2.85 Comparisons of latency and data rate

Table 2.16 shows the summary of measurement result of the implemented E-band ASK transceiver.

Table 2.16 Summary of measurement result

Parameters		Unit	Specifications		Remark
			Unit-A	Unit-B	
TX	RF Frequency	GHz	73.775~75.975	83.775~85.975	
	Center Frequency	GHz	74.875	84.875	
	Output power	dBm	18.3	17.1	Ant. port
	Bandwidth	GHz	2.2		
	IF Frequency	GHz	2.6 ~ 4.8	5.2 ~ 7.4	
	LO-IF	GHz	3.7	6.3	
RX	RF Frequency	GHz	83.775~85.975	73.775~75.975	
	Center Freq.	GHz	84.875	74.875	
	IF Frequency	GHz	5.2 ~ 7.4	2.6 ~ 4.8	
	Bandwidth	GHz	2.2		
	Noise Figure	dB	9.4		1)
	Sensitivity	dBm	-45	-46	BER 10^{-12}
	Dynamic Range	dB	36	39	
Common	Modulation		ASK		
	Data Rate	Gbps	1.25		
	Latency	ns	19.1		one-way
	RF Port		WR-12		
	Temperature	°C	-30 ~ +70		
	Size	mm	130 x 120 x 33.1		

1) Noise Figure is an estimated value

III. Field Test

3.1 Link Budget

The sensitivity of RF receiver is defined as the minimum signal level that the system can detect with acceptable signal-to-noise ratio (SNR). In radiolink, a minimum detectable signal level (MDS) is usually called as sensitivity and is specified by (3.1.1) [40]. Note that the sum of first three terms is the total integrated noise of the system and is sometimes called as noise floor.

$$P_{\text{MDS}} = -174 + 10 \log \text{BW} + \text{NF} + \text{SNR} \text{ [dBm]} \quad (3.1.1)$$

Table 3.1 Link budget analysis

Parameters	Units	Values
Output power, P_o	dBm	19.6
Diplexer loss	dB	-2.5
Output power @ant port	dBm	17.1
Waveguide loss	dB	-1.0
Tx antenna gain	dB _i	45.0
Frequency, f_o	GHz	84.875
Distance of radiolink	km	4.1
Free space path loss	dB	-143.3
Atmospheric loss	dB/km	-0.6
Sub-total of additional loss	dB	-4.0
Total path loss	dB	-147.2
Rain rate, R_p	mm/h	0.0
Rain Attenuation, AR1, $d < D < 22.5\text{km}$	dB	0.0
Rain Attenuation, AR2, $D < d$	dB	0.0
Rx antenna gain	dB _i	45.0
Waveguide loss	dB	-1.0
Rx diplexer loss	dB	-2.5
Received Signal Level	dBm	-44.6
Noise Figure	dB	9.4
Temperature	8C	25
Bandwidth	MHz	2,200
Noise Floor	dBm	-71.6
Required SNR ¹⁾	dB	25.0
Minimum detectable signal le	dBm	-46.6
Link Budget	dB	156.2
Link Margin	dB	2.0

1) Required SNR measured with BERT: 22dB@BER 10^{-6} , 25dB@BER 10^{-12}

For the implemented E-band transceiver, the sensitivity was measured by -46 dBm as shown in section 2.5. According to the link budget analysis, the estimated MDS level is about -46 dBm with the required SNR of 25 dB under BER 10^{-12} criteria. With the output power of 17.1 dBm and antenna gain of 45 dBi for both TX and RX with 1ft diameter, the estimated link budget is estimated by 156.2 dB.

For the 1.25 Gbps Ethernet signal transmission, the link showed about 3dB more sensitivity, or down to -49 dBm, which is equivalent with its SNR of 22 dB. In case of Ethernet transmission, the link is made with only BER 10^{-6} . This explains the increased sensitivity. As the LO carrier is included in ASK modulation spectrum as well as the transmission signal, the received power level looks like higher, but actually the signal exist 15 ~ 20 dB below compared to its LO carrier level, which results in an increased SNR than other typical up/down converter using higher modulation.

3.2 Field Test

Figure 3.1 shows the typical gain and half power beam width (HPBW) of Cassegrain reflector antenna in terms of its reflector dish size. At 80 GHz range, the gain of 1ft antenna, or 12 inch, is typical 45 dBi. The HPBW is typical 0.8 degree, which is called “pencil beam” by the FCC [17], [18].

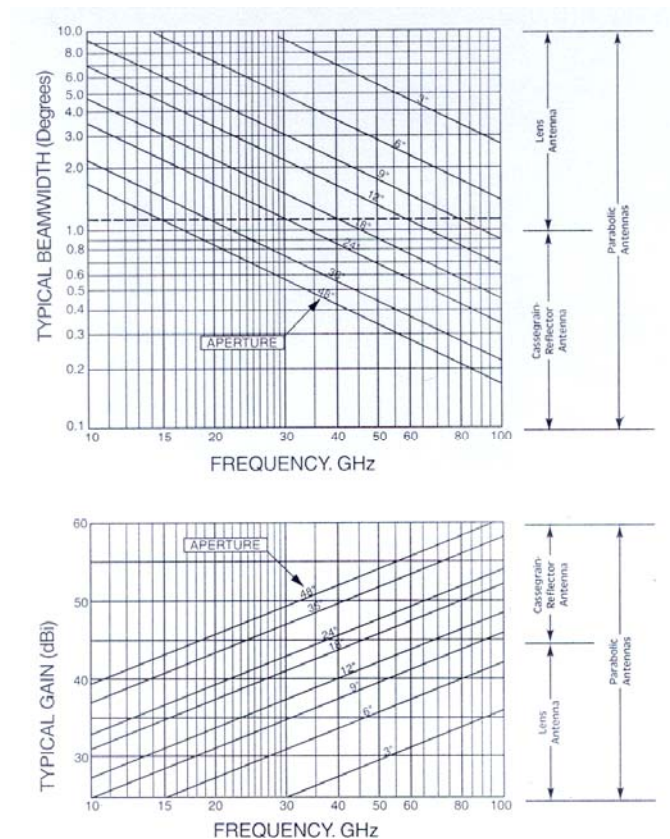


Figure 3.1 Antenna gain & HPBW

As the beam width is too narrow, the procedure of two antenna alignment needs to be conducted carefully with very small angle of steps. To find the beam peak at both sites, one end of the antenna is tilted up and down, left and right first, halting the other site. Tilting is conducted by checking the RSSI voltage, which indicates the received power strength. Once the beam peak is found at one end, the other site of antenna is tilting next carefully.

Figure 3.2 shows the Google Earth view of the field test site. In order to have good line-of-site (LOS), the test site was chosen carefully, having no any obstacles along to the path. According to the estimated link budget, the field test was conducted at a distance of 4.1 km in Ulsan, South Korea.

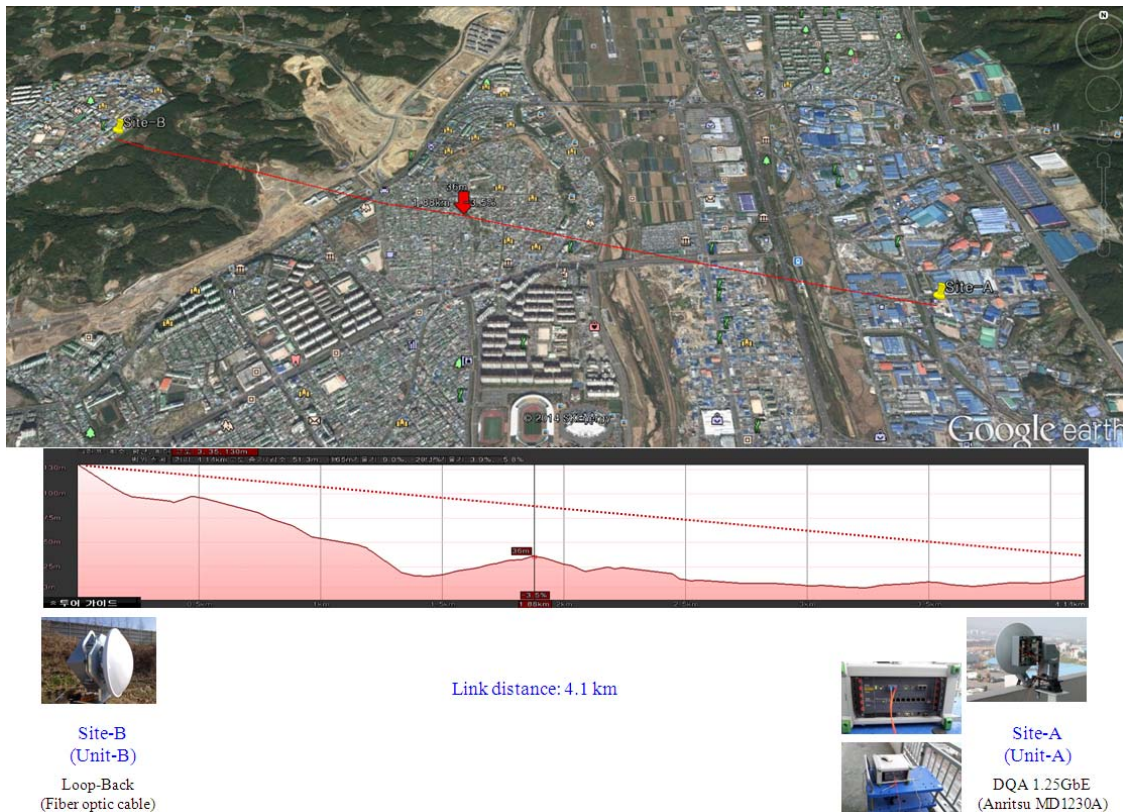


Figure 3.2 Field test site with 4.1 km distance

By using data quality analyzer, DQA, 1.25 Gbps Ethernet signal was plugged in Unit-A TX port. The received signal at the other site of Unit-B apart from 4.1 km was loop-backed to its TX port of Unit-B again so it can be returned back to Unit-A. The received signal at RX port of Unit-A was plugged into DQA again. At 4.1 km, the 1.25 Gbps GbE link was made perfectly without errors. The received power was -44 dBm and there were about 5 dB more margins. The field test result was quite well matched with the indoor test. The input power variation was about +/- 0.5 dB during field test for about 2 hours. The weather was clear, no fog and no wind. The temperature was 16°C.

3.3 Availability Analysis

A fixed broadband radiolink is designed to be available at all times, but all wireless applications using microwave or millimeter wave frequency affects by environment or weather like rainfall directly. Especially planning for millimeter wave spectrum use must take into account the propagation characteristics of radio signals at this frequency range. ‘Available’ means that the BER is at or below a given threshold level. Conversely, an ‘outage’ is the time when the link is not available. The annual link outage is specified by (3.3.1) related to availability [24].

$$Outage = \left(1 - \frac{Availability}{100}\right) \times 525,600 \text{ [min]} \quad (3.3.1)$$

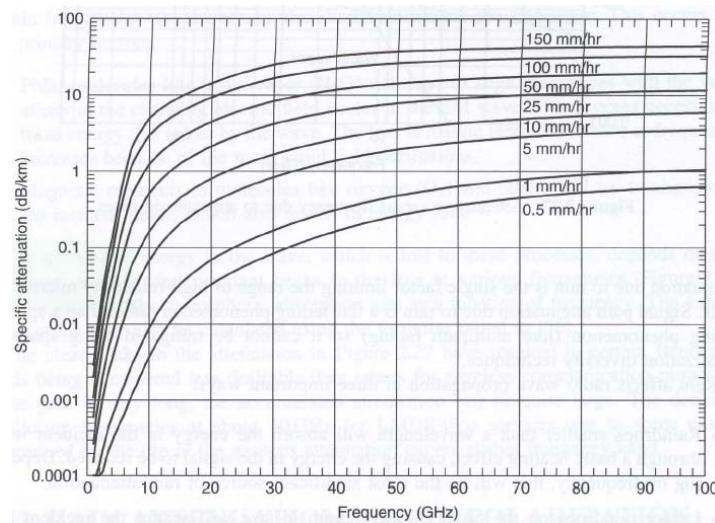


Figure 3.3 Rain attenuation versus frequency

Figure 3.3 shows the rain attenuation versus frequency. Above 30 GHz, the curve saturates and the attenuation levels are almost the same above 60 GHz. At 71 ~ 76 / 81 ~ 86 GHz E-band, the rain attenuation is around 10 dB/km under 25 mm/h of heavy rain.

According to the availability, ITU-R designates 15 rain regions worldwide [25]. It is summarized in Table 3.2. At each rain region, the recommended rain rate is shown in accordance with its specific link outage probability. In South Korea, for example, designated as K-region, the required rain rate is 100 mm/h in order to guarantee 99.999% of availability, or equivalent to link outage of 5.26 min/year.

Table 3.2 Rain rate worldwide recommended from ITU-R

Parameters			Rain Rate [mm/h] @ITU-R Recommended														
Availability	Link outage [min/year]	Provability of rain [%]	A	B	C	D	E	F	G	H	J	K	L	M	N	P	Q
99.999%	5.26	0.001	22	32	42	42	70	78	65	83	55	100	150	120	180	250	170
99.997%	15.77	0.003	14	21	26	29	41	54	45	55	45	70	105	95	140	200	142
99.99%	52.56	0.01	8	12	15	19	22	28	30	32	35	42	60	63	95	145	115
99.97%	157.68	0.03	5	6	9	13	12	15	20	18	28	23	33	40	65	105	96
99.9%	525.60	0.1	2	3	5	8	6	8	12	10	20	12	15	22	35	65	75
99.7%	1,576.80	0.3	1	2	3	5	2	5	7	4	13	4	7	11	15	34	49
99%	5,256.00	1	0.1	0.5	0.7	2.1	0.6	1.7	3.0	2.0	8.0	1.5	2.0	4.0	5.0	12	24

With the implemented parameters in this work, the link distance was estimated by using link budget calculation shown in Table 3.1 in accordance with ITU-R recommendation. In a K-region for 99.99% availability, the recommended link distance is 1.0 km. All available link distance are summarized in Table 3.3. The maximum distance is estimated by 4.9 km under clear weather conditions with no rain.

Table 3.3 Estimated link distance of implemented radiolink

Parameters			Link Distance [km] @BER 10 ⁻¹² or error free														
Availability	Link outage [min/year]	Weather	A	B	C	D	E	F	G	H	J	K	L	M	N	P	Q
99.999%	5.26	torrential	1.3	1.1	1.0	1.0	0.8	0.7	0.8	0.7	0.9	0.6	0.5	0.6	0.5	0.4	0.5
99.997%	15.77	heavy	1.6	1.3	1.2	1.2	1.0	0.9	0.9	0.9	0.9	0.8	0.6	0.6	0.5	0.4	0.5
99.99%	52.56		1.9	1.7	1.5	1.4	1.3	1.2	1.1	1.1	1.1	1.0	0.8	0.8	0.6	0.5	0.6
99.97%	157.68	drizzle	2.3	2.1	1.9	1.6	1.7	1.5	1.4	1.4	1.2	1.3	1.1	1.0	0.8	0.6	0.6
99.9%	525.6		2.9	2.6	2.3	1.9	2.1	1.9	1.7	1.8	1.4	1.7	1.5	1.3	1.1	0.8	0.7
99.7%	1,576.80		3.4	2.9	2.6	2.3	2.9	2.3	2.0	2.4	1.6	2.4	2.0	1.7	1.5	1.1	0.9
99%	5,256.00		4.4	3.8	3.6	2.9	3.7	3.0	2.6	2.9	1.9	3.1	2.9	2.4	2.3	1.7	1.3

1) Antenna: 1ft, Gain: 45dBi, Frequency: 71~76/81~86GHz

2) Datarate: 1.25Gbps, 100% throughput

3.4 Interference Free Scenario

With the implemented radiolink, interference free scenarios were analyzed. Figure 3.4 shows the point-to-point field deployment. Due to the pencil beam characteristic of E-band frequency radiation, two units of radios are being deployed in open site with LOS. Even though the narrow 3 dB beam width of 0.8 ~ 0.9 degree, an interference can occur due to the side lobes of antenna beam pattern when two radiolinks are installed on the same tower closely. In this section, how such interference can be removed is described.



Figure 3.4 Point-to-point multi-link deployment

If unit-A is installed horizontally at site 1, unit-B need to be installed at the same polarity at site 2. If unit-A were installed at vertical polarization, unit-B should be installed at the same polarity at the other site. Thus there exists four possible combinations of deployment with single link of radio. Table 3.4 shows the four possible cases of deployment.

Table 3.4 Deployment case

Case	Site 1	Site 2
I	AH: Unit-A Horizontal	BH: Unit-B Horizontal
II	AV: Unit-A Vertical	BV: Unit-B Vertical
III	BH: Unit-B Horizontal	AH: Unit-A Horizontal
IV	BV: Unit-B Vertical	AV: Unit-A Vertical

In case two links are needed to be installed at the same site, any possibility of interference should be considered. According to the field test, the required separation was measured. With two links in parallel deployment with sufficient separation, it was checked if both of the links shows no interference with each other first. Then by moving one of the links closely to the other, the separation was measured when errors start to occur from any one of links due to the interference. The test was conducted at 1 km of distance. In Table 3.5, the measured results of the required separations are summarized. When different types of radios are installed at the same site, if the polarization is the same, the possibility of interference was relatively high and the required separation was at least 1.5 m.

Table 3.5 Required separations for interference free

Deployment ¹⁾	Required Separation
AH/AV, BH/BV	0 (no interference)
AH/BV, AV/BH	0.5 m
AH/BH, AV/BV	1.5 m

1) In case of the deployment at the same site

With the combination of 4 links of 1.25 Gbps radiolink, a 5 Gbps network can be implemented. By using the interference free scenarios described previously, 4 links of combination at one site can be deployed. Similarly, if there is another type of radio using totally different frequency from the implemented 74.875 GHz or 84.875 GHz, a 10 Gbps network is available.

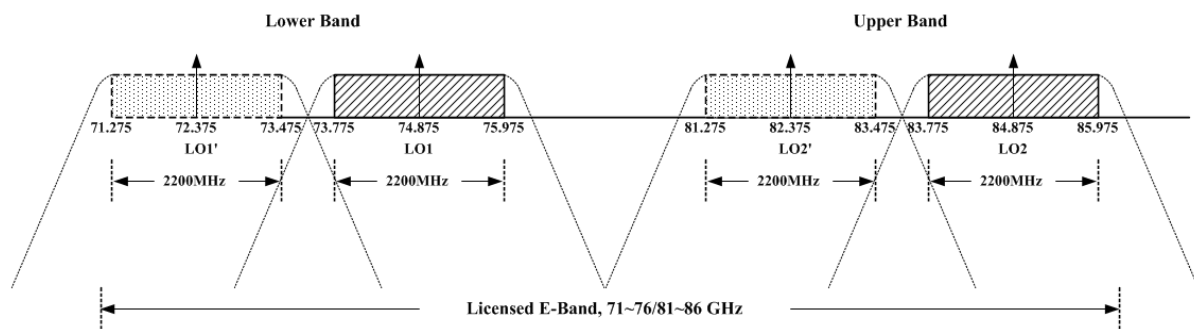


Figure 3.5 Frequency plan for interference free scenarios for 10 GbE

Figure 3.5 shows an available frequency plan for interference free scenarios for 10 GbE. The alternative 2nd sets of LO frequency is 72.375 GHz and 82.375 GHz. By choosing these frequencies as the center frequency of the second radiolink, two different type of 1.25 Gbps radiolink is available. This of course meets the 5 GHz of frequency allocation in 71 ~ 76 GHz and 81 ~ 86 GHz regulation. The possible combination of 8 links with 1.25 GbE for 10 GbE radiolink is summarized in Table 3.6.

Table 3.6 Interference free scenarios for 10 GbE

Radio Unit	SITE 1	SITE 2
74.875 GHz 84.875 GHz	AH: Unit-A Horizontal	BH: Unit-B Horizontal
	AV: Unit-A Vertical	BV: Unit-B Vertical
	BH: Unit-B Horizontal	AH: Unit-A Horizontal
	BV: Unit-B Vertical	AV: Unit-A Vertical
72.375 GHz 82.375 GHz	AH: Unit-A Horizontal	BH: Unit-B Horizontal
	AV: Unit-A Vertical	BV: Unit-B Vertical
	BH: Unit-B Horizontal	AH: Unit-A Horizontal
	BV: Unit-B Vertical	AV: Unit-A Vertical

The challenging 10 GbE radiolink was partially applied to a financial network in service for HFT between Chicago and New York, which is total 12,000 km long distance wireless network. As mentioned in section 1.1, the latency of conventional fiber optic cable is absolutely not comparable with the implemented ultra low latency of E-band transceiver. The newly designed E-band ASK transceiver can be a good alternative for such a time-sensitive network.

IV. Future Work

The implemented E-band transceiver for ultra low latency includes several high cost discrete MMICs of GaAs for the high performance. To reduce the cost of materials, some of advanced research results achieved by using CMOS technology have been announced [55], [56] [57]. As the next phase of the work after the implemented transceiver, a preliminary low cost approach using CMOS design has been investigated for the LNA and mixer. Results are still preliminary, but they already show promise for future work. An initial design result and the implemented chip will be described briefly in this section.

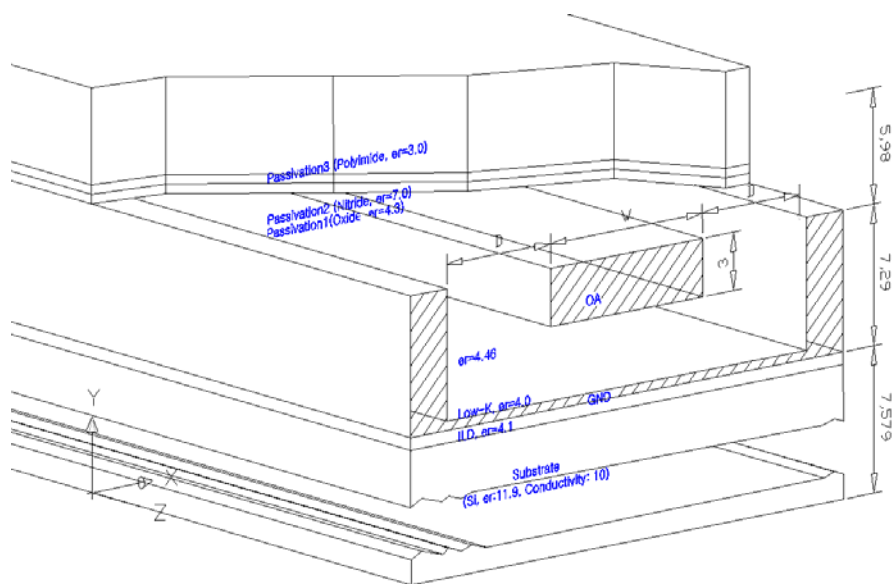


Figure 4.1 Structure of MCPW transmission line

Figure 4.1 shows the structure of MCPW transmission line, which is a basic element for the design of other devices like LNA and mixer, as well as a matching section. The technology is Samsung 65 nm CMOS process. There are a total of 8 metal layers with the process, and the lowest two metal layers were used for a ground plate and the top metal layer with 3 um thickness for the signal line.

To analyze the characteristics of MCPW transmission line, an electromagnetic field simulation is required [58] and Ansoft HFSS was used for the work. By changing the defined dimension of the line width W and separation D from the wall (Figure 4.1), the required dimension of 50Ω transmission line was decided. Figure 4.2 shows the extracted characteristic parameters with its electric field distribution near the conductor of the transmission line.

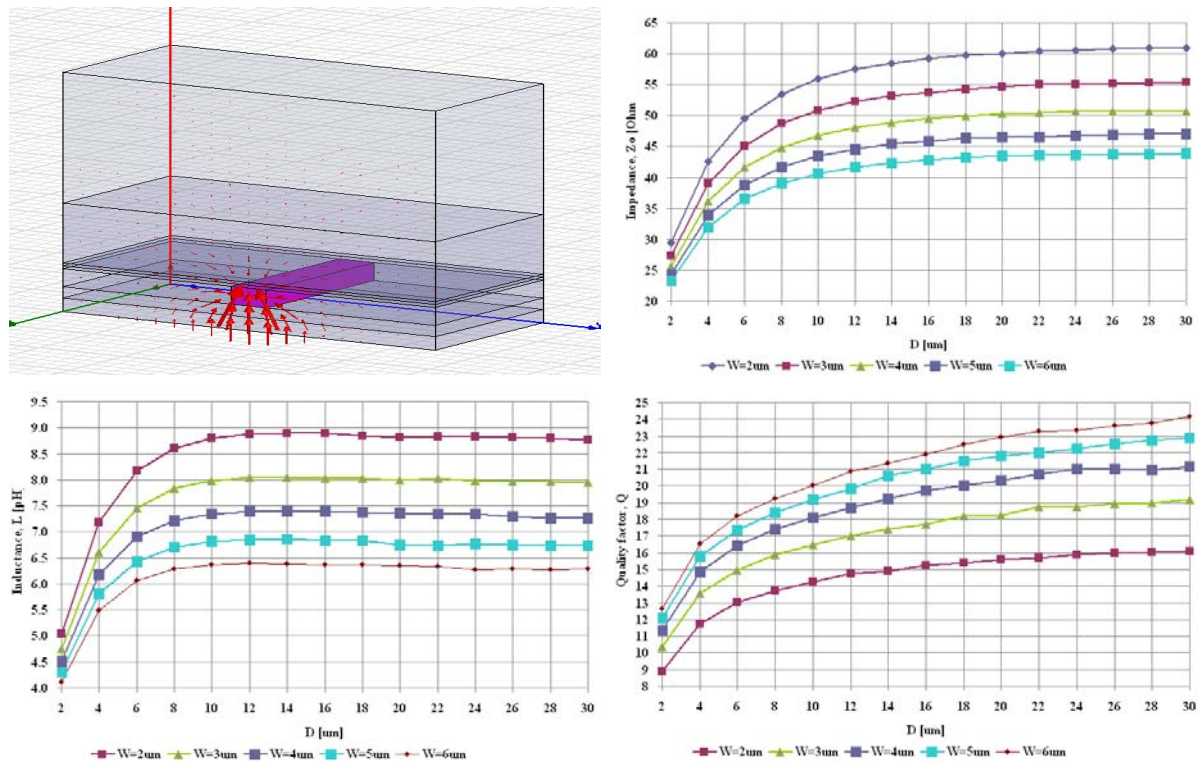


Figure 4.2 Field distribution and MCPW simulation result

The designed 50Ω transmission line has a width of $4.0 \mu\text{m}$ and D of $20 \mu\text{m}$. At 76 GHz , the wavelength is 1.90 mm and the loss is 0.02 dB per unit length of $20 \mu\text{m}$. Line inductance and quality factor Q is defined by (4.1.1) and (4.1.2) respectively, and the extracted inductance is 7.41 pH and quality factor Q is 20.4 .

$$L = \frac{1}{2\pi f \cdot \text{Im}(Y)} \quad (4.1.1)$$

$$Q = \frac{\text{Im}(Y)}{\text{Re}(Y)} \quad (4.1.2)$$

Figure 4.3 shows the schematic of designed 3-stage LNA. Each stage was designed with a common source topology for a stable operation as an initial trial. A cascode topology is good for higher gain with good input/output isolation providing an easy in/out matching, but the design and its operation is known to be sensitive at the millimeter-wave [58], which resulted in failure to work when it is implemented as die. Thus common source topology was chosen first.

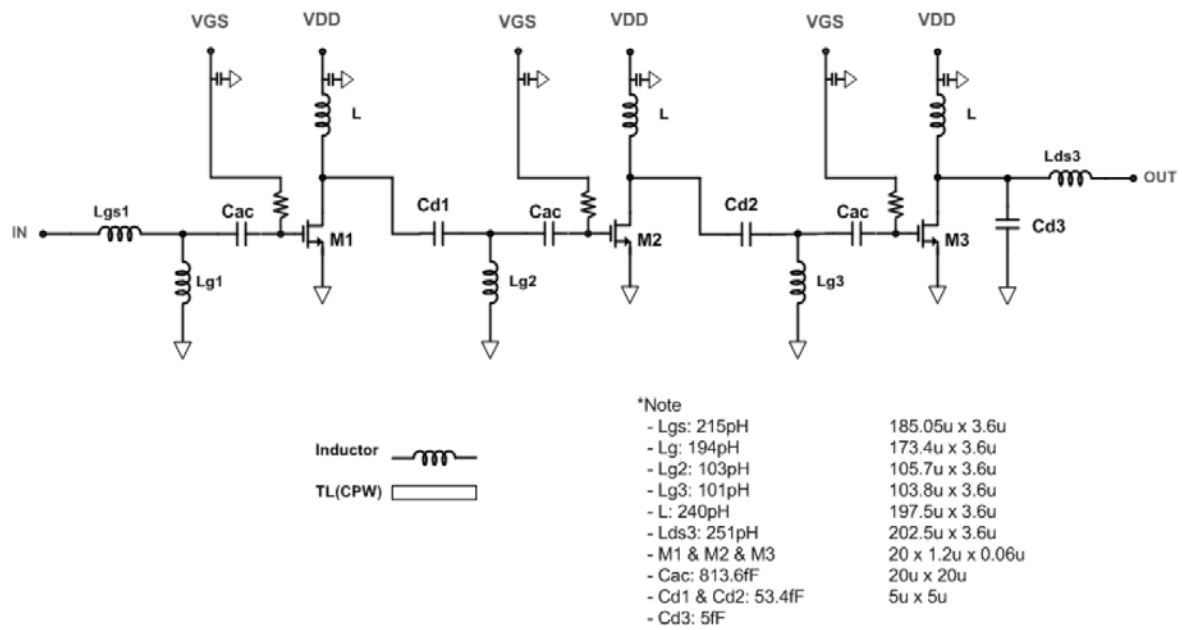


Figure 4.3 Schematic of 3-stage LNA

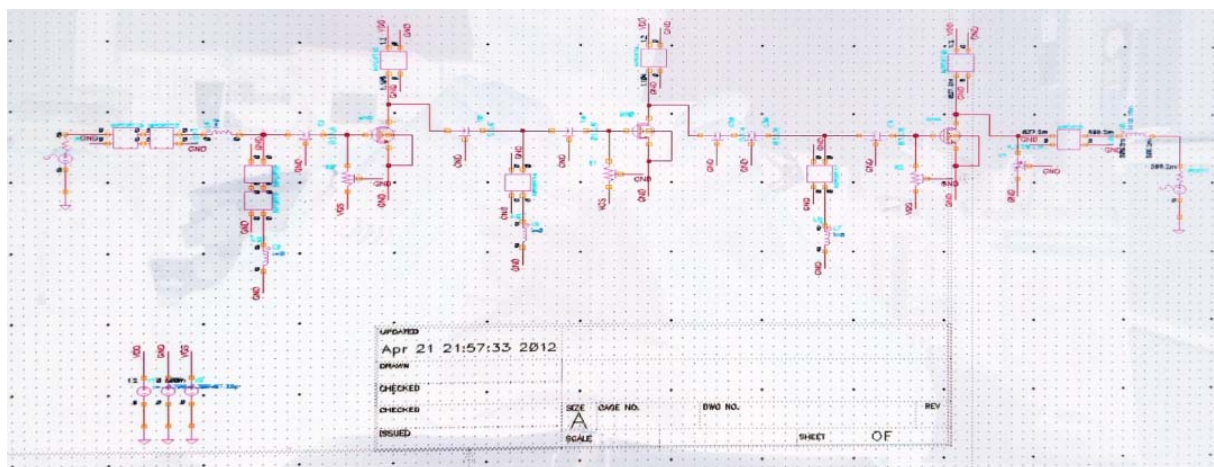


Figure 4.4 Cadences modeling of 3-stage LNA

Figure 4.4 shows the Cadence modeling for simulation. A single stage LNA was designed first and then cascaded to 3-stage. A conjugate matching technique was used for the impedance matching between output of the first stage and input of next stage. Figure 4.5 shows the simulation result of the designed LNA. The designed gain of LNA at 76 GHz was 12 dB typical. Input return loss was less than -18 dB and the output return loss was less than -14 dB. Figure 4.6 shows the chip layout design with the dimension of 750 x 520 μm^2 .

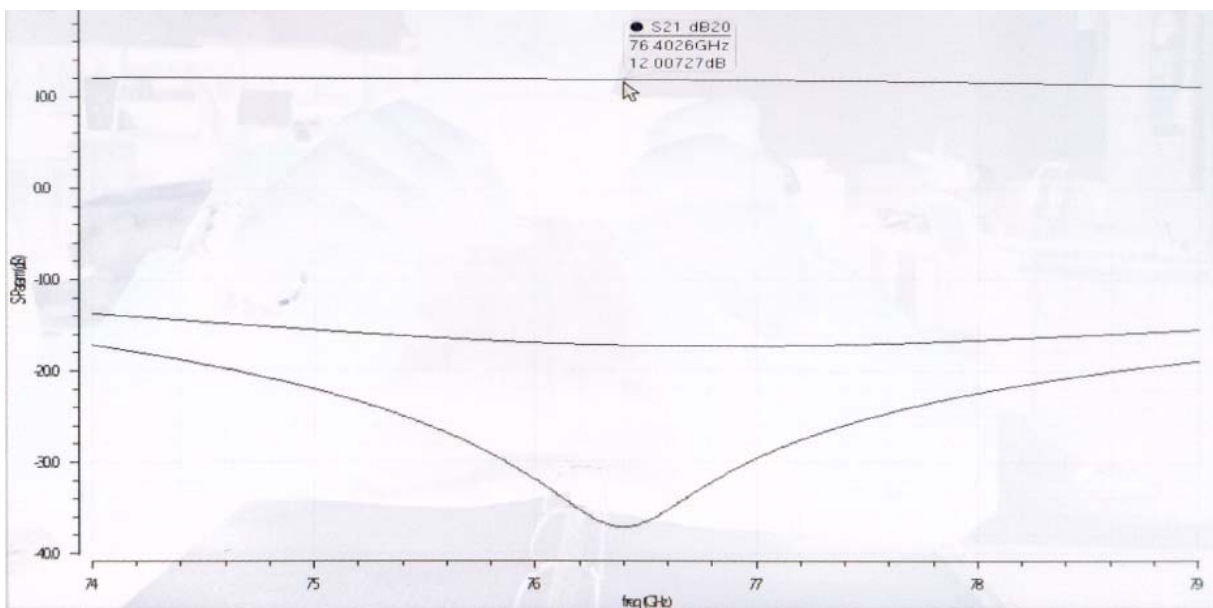


Figure 4.5 Simulation result of designed 3-stage LNA

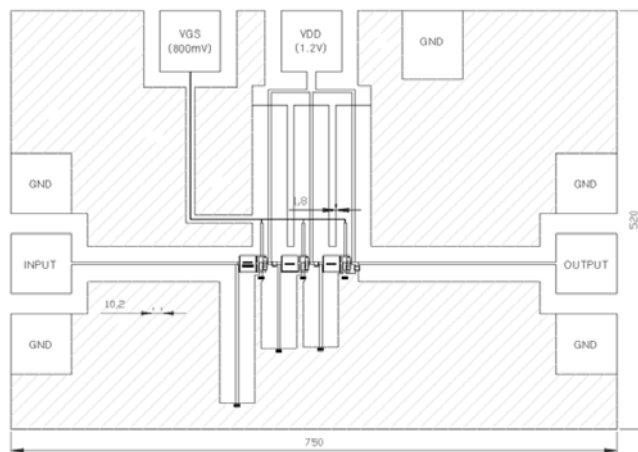


Figure 4.6 Layout design of 3-stage LNA

Figure 4.7 shows the schematic of the designed single balanced mixer at E-band of 71 ~ 76 / 81 ~ 86 GHz. The differential pair of NMOS FET M_2 and M_3 are switched by two LO inputs, which are divided by Marchand balun from LO_IN. During the M_2 or M_3 ON, M_1 is controlled in accordance with RF_IN. The frequency difference of LO_IN and RF_IN is output at the drain of M_2 and M_3 as a differential pair of IF_INT+ and IF_INT-. A $\lambda/4$ transmission line was inserted for drain matching allowing DC bias.

To improve the conversion loss of the mixer as well as a stable operation from load, a differential amplifier as a buffer was added offering good isolation between load and mixer output.

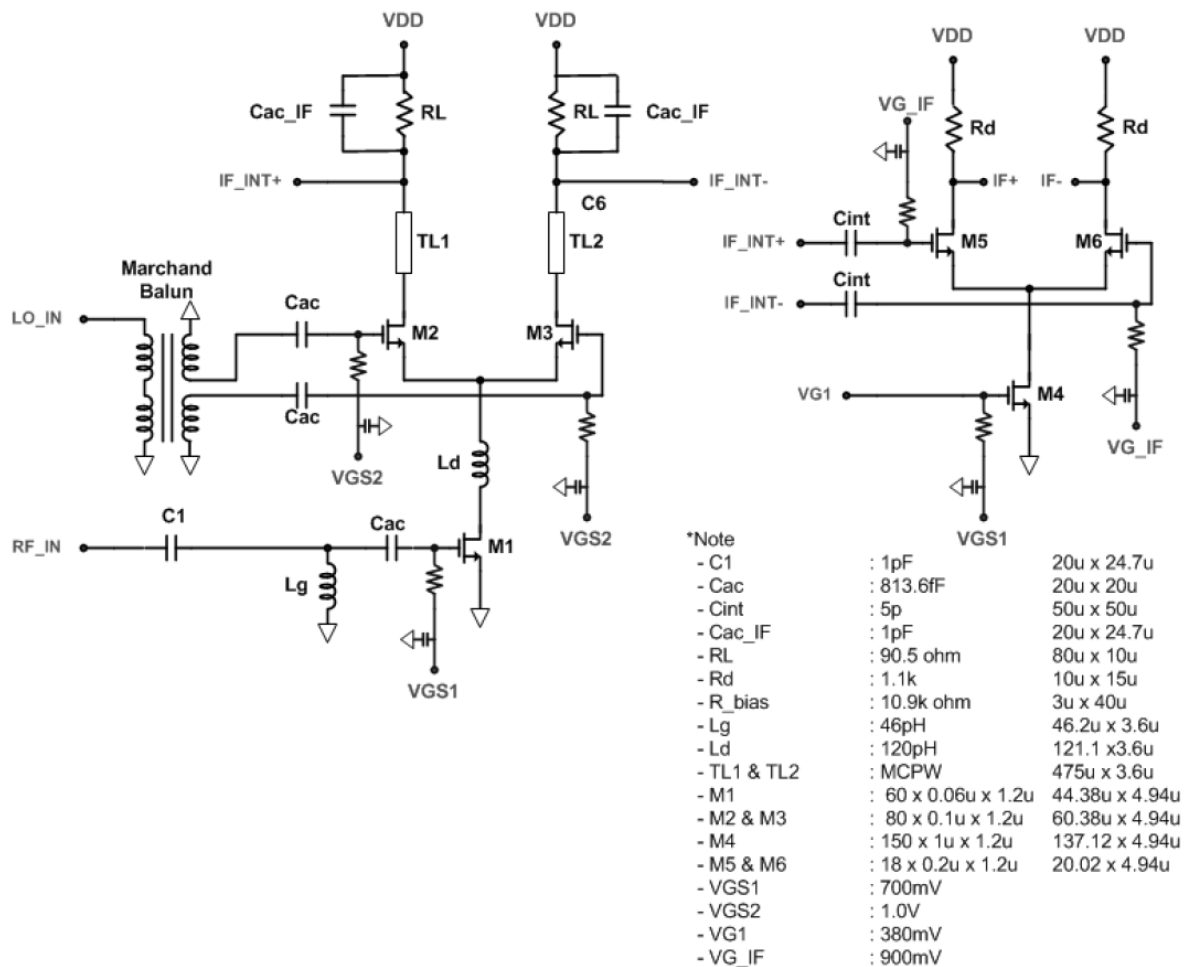


Figure 4.7 Schematic of single balanced mixer with buffer

Figure 4.8 shows the simulation result of the designed single balanced mixer. With LO power of 0 dBm at 76.1 GHz and RF input of -30 dBm at 76.0 GHz, the IF output was -37 dBm at 100MHz, which resulted in a conversion loss of 7 dB, except the buffer gain. Due to the lack of computer memory resources, the simulation took over half a day for only a single setup of simulation, even worse sometimes the simulator abruptly stopped. Thus, note that the simulation result is not final, and needs to be optimized in the future. Figure 4.9 shows the layout design.

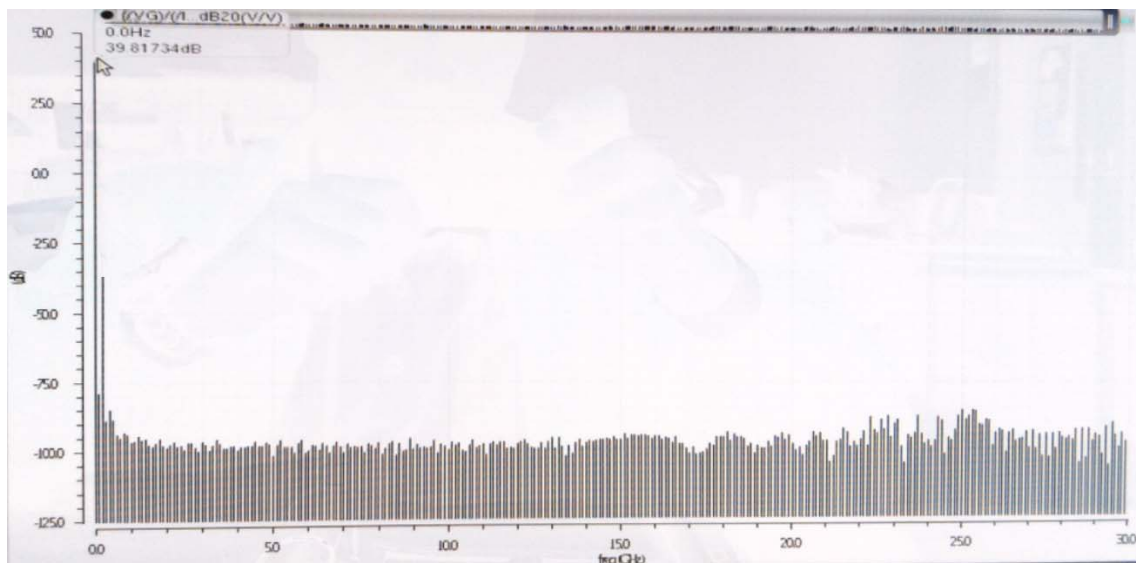


Figure 4.8 Simulation result of mixer

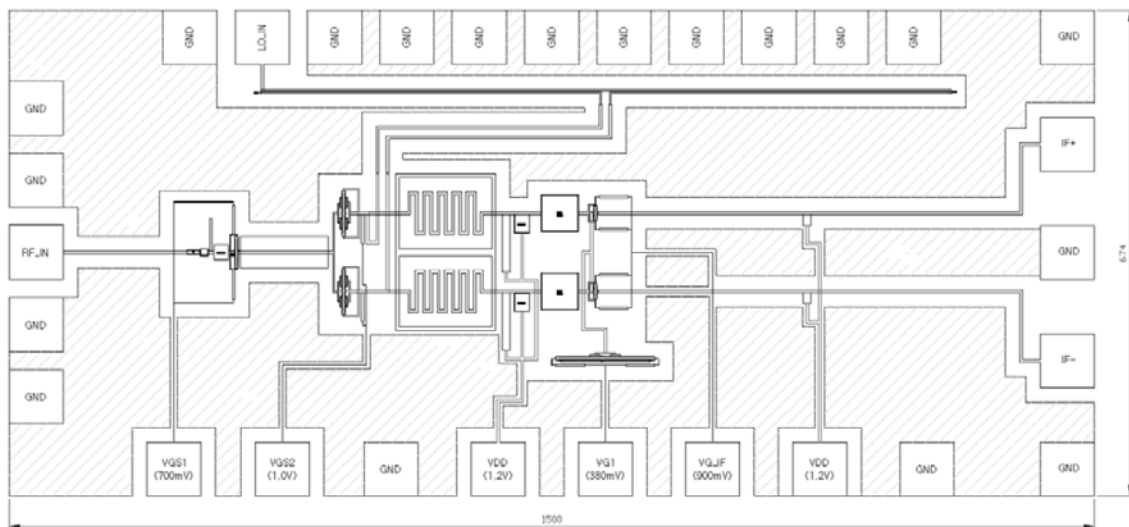


Figure 4.9 Layout design of SBM mixer

Figure 4.10 and Figure 4.11 show the microphotograph of implemented LNA and mixer die, respectively, by using Samsung 65 nm CMOS technology. The chip size is $750 \times 520 \mu\text{m}^2$ for the LNA and $1,500 \times 674 \mu\text{m}^2$ for the mixer.

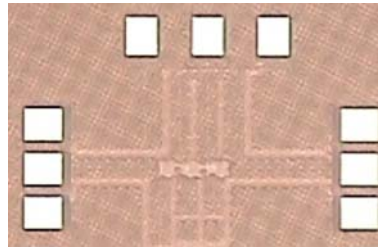


Figure 4.10 Microphotograph of implemented CMOS LNA ($750 \times 520 \mu\text{m}^2$)

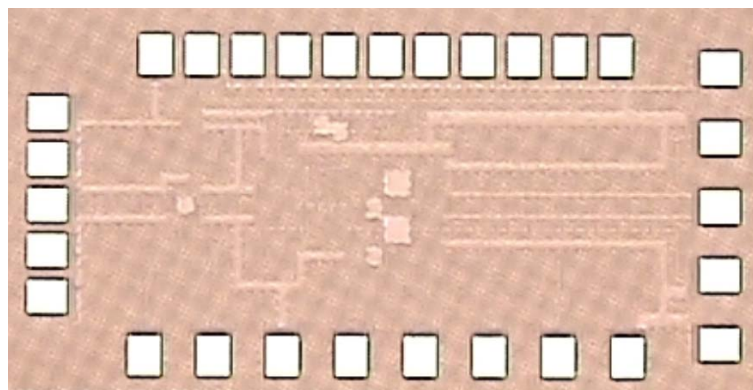


Figure 4.11 Microphotograph of implemented CMOS Mixer ($1,500 \times 674 \mu\text{m}^2$)

V. Conclusion

For the special purpose of a time-sensitive system, such as a financial network, banking network, or medical network for real-time access in hospital, a very low latency of several tenths of a nano-second with a 1.25 Gbps transceiver is required. However, most commercial radiolinks are too slow at 5 ~ 350 μ s of latency through the use of Layer-2 topology with higher level digital modulation. In this work, a unique topology of an ultra low latency transceiver was implemented by using high-speed ASK modulation with the scheme of physical Layer-1 transmission.

The problem was securement of the required bandwidth of 2.5 GHz (actually 2.2 GHz in the work) for 1.25 Gbps transmission with ASK. There are no such allowed wide bands of frequency range in ISM band of 2.4 GHz, 5.8 GHz, 24 GHz, or any other microwave frequency range. Thus 71 ~ 76 GHz and 81 ~ 86 GHz E-band millimeter-wave frequency was chosen, which allows for a 5 GHz bandwidth.

In order to achieve a range of tenths of a nano-second of ultra-low latency with simple low cost, the direct conversion architecture was first tried. It was simple but still needed to be revised to address several problems. First, it was too difficult to build an ASK modulator directly at a 70/80 GHz millimeter-wave, as it was too sensitive at its physical dimension. Secondly, the flatness was important, but it was not easy to secure the required BW. Most of all, the conversion loss was significantly increased when the received power is low.

In order to solve these problems, a heterodyne transceiver was considered. The ASK modulation was conducted at the IF stage. By adopting the heterodyne topology, the burdens of building an ultra wideband ASK modulator in 70/80 GHz millimeter-wave range was alleviated. However, building of the 1.25 Gbps ASK modulator in the IF stage presented another new challenge.

To secure the required in-band flatness, all devices were carefully chosen to cover 2.2 GHz or more, and several wide band design techniques with trial and error were proposed. According to the measurement results, the sensitivity was -45 dBm for 1.25 Gbps under BER 10^{-12} , or error free, and one-way latency was measured by 19.1 ns, which is a superior achievement compared to existing commercial radiolinks worldwide. It was field tested at 4.1 km and showed good match with its link budget.

As a field proven solution, the research result has been partially adapted to a financial network in service between Chicago and New York.

REFERENCES

1. James PGS & Joseph DT 2001, *High-Speed Networking: A Systematic Approach to High-Bandwidth Low-Latency Communication*, John Wiley, USA.
2. Waheed Z, Syed AA, Adeel A, Abid Q 2002, 'Modeling of Processor Delay and Overall Reduction in Network Latencies for Real Time, Interactive Applications', *IEEE*, 76-79.
3. Eugene, H. 2014, *Optics*, Pearson Education Limited, Essex, England
4. Emulex Inc., 'Achieve Ultra-Low Latency for High-Frequency Trading Applications', Cisco, <http://www.emulex.com/resources>, accessed March 2013
5. Tomi. K. 2014, 'Traders Pump up the Volume in Rally to New Highs', *Wall Street Journal*, May
6. Clive C 2013, 'Time is money when it comes to microwaves', *Financial Times*, May 10, <http://www.ft.com/cms/s/2/2bf37898-b775-11e2-841e-00144feabdc0.html#axzz2zhLNa6yp>
7. Lockwood, JW, Gupte A, Mehta N, Blott M, English T & Vissers K 2012, 'A Low-Latency Library in FPGA Hardware for High-Frequency Trading (HFT)', *High-Performance Interconnects (HOTI), IEEE 20th Annual Symposium*. pp.9 ~ 16.
8. Brook M, Sharp C, Ushaw G, Blewitt W & Morgan G 2013, 'Volatility Management of High Frequency Trading Environments', *Business Informatics (CBI), IEEE 15th Conference*, pp. 101 ~ 108.
9. Irene A 2013, *High-Frequency Trading: A Practical Guide to Algorithmic Strategies and Trading*

Systems, John Wiley, USA.

10. Elaine W, Michael P & Wellman 2013, 'Latency Arbitrage, Market Fragmentation, and Efficiency: A Two-Market Model', *Proceedings Article*, University of Michigan.
11. Kohli, J 1989, 'Medical imaging applications of emerging broadband networks', *Communications Magazine, IEEE*, Volume: 27, pp. 8 ~ 16.
12. Sakamoto M & Murase M 2007, 'Parallel Implementation for 3-D CT Image Reconstruction on Cell Broadband Engine', *Multimedia and Expo, IEEE International Conference*, pp. 276 ~ 279.
13. Colombo, Claudio, Cirigliano & Massimo 2011, 'Next-generation access network: A wireless network using E-band Radio frequency (71–86 Ghz) to provide wideband connectivity', *Bell Labs Technical Journal*, Volume: 16, pp. 187 ~ 205.
14. Kim HC, Lee DM, Chon KN, Jang BC, Kwon TK, Choi YH 2010, 'Performance impact of large file transfer on web proxy caching: A case study in a high bandwidth campus network environment', *Communications and Networks, IEEE Journals & Magazines*, Volume: 12, pp. 52 ~ 66.
15. Wikipedia 2014, 'ISM band', *Wikipedia*,, http://en.wikipedia.org/wiki/ISM_band
16. LightPointe 2014, 'Millimeter-Wave (MMW) Radio Transmission: An Application and Technology Primer', LightPointe, www.lightpointe.com
17. ZhenQi C & Fa FD 2010, 'Effects of LO Phase and Amplitude Imbalances and Phase Noise on M-QAM Transceiver Performance', *IEEE Transaction on Industrial Electronics*, vol 57, May. pp.

1505 ~ 1517.

18. FCC 2005, 'Memorandum Opinion and Order in the Matter of Allocations and Service Rules for the 71-76 GHz, 81-86 GHz, and 92-95 GHz Bands', *FCC 05-45A*.
19. 국립전파연구원, 2013, '국립전파연구원고시 제2013-2호', *국립전파연구원고시*
20. Jonathan W, 'Licensing and License Fee Considerations for E-band 71-76 GHz and 81-86 GHz Wireless Systems', *E-band Communications Corp.*
21. CEPT(ECC) 2009, 'Radio Frequency Channel Arrangements for Fixed Service Systems operating in the Bands 71-76 GHz and 81-86 GHz', *ECC REC05-07*.
22. OFCOM 2013, 'Spectrum Management Approach in the 71-76 GHz and 81-86 GHz bands', *OFCOM, Dec.*
23. ETSI 2006, 'Fixed Radio Systems; Point-to-Point Equipment; Radio equipment and antennas for use in Point-to-Point Millimeter wave applications in the Fixed Services frequency bands 71 GHz to 76 GHz and 81 GHz to 86 GHz', *ETSI-TS-102-524*.
24. Harry R. A 2003, *Fixed Broadband Wireless System Design*, Wiley, USA.
25. ITU-R 1994, 'Characteristics of Precipitation for Propagation Modeling', *Recommendation ITU-R PN.837-1*
26. Marian CV, Croitoru V & Oprea D 2013, 'Proposed communication protocol between network nodes and address exchange', *Signals, Circuits and Systems (ISSCS), IEEE International*

Symposium, pp. 1 ~ 4.

27. O3b Networks, 'What is Network Latency and Why Does It Matter?', *O3b Networks*, http://www.o3bnetworks.com/media/40980/white%20paper_latency%20matters.pdf, accessed August 2012
28. SIAE 2013, '70/80 GHz 2.5 Gbps Full Outdoor', ALFOplus80, SIAE MICROELETTRONICA. <https://www.siaemic.com>
29. E-band Communications, 'E-Link 1000Q 4G Evolution Series', *E-band Communications*, www.e-band.com
30. E-band Communications, 'E-Link 2500 Solution 4G Evolution Series', *E-band Communications*, www.e-band.com
31. Sub10 Systems, '70/80 GHz Wireless Backhaul for Macro Cell Backhaul & Enterprise Connectivity', *Liberator-E1000c*, *Sub10 Systems Limited*, www.sub10systems.com
32. Huawei Technologies, 'RTN 380, The Fiber-speed Microwave', *Huawei Technologies Co.* www.huawei.com
33. Elva-1, 'PPC-1000, Gigabit Ethernet link', *ELVA-1*, www.elva-1.com
34. BridgeWave Communications, '80 GHz Extended Range Gigabit Wireless Links', *BridgeWave Communications Inc.*, www.bridgewave.com
35. BridgeWave Communications, '80 GHz 3000 Mbps Ultra-High Capacity Wireless Links', *Bridge-*

Wave Communications Inc., www.bridgewave.com

36. Fujitsu Wireless, 'Fujitsu Network BroadOne GX4000 Series', *Fujitsu Wireless Systems Limited*,
<http://jp.fujitsu.com/group/fwl/>
37. Sub10 Systems, 'Gigabit Full-Duplex over distances up to 4 km', *Liberator-E1000e*, *Sub10 Systems Limited*, www.sub10systems.com
38. Siklu Communication 2013, 'EtherHaul™-1200 – Gigabit Ethernet Wireless Solution', *EH-1200 Datasheet*, Siklu Communication Ltd.
39. Zabidi SA, Khateeb WA & Islam MR 2010, 'The effect of weather on free space optics communication (FSO) under tropical weather conditions and a proposed setup for measurement', *Computer and Communication Engineering (ICCCE), IEEE International Conference*, pp. 1 ~ 5.
40. Behzad R 1998, *RF Microelectronics*, Prentice Hall, USA.
41. David M 1985, 'Necessary Bandwidth and Special Properties of Digital Modulation', *NTIA Report 84-168*, US Department of Commerce
42. Yoneyama T & Nishida S 1981, 'Nonradiative Dielectric Waveguide for Millimeter-Wave', *Microwave Theory and Techniques, IEEE Transactions*, Volume 29, pp. 1188 – 1192.
43. Haiyoung L 1995, 'Wideband characterization of a typical bonding wire for microwave and millimeter-wave integrated circuits', *Microwave Theory and Techniques, IEEE Transactions*, Volume 43, Issue 1, pp. 63 ~ 68.

44. Comotech corp. 2010, 'AirLight, E-band Point-to-point Fixed Wireless Solution', Comotech Corp., www.comotech.com

45. Youngsu K, Oneryul R, Younggeun Y & Jae-ha C 2003, 'Design and Fabrication of Ka-Band NRD Guide Filter with Newly Designed Inductive Post Structure', *KEES*, vol.14, No 4, pp. 369 ~ 376.

46. Youngsu K, Oneryul R, Hyungdong C & Younggeun Y 2002, 'Design and Fabrication of NRD Guide Filter Using Inductive Iris' *KEES*, vol.13, No.8, Sep. pp. 741 ~ 747.

47. Vasil P & DS Budimir 1994, 'Design of Waveguide E-Plane Filters with All-Metal Inserts by Equal Ripple Optimization', *IEEE Trans. MTT*, Vol.42 No.2, Feb.

48. Levent K, Mohammad M & Edward SR 2010, 'Abnormal group delay and detection latency in communication systems', *Antennas and Propagation Society International Symposium, IEEE*, July.

49. Jones, E.M.T., Young, L., Matthaei, G.L. 1981, *Microwave Filters, Impedance Matching Networks and Coupling Structure*, Artech House, Norwood, MA, USA

50. G.Matthaei, L. Young "Microwave Filters, Impedance Matching Networks and Coupling Structure", Artech House 1981

51. F. Arndt, J. Bornemann, D. Heckmann, C. Piontek, H. Semmerow & H. Schueler 1986, 'Modal S-matrix method for the optimum design of inductively direct-coupled cavity filters', *IEE Proceedings*, vol.133 No.5 Oct. 1986

52. Bui LQ, Ball D & Itoh T 1984, 'Broad-Band Millimeter-Wave E-Plane Bandpass Filters', *IEEE Trans.*, Vol. MTT-32, Dec.

53. Xiao PL, Kawthar AZ & Ali EA 1991, 'A Rigorous Three Plane Mode-Matching Technique for Characterizing Waveguide T-Junctions, and its Application in Multiplexer Design', *IEEE MTT* vol.39, No.12 Dec.

54. Hui WY, Amr EA, Ji FL, Xiao PL, Kawthar AZ & Alain M 1993, 'Wide-Band Waveguide and Ridge Waveguide T-Junctions for Diplexer Applications', *IEEE MTT* vol.41 No.12 Dec.

55. Antonio M & Tullio R 1994, 'Design of Optimum Three Port Symmetrical Junctions for Diplexer Application', *IEEE MTT-S Digest*.

56. Chinh HD, Sohrab E, Ali MN & Robert WB 2005, 'Millimeter-Wave CMOS Design', *IEEE Journal of Solid-State Circuits*, Vol 40, No. 1, Jan. pp. 144 ~ 155.

57. Roc B, Gui L, Abe A, Keya K & Yang X 2010, 'A 43.5mW 77GHz Receiver Front-End in 65nm CMOS suitable for FM-CW Automotive Radar', *IEEE Custom Integrated Circuits Conference, CICC '10*.

58. Yoichi K, Toshihide S. Masaru S, Tatsuya H, Kajukiyo J 2009, 'A 77GHz Transceiver in 90nm CMOS', *IEEE ISSCC Dig. Tech. Papers.*, pp. 310-311, Feb.

59. Jri L, Yi AL, Meng HH & Shih JH 2010, 'A Fully-Integrated 77-GHz FMCW Radar Transceiver in 65-nm CMOS Technology', *IEEE, Journal of Solid-State Circuits*, Vol. 45, No. 12, Dec.

ACKNOWLEDGEMENT

I would like to express my deepest gratitude to my advisor, Dr. Franklin Bien for his technical support, mentorship, encouragement, and advisement. I would never have been able to finish my doctoral dissertation without his help and guidance.

I would like to give my special thanks to all my committee members Dr. Jae Joon Kim and Dr. Ki Jin Han for guiding my research and teaching at graduate school, and specially many thanks to Professor Jongsoo Kim and Professor Chong Koo An for encouraging and helping me to finish my research. I would also like to thank Professor Jae Ha Choi for his deep encouraging and help. I would also like to thank Professor Zeungnam Bien for his encouragement and advice on school and daily life.

I would also like to thank my President Mr. Sang Hun Kim and all Comotech members providing me the chance to finish my doctoral program providing me conveniences. I would also like to express my deep gratitude to my ex boss, vice president Soo Chan Lee for his willingly allowance to join the doctoral program at UNIST.

I would like to thank all other professors and staffs in school of Electrical and Computer Engineering addressing deep encouragement and providing convenience in my school life. Many thanks to all my lab members in BICDL especially Yunho, Huy, Heedon, Kyungmin, Sanghyun. Without your help, I am sure I would never have been able to finish my dissertation successfully.

Finally, I would like to express my deepest gratitude to my wife for her encouragement and patience. Love you. Many special thanks to my son, my daughter, and my family for cheering me with love. I would also like to thank all my friends who cheer me up whenever I spend difficult time.